THE ELECTRICAL AND OPTICAL PROPERTIES OF ZINC SULPHIDE PLATELETS

by

A. R. Cusdin, B.Sc.(Eng.)

Thesis submitted for the degree of Doctor of Philosophy in the University of London

Department of
Electrical Engineering
Imperial College,
London.

December, 1969

Abstract

This work describes the growth and properties of pure single crystal zinc sulphide platelets. Both the practical and theoretical aspects of the growth of these crystals from the vapour phase are investigated. The experimental observations are shown to be in agreement with the predictions of a simple model for the evaporation and condensation rates of zinc sulphide.

Chemical analysis of the crystals showed that all impurities except silicon were at or below the limits of detection of the methods used (of the order of parts per million). Optical and X-ray examination showed that many crystals had a highly perfect hexagonal structure.

Attempts to produce double carrier injection using cuprous sulphide and indium contacts as hole and electron injectors respectively, apparently failed. However, when silver contacts were used to form a thin Ag - ZnS - Ag sandwich structure, it was found possible to induce a conductivity change in the crystals of about six orders of magnitude by the application of a high voltage between the contacts. The original conductivity could then be restored by discharging a small capacitor through the device or by applying a short pulse from a pulse generator. This conductivity switching phenomenon has been investigated experimentally and is interpreted in terms of a modification in the shape of the conduction band profile in the zinc sulphide crystals.

The author wishes to thank Professor J. C. Anderson, Dr. D. W. G. Ballentyne and Dr. E. A. D. White for many helpful discussions about this work and for their supervision of it. He also wishes to thank the Analytical Services Laboratory, Imperial College, for performing chemical analyses of the zinc sulphide starting material and crystals.

Sincere thanks are also due to Mrs. W. M. Baxter who has devoted a great deal of her spare time to typing this thesis.

To my wife Linda

Contents

		Page
Chapter 1	Introduction	10
Chapter 2	Crystal growth	13
2.1	Introduction	13
2.2	Previous work on the growth of zinc sulphide crystals	13
2.2.1	Growth from the vapour phase	14
2.2.2	Growth from solution	19
2.2.3	Growth from the pure melt	20
2.3	Choice of method of crystal growth	22
2.4	The apparatus for crystal growth	22
2.4.1	The furnace	22
2.4.2	Crystal growing tube	28
2.4.3	The argon gas supply	30
2.4.4	Material handling	32
2.5	Crystal growth procedure	34
2.5.1	Preparation of the crystal growing tube	34
2.5.2	Starting material	35
2.5.3	Charge sintering	36
2.5.4	Growing the crystals	37
2.6	Results	39
2.6.1	Description of the crystals	40
2.6.2	Orientation	45
2.6.3	Effect of growth conditions on crystalline yield	46

		Page
2.7	Theoretical considerations	52
2.7.1	Mode of vapourisation of zinc sulphide	52
2.7.2	Determination of $p_e(Zn)$	53
2.7.3	Determination of the actual zinc vapour pressure p(Zn)	54
2.7.4	Theoretical calculation of the evaporation rate of zinc sulphide	58
2.7.5	Theory of condensation and crystal growth	65
2.7.5.1	Condensation theory	66
2.7.5.2	Mechanisms for the growth of zinc sulphide platelets	81
Chapter 3	Material characterisation	85
3.1	Introduction	85
3.2	Chemical analyses	85
3.2.1	Starting material	86
3.2.2	Crystals	89
3.3	X-ray diffraction experiments	91
3.4	Optical examination	96
3.5	Spectrometric observations	102
3.5.1	Transmission measurements	102
3.6	General observations	109
Chapter 4	Contacts to zinc sulphide	111
4.1	The theory of contacts to semiconductor materials	111

		Page
4.1.1	General description of a metal - semiconductor contact	111
4.1.2	Carrier concentrations and conductivity in zinc sulphide	112
4.1.3	Metal - zinc sulphide junctions	115
4.1.4	Hole injecting contacts	126
4.2	Methods of making contacts to zinc sulphide	132
4.2.1	Radiation wetted indium contacts	132
4.2.2	Evaporated contacts	135
4.2.3	Silver paste contacts	137
4.3	Initial measurements of conduction	138
4.3.1	Sample mounting	138
4.3.2	The cryostat	138
4.3.3	Measuring apparatus and power supply	141
4.3.4	D.C. results	141
4.3.5	Oscillations	143
4.3.6	Discussion of results	144
Chapter 5	Conductivity switching in zinc sulphide	148
5.1	Introduction	148
5.2	First observations of conductivity switching	148
5.3	Definitions of the switched states and criteria for switching	152

		Page
5.3.1	Definitions	152
5.3.2	Effect of contact material on conductivity switching	155
5.3.3	Transition from the OFF state to the ON state	159
5.3.4	Transitions from the ON to the OFF state	161
5.4	Conduction in the ON state	163
5.4.1	Linearity	163
5.4.2	Memory	166
5.4.3	Temperature variation of ON state resistance	166
5.4.4	Frequency dependence of the ON state conduction process	169
5.4.5	Effect of optical stimulation on the ON state	170
5.5	Conduction in the OFF state	170
5.5.1	General description of the OFF state conduction	170
5.5.2	Possible conduction mechanisms and their associated current voltage characteristics	172
5.5.3	Results of the D.C. conduction experiments	175
5.5.4	Frequency dependence of the OFF state conductivity	189

Page

5.6	Thermally stimulated current (T.S.C.) measurements	189
5.6.1	The T.S.C. method	189
5.6.2	Results	192
Chapter 6	Theoretical discussion of conductivity switching	199
6.1	Review of previous work	199
6.2	Proposed band model for switching crystals	205
6.2.1	General description	205
6.2.2	Potential distribution in a device for zero applied voltage	208
6.2.3	Current conduction in devices in the ON state	216
6.2.4	Conduction in the OFF state	223
6.2.5	Origin of the positive charge	225
6.2.6	The forming process	230
6.2.7	The switch ON process	233
6.2.8	The switch OFF process	234
6.3	Discussion of the model and conclusion	239
References		242

CHAPTER I

Introduction

Zinc sulphide is a wide band gap semiconductor having a direct band gap of about 3.6eV[1a] at 300°K. Although originally classified as an ionic solid[2], its bonding is now thought to be at least partly covalent in character. Estimates vary from about 62% to 82% ionicity[1b].

It has long been known that ZnS is an electroluminescent compound[3] and a great deal of work has been done in the past on its luminescent properties. However, very little has been published on its conventional transport properties, partly because of the difficulty of growing suitable single crystals[1a]. The growth of satisfactory single crystals for experimental investigation therefore constituted a major part of this work. The assessment of crystal quality was a difficult problem, but optical methods (polarized light microscopy and transmission spectroscopy) were found to be the most useful techniques in this respect.

One of the problems with ZnS electroluminescent devices is their low efficiency. Typically, the energy conversion efficiency of an a.c. electroluminescent cell is about 5%[1c]. However, since the cell is a good capacitor, it draws a large quadrature current which dissipates power in the external circuit without contributing to the light output. The overall efficiency may thus be considerably lower than 5%. D.C. efficien[illegible] may be even lower than the a.c. efficiencies, mainly because

of the inability of contacts to inject carriers efficiently into the ZnS. Part of this work was therefore devoted to the investigation of the properties of certain contacts to ZnS single crystals in the hope that efficient carrier injection and d.c. electroluminescence might be achieved. It was of particular interest to investigate the possibilities of double carrier injection (the simultaneous injection of electrons and holes) since this is a means of maintaining space charge neutrality within the crystal even at high injection levels. Without space charge neutrality it is impossible to achieve efficient injection at high carrier densities since the space charge of the carriers themselves opposes the flow of current. Given the ability to achieve efficient carrier injection it might then be possible to produce population inversion and laser action in ZnS.

In the course of the investigation of contact properties a conductivity switching phenomenon was discovered which was similar to some of the switching phenomena recently reported in thin insulating films, (see, for instance, references 51 to 59). It was found possible to switch the conductivity of ZnS single crystals between two stable states, differing typically by six orders of magnitude, by the application of an electrical stimulus to two contacts attached to the crystal. The application of a high voltage caused the crystals to switch from a resistance state in excess of $10^{10}\Omega$ to one of the order of $10^{4}\Omega$. The high resistance state could

then be retrieved by the application of a short pulse of current between the same contacts as were used to switch on the device. At 77°K the low resistance state could be retained by the crystal for at least 24 hours without the need to supply any electrical bias to the contacts.

This type of conductivity switching device has many possible applications as a potentially cheap bistable element. Apart from its simplicity, it has the advantages of non-destructive readout, memory without power consumption and it is a two terminal device. One possible use might be in display panels where it is required to maintain the display pattern during a scanning period.

Being a single crystal device the ZnS switch provides a new and interesting addition to the range of conductivity switching devices so far reported, in that the amorphous nature of previous devices has not made theoretical interpretation any simpler. The switching effect was therefore investigated experimentally and a theory was developed to explain the experimental observations.

CHAPTER 2

CRYSTAL GROWTH

2.1 Introduction

A review of previous work on the growth of zinc sulphide crystals will be given in this chapter, followed by a description of the experimental techniques used in the present work. The results of the crystal growth experiments will then be presented and possible growth mechanisms will be discussed. The review of previous work is not intended to be an exhaustive one as its purpose is merely to indicate the present "state of the art" and to show why the method used here was chosen.

2.2 Previous work on the growth of zinc sulphide crystals

Most of the standard methods of crystal growth have been applied to the growth of zinc sulphide at some time or other. Allen & Crenshaw[4] (1912), described growth from a flux of molten sodium chloride but apparently little success was achieved with this class of crystal until after Frerichs[5] (1946) was successful in growing usable crystals of cadmium sulphide by reaction of cadmium vapour with hydrogen sulphide. Frerichs' success opened the way for others and at the same time the increasing interest in II - VI compounds as semiconductors created the necessary demand to act as a stimulus for the production of better crystals.

Zinc sulphide melts at a temperature of about 1830°C[6] and a minimum pressure of 3.7 atmospheres. However, in order to prevent material loss by sublimation, it is necessary to surround the zinc sulphide with an atmosphere of argon at about 80 atmospheres pressure. Growth from the pure melt, therefore, obviously presents serious technological problems. For this reason, most work has naturally concentrated on growth from the vapour phase.

2.2.1 Growth from the vapour phase

Zinc sulphide crystals can be grown from the vapour phase either by a forced convection technique, such as used by Frerichs[5] or else by a sealed tube method in which material is transported by virtue of a free energy difference between points at differing temperatures. The simplest case of the sealed tube approach is the sublimation of pure zinc sulphide at high temperature and its subsequent recrystallisation at a lower temperature in a closed, evacuated (or gas filled) tube. Transport in this case is achieved by the difference in free energy of evaporation of zinc sulphide at two points at different temperatures, which gives rise to a pressure differential between the two temperature zones. This system has been studied by Reynolds and Czyzak[7], Nishimura and Tanabe[8], Patek[9], Piper and Polich[10], and Samelson[11]. A useful modification of the closed tube method of growth is the transport of material by a chemical reaction whose equilibrium constant is temperature

dependent. A typical example of such a reaction is

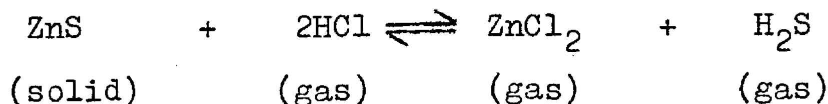

$$\underset{\text{(solid)}}{ZnS} + \underset{\text{(gas)}}{2HCl} \rightleftharpoons \underset{\text{(gas)}}{ZnCl_2} + \underset{\text{(gas)}}{H_2S}$$

where the free energy change forces the reaction to the left as the temperature decreases. The nett result is that ZnS is transported down the temperature gradient from a reservoir at the high temperature zone.

A general investigation of halogen transport reactions, with special reference to iodine transport has been undertaken by Nitsche[12] et al. and Jona and Mandel[13] have investigated parameters controlling the transport rate in the ZnS:I system. Samelson[14] and Patek[9] have described growth of zinc sulphide crystals in a hydrogen chloride atmosphere.

Chemical transport reactions offer much greater control over material transport rates than is possible in the pure system, and they also allow the range of temperatures at which crystals can be grown to be greatly extended. This enabled Samelson[14], for example, to grow zinc sulphide at a low enough temperature to produce structurally pure cubic crystals. The main disadvantage of halogen transport is the rather large amount of transporting agent included in the crystals. Samelson[14] found his crystals contained between 200 and 600

parts per million (p.p.m.) of chlorine and Nitsche found the iodine content of his crystals to be of the order of 100 p.p.m. by weight. Since the halogens are often required as dopants in II - VI compounds these concentrations may not always be undesirable, but in any attempt to produce pure crystals this sort of impurity level is prohibitive.

The sealed tube method of growth as applied to the pure zinc sulphide system removes the objection of halogen doping but increases the difficulty of control of crystal growth. Indeed Patek[9] believed that it was impossible to grow zinc sulphide crystals unless at least 20 p.p.m. of chlorine was present. Early attempts (e.g. Reynolds and Czyzak[7]) were unsuccessful when the growing tube was evacuated and H_2S atmosphere was generally recognised to give the most controllable and reproducible results (see Patek[9] and Samelson[11]). One objection to the use of a vacuum was the limitation that it placed on the maximum operating temperature due to the softening and collapse of the silica growing tubes.

Inert gas atmospheres, helium and argon, were also tried in order to prevent collapse of the silica tube but Patek[9] found that these atmospheres drastically reduced the crystal growth rate and also led to a certain amount of segregation of zinc and sulphur. Greene[15] et al. however, had already grown large crystals of ZnS in an argon atmosphere using a quartz seed plate arrangement. They were able to achieve temperatures of up to 1600°C in their silica tubes by enclosing them in an

outer mullite tube to provide a rigid structure. Crystal growth took place at 1475°C to 1500°C. By the use of higher temperatures Greene[15] et al. were, therefore, able to overcome the effect argon has in reducing the rate of crystal growth.

Piper and Polich[10] introduced two modifications to the method used by Greene[15] et al. They used a **silica** tube with a pointed end to act as a nucleation point for the zinc sulphide instead of the quartz seed plate. One nucleus usually dominates in this arrangement and eventually leads to a single crystal filling the growing tube. Secondly, they arranged to pull the whole growing tube through an inverted V-shaped temperature profile. The charge was on one side of the temperature maximum and the growing zone on the other. As the pulling progressed the charge increased in temperature and the growing zone decreased in temperature. Material was thus made to pass from the charge to the growing zone and be deposited there as a crystal growing in the opposite direction to that in which the tube was being pulled. In this way the growing face of the crystal maintained itself at a roughly constant temperature throughout a run.

The methods of Greene[15] and Piper and Polich[10] are useful for the production of large volume single crystals whereas the methods of Patek[9] and Samelson[11] are useful where many small plate and needle type crystals are required.

The forced convection vapour growth techniques depend on a flow of transporter gas to assist material transport from an evaporation zone to a crystallization zone. The gas may, or may not, take part chemically in the crystal growth process. The method of Frerichs[5] used hydrogen sulphide to transport sulphur to the crystallization zone in a chemically combined form. This method was modified by Bishop and Liebson[16] who used argon to transport zinc and sulphur vapours separately to the crystallization zone. In these methods the evaporation zone temperatures were both lower than the crystallization zone temperature.

Kremheller[17] evaporated zinc sulphide powder as a source material and used an inert gas to transport the vapour to the crystallization zone which was at a lower temperature than the evaporation zone. He used a U-shaped quartz rod on which to nucleate crystals instead of depending on the walls of the growing tube to provide nucleation sites. His finding was that it became increasingly difficult to grow crystals as successive runs were carried out. However, the use of a new quartz nucleation rod, or the addition of a little zinc oxide or copper to the charge seemed to stimulate growth again. He correlated these findings with the increasing purity of zinc sulphide crystals obtained with successive runs and concluded that it was very difficult (if not impossible) to grow chemically pure single crystal zinc sulphide by this means. He therefore devised a means of

purifying contaminated crystals after growth. This method seems rather unsatisfactory, however, when one is aiming at the highest purity.

Fochs[18] has described a method in which both cadmium sulphide and zinc sulphide were successfully grown in a silica tube with or without gas flow. The essential part of his experiment was the control of nucleation on the silica so that only a few nuclei were allowed to develop. It is this method which is used in the present work.

Two papers have recently been published by Dev[19] and Caveney[20] in which similar crystal growth techniques using the flow method are reported. As far as can be judged, however, the crystals obtained were in both cases inferior to those obtained here.

2.2.2 Growth from solution

Little work seems to have been done on growth from solution. Allen and Crenshaw's[4] work has already been mentioned. Gilman[21a] mentions some unpublished work by Linares who used 79% zinc fluoride flux with 21% zinc sulphide and grew crystals by slow cooling at between 1 and 5°C/hr. from 1000°C to 800°C. Cubic zinc sulphide was grown, but no other details are given. Gilman[21b] also refers to work done by Laudise and Ballman on the hydrothermal growth of zinc sulphide from NaOH solution. Little information about crystals of zinc sulphide grown by this method seems to have been given. White[22] has suggested

that $(NH_4)_2S$ or H_2S might be suitable hydrothermal solvents for the growth of zinc sulphide, but no information has been found regarding experimental attempts in this direction.

Growth from liquid gallium solution is reported by Bertoti[23] et al. Both cubic ribbons and plates and hexagonal needles were obtained by dendritic growth. The photographs of the crystals shown indicate that they would not be readily adaptable for optical or electrical work as they have a very disordered and uneven morphology.

2.2.3 Growth from the pure melt

Despite the technological difficulties involved in melting zinc sulphide this method has been used successfully. Addamiano[24] was able to grow pure hexagonal zinc sulphide crystals by controlled cooling of the melt in an atmosphere of argon. These crystals were rods ½ cm. diameter by 2 or 3 cm. long. Regular shaped crystals up to 5 x 5 x 1.5 mm could be cut from the rods. The density of these crystals was found to be greater than that of vapour grown crystals and was in fact, equal, within experimental error, to the theoretical density calculated from the wurtzite cell dimensions. The molten zinc sulphide was cooled from the bottom upwards and this resulted in a segregation of impurities such that the bottom of the rod was silicon rich and the top of the rod was copper rich. The middle portion of the rod was found to be spectroscopically pure. However, the analysis makes no mention of chlorine or oxygen. It was found that the phase

transition wurtzite to sphalerite was very difficult to induce in these crystals and no conversion was observed even after 500-hr. heating at 975°C.

Ebina and Takahashi[25] have investigated the structure of some melt grown crystals and compared the results with the structures of vapour grown and natural crystals. Some of the crystals investigated by them were grown by Addamiano. They claim that all the melt grown crystals were cubic with a considerable amount of stacking disorder. They suppose that stacking faults in these crystals separate regions of twin orientation and they calculate the distance between faults to be 21Å to 24Å, showing the twinning to be of short range. In contrast the natural crystals were pure cubic with no twinning and the vapour phase grown crystals were pure hexagonal showing low fault densities.

Recently Kukimoto[26] et al. have described a furnace for the growth of zinc sulphide from the melt by the Bridgman method. Temperatures up to 2500°C at argon pressures up to 120 atmospheres could "easily" be obtained. Pulling rates were usually 20 - 30 mm/hr. and temperature and argon pressure were usually 2000°C and 80 atmospheres respectively. Crystals 50mm long and 12mm diameter were produced. X-ray oscillation photographs indicated that the crystal structure was a modified cubic form with various stacking disorders.

2.3 Choice of method of crystal growth

The requirement of the present work was for chemically and structurally pure crystals with a large ratio of surface area to thickness, i.e. thin plates. Surfaces were required to be optically smooth and without mechanical damage. The best surface was therefore one which could be used in the "as grown" condition rather than one obtained by cutting and polishing. The logical choice of crystal growth method was therefore a vapour phase technique. A pure system was desirable in order to obtain the required crystal purity, although past work had tended to show that it was more difficult to grow good crystals in pure systems.

The argon transport technique of Fochs[18] was chosen since it offered the advantages of short crystal growth runs (2 to 4 hours as compared with 48 hours to 10 days for the pure, sealed tube system) and easy control of growth conditions via the gas flow rate and temperature gradient. There was also the possibility that beneficial segregation of impurities could occur during growth.

2.4 The apparatus for crystal growth

2.4.1. The furnace

The furnace used for crystal growth was a two zone

(a) Side view

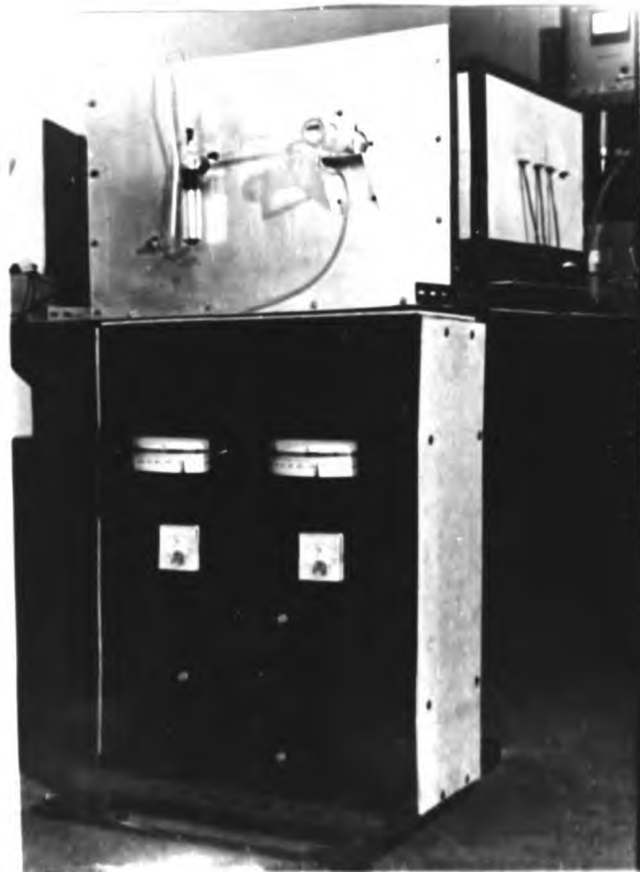

(b) Front view

Figure 2.1 Furnace used in crystal growing

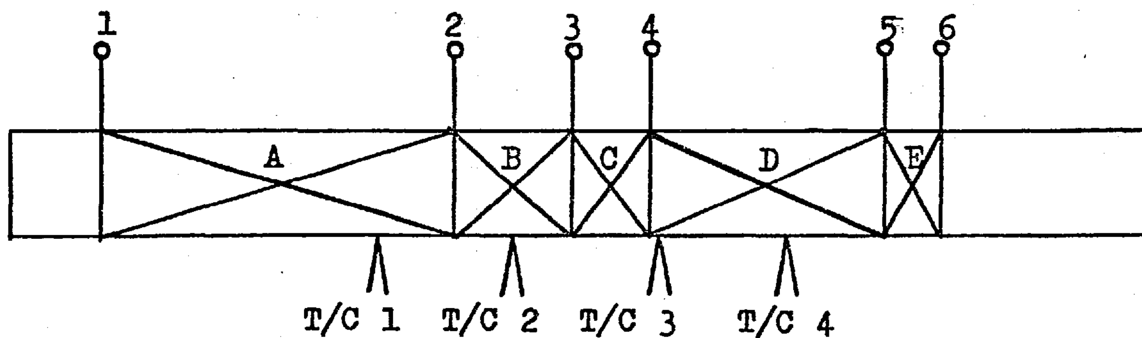

Windings

A.	Cool zone	58 turns	23.5 cm
B.	Cool zone	19 turns	7.6 cm
C.	Hot zone	16 turns	5.1 cm
D.	Hot zone	50 turns	14.9 cm
E.	Guard zone	18 turns	4.1 cm

Terminals

1. Cool zone supply
2. Cool zone tap
3. Centre tap
4. Hot zone tap
5. Hot zone supply
6. Guard zone supply

Figure 2.2 Diagram of the furnace windings

Scale: 1/5 full size

muffle furnace capable of operating up to temperatures of 1500°C. Two views of it are shown in the photograph of figure 2.1. The winding consisted of 161 turns of 0.8 mm diameter platinum/10% rhodium wire wound on a 7 cm O.D. Morgan sintered alumina tube. The total winding length was 55.2 cm and the total tube length 75 cm. A non-uniform winding density was used in order to create the desired temperature profile. Figure 2.2 shows the layout of the furnace windings on the tube. The whole winding was encased in a layer of high purity alumina cement (Morgan 961) in order to hold the platinum wire in place and protect it from the air.

Four platinum/platinum-rhodium thermocouples were embedded in the alumina cement in the positions shown in figure 2.2. The whole winding assembly was then laid in a U-shaped groove cut in a line of furnace bricks and another layer of furnace bricks was placed over the top of it. The winding terminations and thermocouple leads were brought out between the furnace bricks. Vermiculite insulation was used to fill the two inch gap between the furnace bricks and the outer furnace case.

The whole furnace was mounted on wheels so that it could

be moved easily into position for crystal growing when required.

Power was fed to each winding separately from a twin track 4.2 kVA variac. Temperature control was achieved by using two Ether Transitrol type 991 anticipatory controllers fed from two of the four thermocouples attached to the furnace windings, to control the power input to the hot and cool zone windings respectively. The control relay contacts were shunted with resistors so that, under normal working conditions, the power actually being controlled was only about one third of the total input power to the windings. This allowed the short term temperature variations in the furnace to be kept to within $\pm$ 1°C as measured under crystal growing conditions.

Figure 2.3 shows a set of temperature profiles for the furnace taken inside the silica crystal growing tube for various settings of the hot and cool zone controllers. The control thermocouples were always numbers 1 and 3. Number 2 thermocouple was often used as a monitor and its output was fed to a chart recorder. It was found that the presence of the silica growing tube significantly affected the temperature profile and therefore all measurements were made with one in

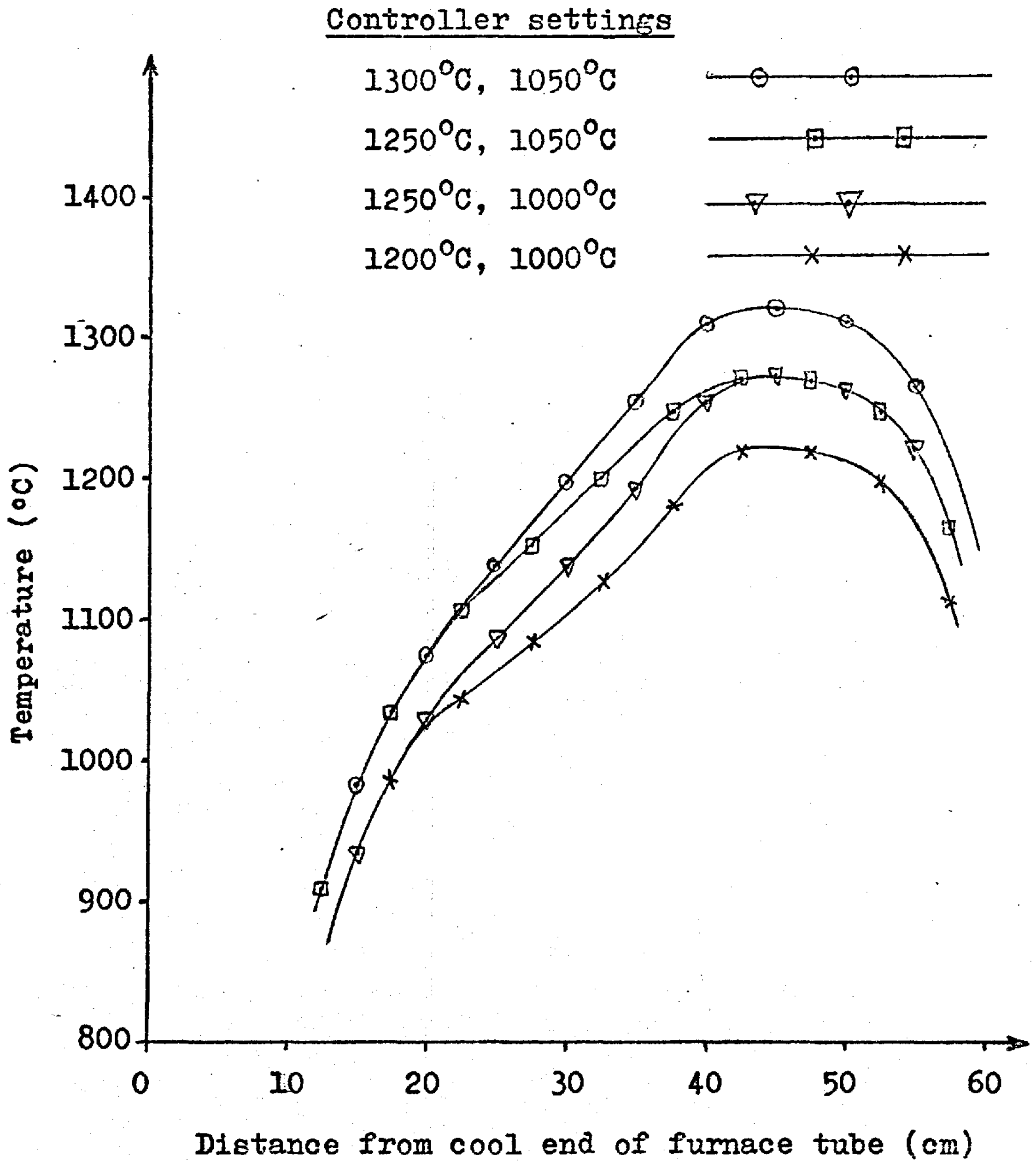

Figure 2.3 Temperature profiles of the furnace

position. The argon flow rates normally used in crystal growing (up to 850 cc per minute) however, had no measurable effect on the profile.

2.4.2 Crystal growing tube

The crystal growing tubes used were constructed out of transparent silica tubing and were in the shape of U-tubes with arms of unequal bore. A drawing of such a tube is shown in figure 2.4. The small tube had a bore of about 0.5 cm. whilst the larger tube bore was 3.5 cm. A B50 ground silica socket was joined to the open end of the larger tube and a B7 silica cone terminated the smaller tube. The usual overall length of the growing tube was about 30 inches but this was not critical.

The principle of operation was that argon entered the system in the small bore tube, passed over a zinc sulphide charge at the closed end of the large tube, picking up zinc sulphide vapour as it did so, and then continued down the large tube to a cooler zone where it deposited the zinc sulphide in the form of crystals. The argon was then exhausted at the end of the large tube which was usually terminated with a B50 glass cone with an optical viewing window as shown in figure 2.4

One of the main reasons for using a U-tube arrangement as opposed to a double-ended straight through arrangement was that the growing tube could be completely removed from the furnace without the need to disconnect either the gas input or the exhaust system. This allowed one to maintain a completely

Key.

1. Plate glass viewing window.
2. Silicone rubber support.
3. B7 gas inlet cone.
4. B10 exhaust socket.
5. B50 glass cone.
6. B50 silica socket.
7. Main growing tube.

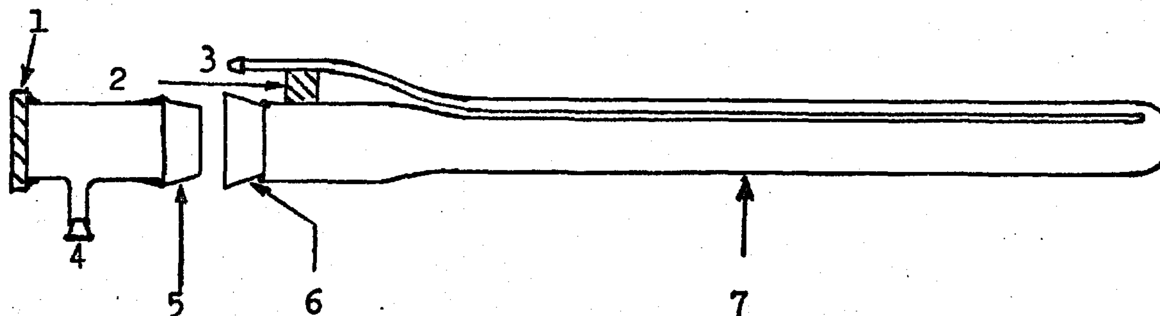

Figure 2.4 The silica crystal growing tube.

(not to scale)

pure system while at the same time being able to quench the grown crystals very rapidly. Also the furnace could be maintained at the growing temperature if another run was required rapidly.

Another reason for using the U-tube system was that the incoming argon gas was warmed before entering the main growing tube. This lessened any disturbing effect it might otherwise have had on the stability of the temperature in the growing tube.

2.4.3. The argon gas supply

From a study of manufacturers data it was concluded that Air Products High Purity Argon was the best gas supply available. Table 2.1 is a reproduction of the specification of this gas. In addition to this specification it was made a condition of purchase that every cylinder be labelled with its oxygen content in p.p.m. and its dew point, so that any possible correlation between crystal growth and gas impurity might be made. In fact none was observed. It can be seen from Table 2.1 that the most significant impurity was nitrogen. As far as is known, however, nitrogen acts as an inert gas in relation to zinc sulphide and may therefore be discounted as an impurity. Thus, discounting nitrogen, the total active impurity level of the argon was typically less than 10 p.p.m. by volume and probably much less than this since 7 p.p.m. of the impurities counted were on or below their limits of detection. A deoxidizing tube filled with titanium granules heated to 700°C was built into the gas supply system but no difference was

TABLE 2.1

INDUSTRIAL GAS SPECIFICATION

GASEOUS ARGON : HIGH PURITY

Analysis	Guarantee ppm by volume	Typical ppm by volume
Oxygen	less than 3	2
Nitrogen	less than 10	6 - 9
Moisture	less than 1	less than 1

Note: 1ppm moisture is equivalent to a dewpoint of -105°F

TRACE CONTAMINANTS

Analysis	Typical ppm by volume
Carbon Dioxide	less than 0.5*
Carbon Monoxide	less than 1.0*
Hydrogen	less than 5*
Nitrous Oxide	less than 0.1*
Total Hydrocarbons	1.0*
Methane	0.5*
Acetylene	less than 0.05*

* Minimum detectability by the methods used.

observed in the growth of the crystals.

One of the advantages of having the furnace on wheels was that the crystal growing tube could be fixed rigidly in position and the furnace moved up to it instead of the usual procedure where the furnace is fixed and the growing tube is mobile. This allowed all gas input tubes to be rigid and they could therefore be made of glass. There was no need to use flexible plastic tubing or flexible joints, both of which can allow oxygen to diffuse into the system. All joints on the input side of the furnace were ground glass and sealed with picene black wax.

The argon flow rate was measured on a Fischer and Porter flow meter graduated 0 to 13 in equal divisions. A calibration experiment revealed that the scale was linear in terms of volume flow rate registering 65cc/minute per division.

Control of the flow of argon was achieved with an Edwards type OS1D needle valve placed before the flow gauge. An argon pressure of 15 p.s.i.g. was maintained behind the needle valve. The result was a very stable flow without any noticeable spurious fluctuations.

2.4.4 Material handling

All the handling and weighing of the zinc sulphide starting material and of the sintered charges was done in the glove box shown in figure 2.5. This glove box was filled with dry nitrogen from an Air Products cylinder when in use and was continuously dried at all times with silica gel kept in open

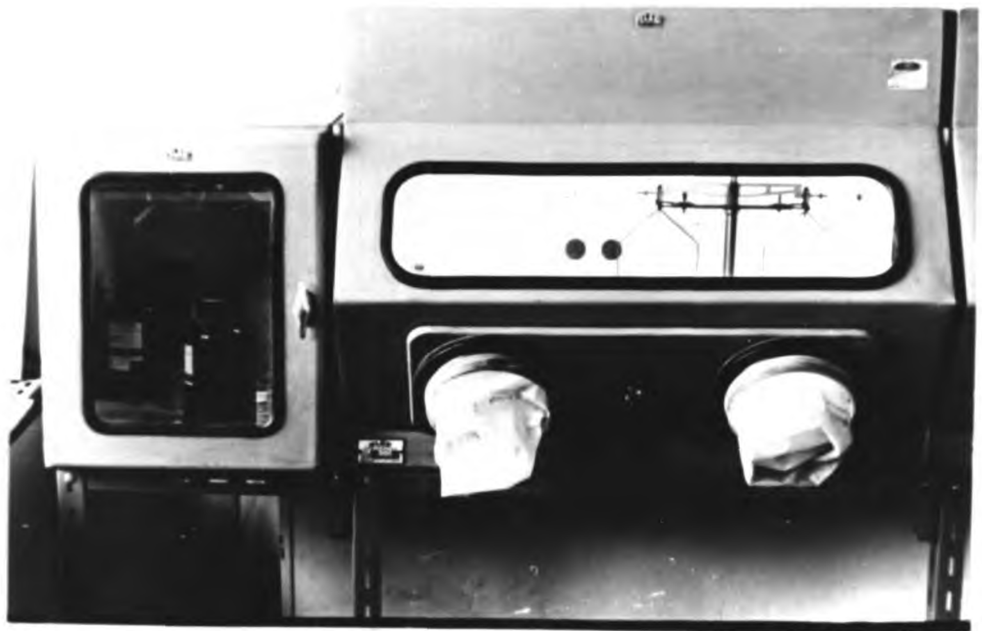

Figure 2.5 The glove box used for material handling

beakers inside it. After a thorough initial cleaning the box was used solely for the handling of zinc sulphide for a period of two years. No other materials were introduced, other than tools and containers, which could contaminate the zinc sulphide. The box was equipped with an air lock input port so that there was no direct entry to the inner compartment from outside. All containers and tools which were taken into the glove box were cleaned beforehand. All charge material taken into or out of the glove box was handled inside a pyrex ampule made out of a B35 cone and socket whose plain ends had been sealed off. It was felt that, in the absence of a clean room, these were the best precautions that could be taken against contamination of the starting material.

2.5. Crystal growth procedure

2.5.1. Preparation of the crystal growing tube

The factor most important to the growth of the required crystals was the control of nucleation sites on the walls of the silica growing tube. This control was achieved by taking great care with the preparation of the tube before a crystal growth run.

A mixture of concentrated hydrochloric and nitric acids, in the ratio 1:1, was used for the initial cleaning of a tube after a previous run. The tube was then well rinsed in de-ionized water and given a half-hour etch (both inside and

outside) in the following mixture:-

250 ml AnalaR hydrofluoric acid

200 ml AnalaR nitric acid

100 ml de-ionized water.

This etch removed the surface of the silica tube and with it any embedded impurities. After etching the tube was again thoroughly rinsed in de-ionized water and dried by warming whilst passing a stream of pure argon through it.

Once etched the tube had to be flame polished in order to smooth the surface of the silica and thereby reduce the number of nucleation sites for crystal growth. This was a very critical step and demanded great care. In order to ensure that the inner surface of the tube was smooth, it was necessary to thoroughly melt the silica wall a little at a time, working round in a spiral fashion until the whole tube had been polished. During flame polishing a stream of pure argon was kept flowing through the tube in order to prevent contamination and to provide a means of counteracting the pressure of the oxy-hydrogen flame used for polishing.

2.5.2. Starting material

Zinc sulphide starting material was obtained from:-

1. Levy West & Co., Ltd.,
   Harlow,
   Essex.
2. British Drug Houses Ltd.,(BDH)
   Poole,
   Dorset.
3. E. Merck A.G.,
   Darmstadt,
   Germany.

The Levy West material was in powder form, the BDH material in microcrystalline form, and the Merck material sintered into 1 g tablets. All materials were nominally chlorine free. The chemical analyses of these materials are given in Chapter 3.

2.5.3. Charge sintering

All the various charge materials used for crystal growth required sintering before use in order to remove adsorbed gases and to crystallize the charge surface so as to obtain a controlled evaporation rate. For convenience charges were sintered in silica test tube moulds about 2 cm diameter and 7 cm long which could hold approximately 35 g of ZnS.

The sintering was done in a flow of pure argon at various temperatures ranging from 900°C to 1250°C and an old crystal growing tube was used for the purpose. Apart from preventing gradual changes in the evaporation rate during crystal growth, charge sintering also had the effect of distilling off any voltile impurities from the charge including any free zinc and sulphur which might have been present. This distillation process was particularly in evidence with one batch of material which was later found to contain 3700 p.p.m. chlorine. In that case zinc chloride was clearly visible as a transparent condensate in the cooler parts of the sinter tube soon after sintering began.

Yet another advantage of sintering was the greater ease

with which sintered charges could be handled compared with powder charges.

2.5.4 Growing the crystals

The furnace was always brought up to temperature and allowed to remain at its control points for at least two hours before the beginning of a run. This allowed the furnace insulation to achieve thermal equilibrium with the element which in turn ensured that short term temperature stability was within the limits of $\pm 1°C$ as previously stated.

Meanwhile the crystal growing tube was prepared and fixed in position and the argon gas flow started. The initial gas flow rate was always much higher than that used for crystal growing in order to thoroughly flush out the system. The charge was placed in the correct position in the U-tube using a long silica spoon. Another method of getting the charge to its correct position in the growing tube is to place the charge just inside the entrance to the tube and then to tip the whole assembly. This has the advantage of allowing the growing tube to be brought to the correct temperature in the furnace before charge evaporation begins, since one can tilt furnace and tube together. This was, in fact, tried at one stage, but it was found that the zinc sulphide charge always left behind it a trail of powder along the bottom of the tube, which defeated the object of the flame polishing by providing a new set of dense nucleation sites. The spoon method of inserting the charge was therefore chosen. Having inserted the charge, the

growing tube was closed with the B50 glass cone with the viewing window (figure 2.4) and the exhaust tube was fixed in position. The system was allowed to flush out for a further half-hour at the high gas flow rate after which the flow was reduced to that required for the run. The furnace was then wheeled into position around the silica tube and the crystal growing run had commenced. During crystal growing runs a flow of dry nitrogen ($\frac{1}{2}$ litre/min.) was maintained through the furnace tube to act as a blanket for the silica tube against oxygen. By so reducing the oxygen concentration around the silica tube it was hoped equally to reduce the diffusion of oxygen through the walls of the tube into the crystal growing zone. This flow did not measurably alter the temperature profile in the region of interest.

The insertion of the cold silica tube into the furnace tended to upset the temperature stability of the furnace temporarily. However, control was usually re-established within two or three minutes of inserting the tube, after which the normal stability of temperature in the furnace was maintained. This temporary departure from stability did not seem to matter since the large mass of zinc sulphide charge was always much slower to warm up than the silica tube and hence evaporation did not take place until stable conditions were re-established. A crystal growth run usually lasted two to four hours although some runs were performed for much shorter and much longer times. At the end of the run, the furnace was

wheeled away from the silica growing tube which was allowed to cool naturally in the air until it was at least cool enough to touch with the hand. This made sure that the crystals were quenched and retained their "as grown" structure. Before removal of the crystals a note was made of the positions of the various crystallization zones as appropriate. The crystals were then removed and sorted and the charge returned to the glove box for weighing. It was unfortunate that the glove box was not big enough to allow the crystals to be extracted inside it. However, sorting was done inside the box and the crystals were put into petri dishes inside vaccum desiccators for storage. The desiccators contained silica gel drying agent.

2.6 Results

A total of 86 crystal growing runs was performed in which the effects of varying the growth conditions were studied.

The growth sequence after the start of a run followed a consistent pattern. During the first three or four minutes nothing happened owing to the delay while the charge was heating up. Then a very thin haze appeared in the tube in front of the charge (when viewed from the cool end of the tube). This signified that evaporation had begun. The next stage was dependent upon the prevailing growth conditions. Either thin whiskers would appear very rapidly, growing radially inwards from the walls of the tube or else there would be no whiskers but simply a gradual increase in nucleation followed by slow growth from some or all of the nuclei. In extreme cases

nucleation would take place over the whole tube surface producing a polycrystalline deposit. This was invariably the result of neglecting the flame polishing of the tube.

The final stage of growth was either the broadening of the fine whiskers into thin ribbons, plates or butterfly twins, or else the slow growth of thicker rods and plates from the nuclei established on the **wall of the** tube.

2.6.1 Description of the crystals

During the course of investigations, eight different forms of crystalline deposit were encountered. They were:

(i) Polycrystalline substrate covering the whole tube surface.

(ii) Chunky three dimensional crystals like grains of sugar.

(iii) Clusters of short rods.

(iv) Slow-growing plates.

(v) Whiskers and fine needles.

(vi) Ribbons.

(vii) Butterfly twins.

(viii) Fast-growing plates.

As mentioned previously the polycrystalline substrate was always the result of the lack of flame polishing.

The three dimensional crystals were rather an exception. It was later found that they were only produced when the Levy West material with the exceptionally high chlorine content was used. When such crystals grew it was always totally impossible

to grow any needle or plate type crystals at the same time. The production of three dimensional crystals was therefore attributed to the presence of excess chlorine which was thought to promote growth in normally unfavourable crystallographic directions.

The clusters of short rods were found to grow from small polycrystalline areas at separated points on the walls of the tube. The rods were of the order of 100 to 500 microns across and 1 to 10 mm. long.

Slow growing plates usually grew from the clusters of short rods, giving the impression that these plates had grown by a slow broadening of the rods. The surfaces of these plates were rough giving a heavily striated appearance. There were also other striations perpendicular to the roughness ones. Typical thicknesses were in the range 100 to 500 microns and areas were of the order of a square centimetre.

The growth of whiskers has already been described. These very fast growing crystals were estimated to be about 4 microns in diameter. When a large number of these whiskers was produced in a particular run they had a tendency not to develop into plates but rather to thicken only slightly into fine needles. These needles were of the order of 10 microns in diameter and could be up to 9 cm. long, though they were more usually 2 or 3 cm. long. They could be bent through 360° or more without fracture.

Ribbons, butterfly twins and fast-growing plates were all observed to develop from whiskers by a process of broadening.

The thickness of these crystals was generally between 2 and 20 microns. Ribbons were a fraction of a millimetre wide and usually 2 or 3 cm. long. The areas of the butterfly twins and fast-growing plates depended on their state of development, but lengths of 1 to 2 cms. were common and breadths of up to 8 mm. were obtained. Ribbons were generally produced when the original density of whiskers was fairly high. Butterfly twins and fast-growing plates, on the other hand, were produced when the spacing between whiskers was much greater. No criterion could be found, however, to determine which of these latter two habits was the more likely to grow.

Ribbons, butterfly twins and fast-growing plates were characterised by their flat surfaces and their very low striation densities. Some crystals had areas as large as $\frac{1}{2}cm^2$. with no striations visible to the naked eye. All were totally transparent to visible light showing no colouration whatsoever.

Figure 2.6 illustrates some of the crystals which have been grown. Although the aim in this case was to grow smooth, unstriated plate crystals, several different types of crystal are shown in figure 2.6 for comparison.

An interesting feature of ribbons and fast-growing plates, as well as some of the slow-growing plates, was that most (if not all) had one straight edge and one ragged one. The inference to be drawn is that the crystals grew only in the direction of the ragged edge, the straight edge being defined

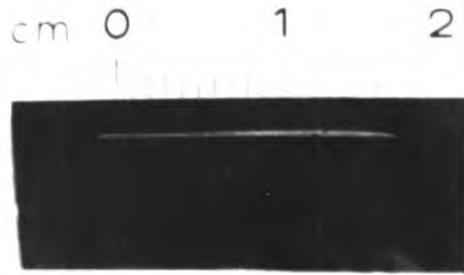

(a)

Butterfly twin in early stages of development

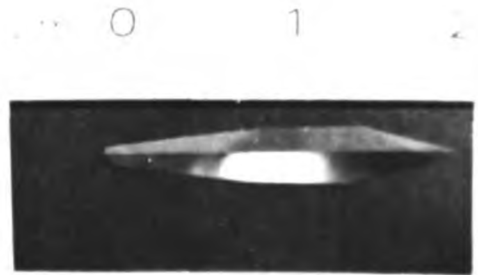

(b)

Butterfly twin in well developed form

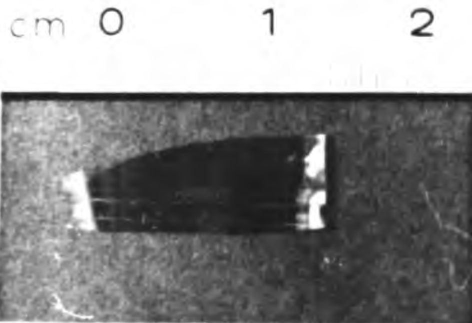

(c)

Fast-grown plate

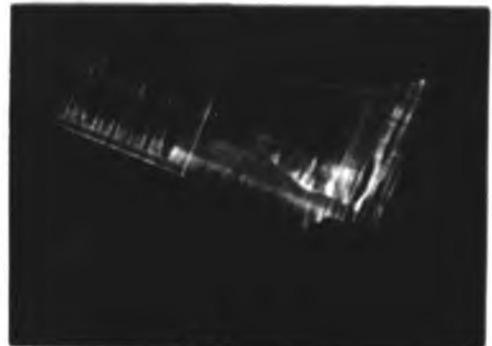

(d)

Slow-grown plate

(e)

Fine needle

Figure 2.6 Selection of some of the ZnS crystals grown.

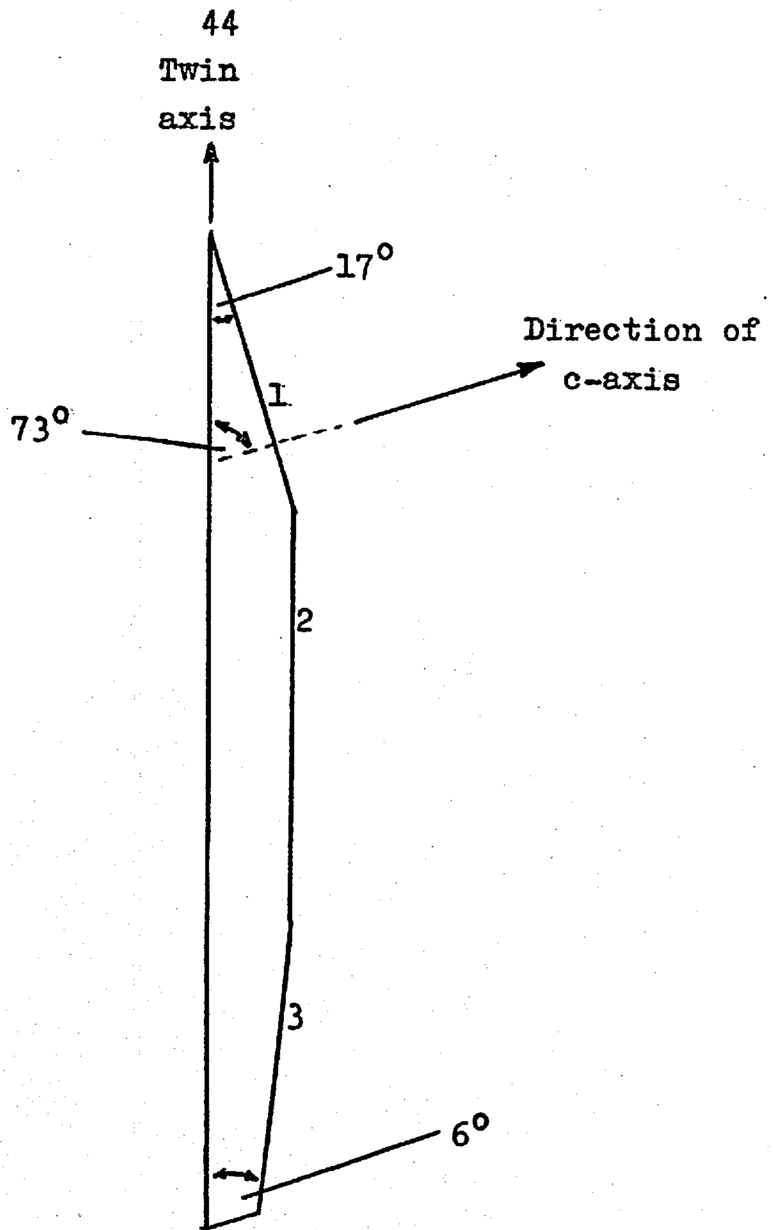

Figure 2.7 Drawing of one face of a butterfly twin.

by the original whisker with little or no growth in that direction.

Butterfly twins had a dihedral angle between their two faces of 120°. Figure 2.7 is a diagram of one face of the large butterfly twin shown in figure 2.6. The crystal face is bounded by three different edges whose inclination to the twin axis is shown. Edge 1 is at about 17° to the twin axis and is exhibited by all butterfly twins. It is the edge at the tip of the twin furthest from the wall of the tube. The c-axis of the twins examined was perpendicular to this edge, lying in the plane of the twin face. It was therefore at about 73° to the twin axis. Edge 1 was probably a fully developed edge. Edge 2 was made up of many short lengths of apparently randomly oriented edges. It was roughly parallel to the twin axis. Edge 3 was straight and at about 6° to the twin axis. It therefore did not correspond to a low index plane and probably would disappear, together with edge 2 in a fully developed crystal.

2.6.2 Orientation

Orientation was done by the Laué X-ray transmission method. Practical details are given in Chapter 3.

The major faces of the slow-growing plates were found to be either (10.0) or (12.0), whereas the major faces of the fast-growing plates, ribbons and butterfly twins were (11.0) only. (All indexing is referred to hexagonal axes).

The surface roughness striations on the slow-growing plates were found to be parallel to the c-axis.

All needles examined had the c-axis as the axis of the needle.

2.6.3 Effect of growth conditions on crystalline yield

The effect of flame polishing the growing tube has already been discussed. This section deals with the variation of crystalline yield with changes in the gas flow rate, temperature, temperature gradient and charge size.

The crystalline yield was assessed by visual inspection of the density of outgrowth from the walls of the growing tube. This eliminated polycrystalline substrates from the discussion. A figure of merit between 1 and 10 was assigned to each run according to the density of outgrowth produced.

In order to ascertain whether there was any correlation between the yield and the growth parameters listed above, the yield was plotted in turn against these parameters as variables in figures 2.8 to 2.11 inclusive. The graphs show no correlation at all between yield and either evaporation temperature or temperature gradient. A slight trend can be seen in figure 2.10 showing that the yield tended to increase as the argon flow rate decreased, but the correlation was none too convincing.

Figure 2.11 is a graph of yield against $\frac{F}{\dot{m}_{ZnS}}$. "F" is the argon flow rate as measured in divisions on the flow meter and $\dot{m}_{ZnS}$ is the mass evaporation rate of zinc sulphide from the charge in g/hr. It will be shown later (equation 2.37) that $\dot{m}_{ZnS}$ is functionally related to gas flow rate, evaporation

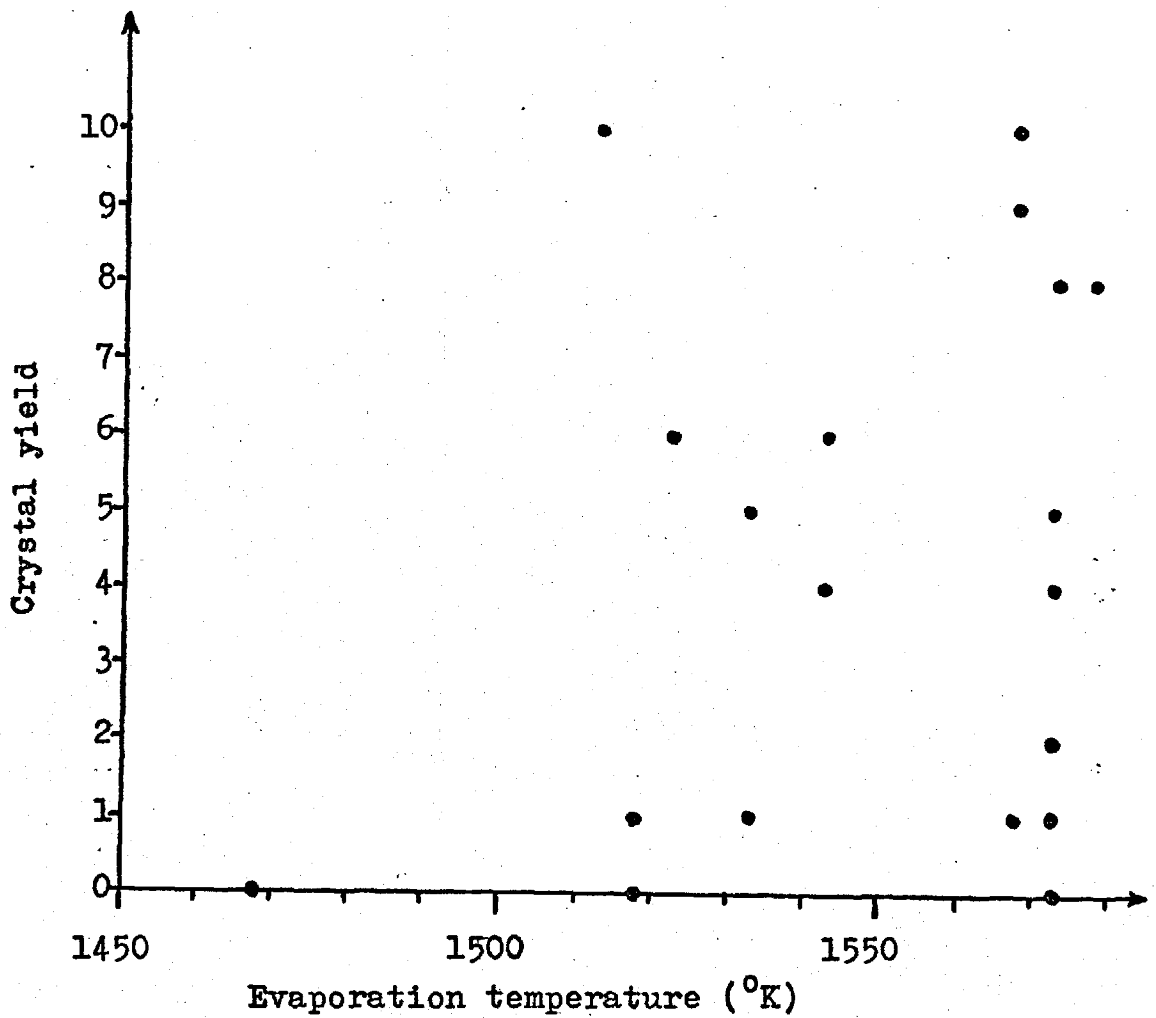

Figure 2.8 Crystal yield versus evaporation temperature

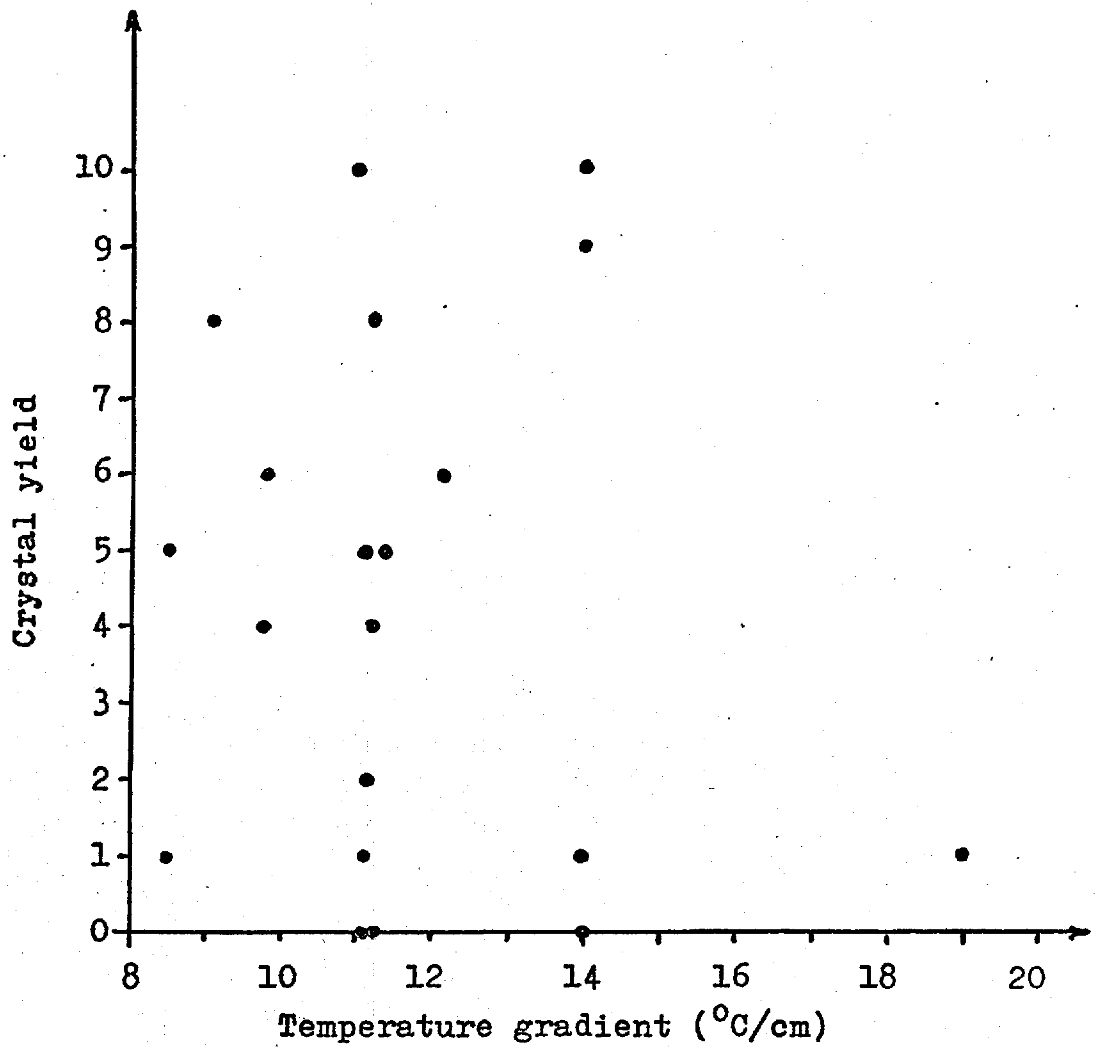

Figure 2.9 Crystal yield versus temperature gradient

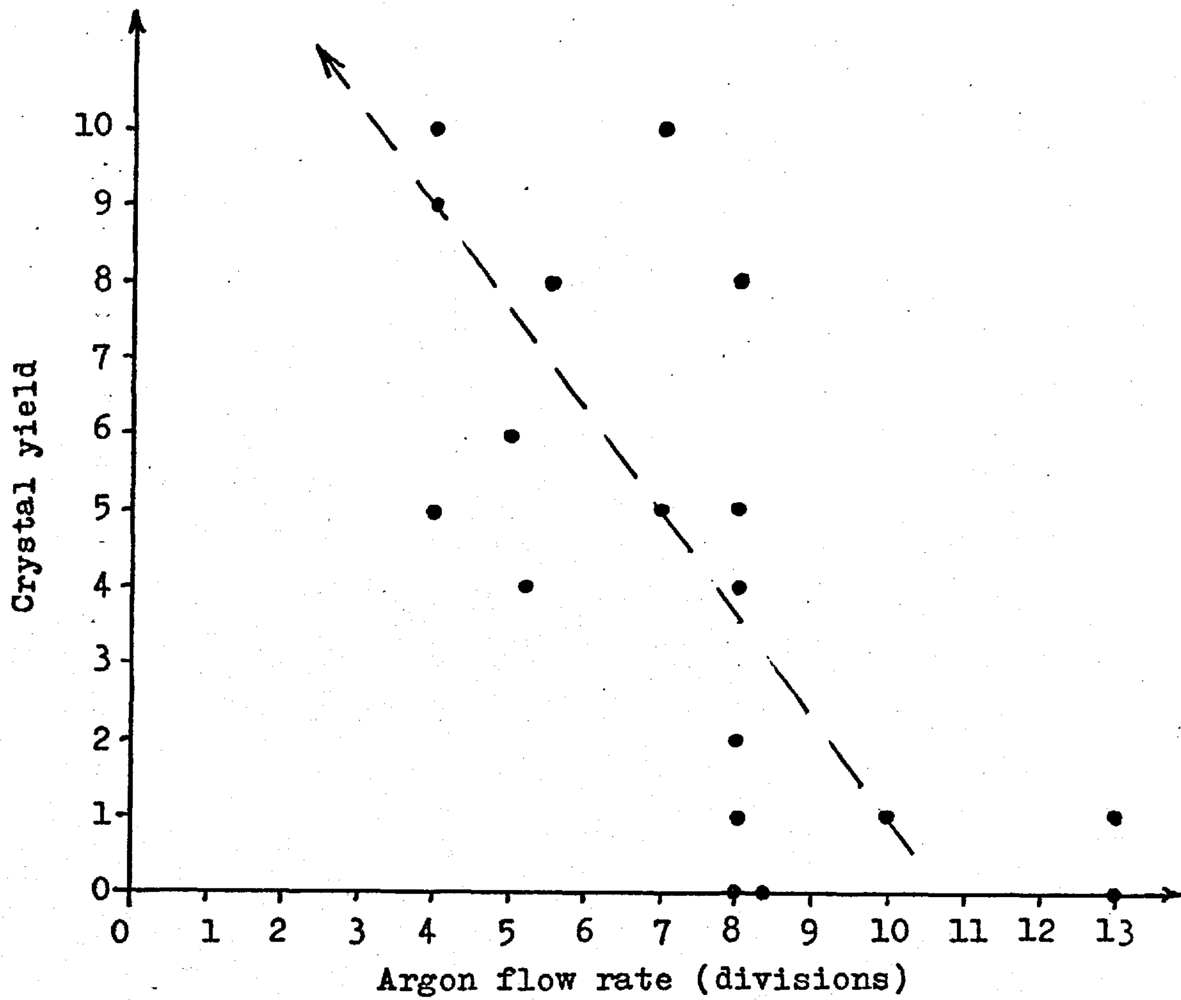

Figure 2.10 Crystal yield versus argon flow rate.

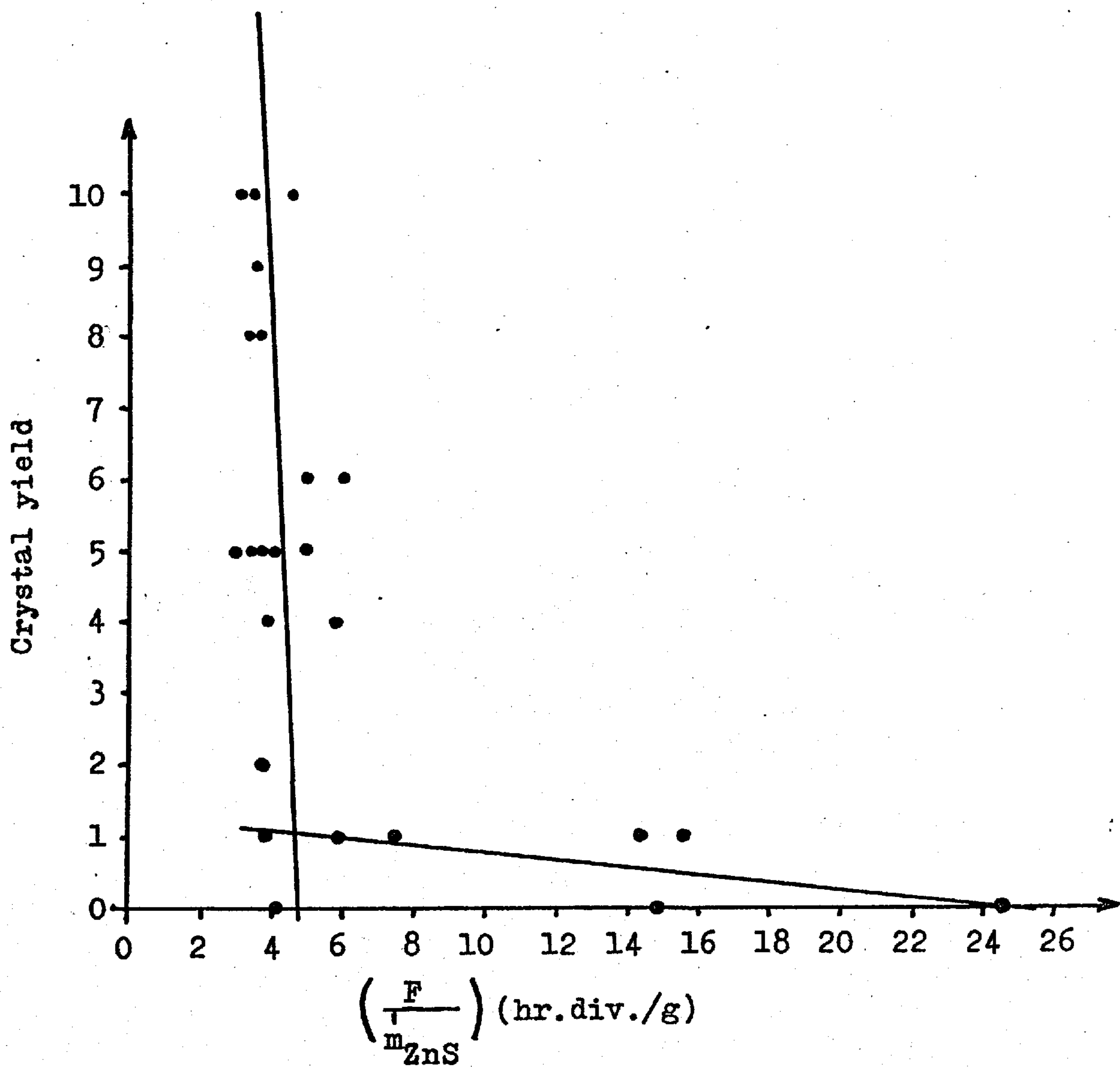

Figure 2.11 **Crystal yield versus** $\left(\frac{F}{m_{ZnS}}\right)$

temperature, and charge size. Thus, figure 2.11 is effectively the relation between all these parameters and the yield. There is an obvious correlation in that a critical value of $\frac{F}{\dot{m}_{ZnS}}$ exists below which the yield rises very sharply. An exact evaluation of this critical point is not possible owing to the scatter of the data, however, a good estimate would be that $\frac{F}{\dot{m}_{ZnS}}$ is between 4 and 5 at the critical point. Now $\frac{F}{\dot{m}_{ZnS}}$ represents the volume of argon, as measured at room temperature, containing unit mass of zinc sulphide. In other words, it is proportional to the reciprocal of the molar concentration of zinc sulphide in the argon carrier gas. There exists, therefore, a critical concentration of zinc sulphide below which single crystal growth is very unlikely to occur. This point will be dealt with again in the theoretical section on crystal growth.

One further observation may be made with the help of figure 2.11. Although the highest yields were obtained for the highest molar concentrations of zinc sulphide, the most desirable crystals were obtained when the figure of merit was about 5. It is now easy to see why the growth of the required crystals was so uncertain. Owing to the very steep slope of figure 2.11 in the operating region, an impossibly close control of $\dot{m}_{ZnS}$ would have been necessary in order to maintain the figure of merit at a close enough value to 5 for consistent crystals to have been grown.

2.7 Theoretical considerations

2.7.1 Mode of vapourisation of zinc sulphide

The generally accepted view on the vapourisation of zinc sulphide is that it is almost totally dissociated in the vapour phase into zinc and diatomic sulphur gases. There is much evidence to support this view(1d), in particular two investigations using mass spectrometric techniques(27, 28), and one using zinc vapour to suppress the sulphur vapour pressure(29). Goldfinger and Jeunehomme(27) found that the ratio $\frac{p(S_2)}{p(ZnS)}$ was greater that 10^5. The pressure due to ZnS gas is therefore neglected in the present calculations and zinc sulphide is assumed to evaporate according to the equation:

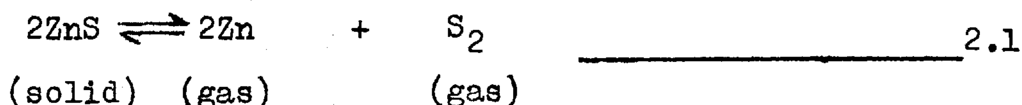

$$\underset{(solid)}{2ZnS} \rightleftharpoons \underset{(gas)}{2Zn} + \underset{(gas)}{S_2} \qquad 2.1$$

K is the equilibrium constant for this reaction and is given by

$$K = [p_e(Zn)]^2[p_e(S_2)] \qquad 2.2$$

where $p_e(X)$ stands for the equilibrium vapour pressure of component X expressed in atmospheres.

In the absence of excess solid of either zinc or sulphur, equilibrium is established between zinc sulphide solid and zinc and sulphur gases so that

$$p_e(Zn) + p_e(S_2) \text{ is a minimum.}$$

Differentiating equation 2.2 we obtain

$$0 = 2[p_e(Zn)][p_e(S_2)].d[p_e(Zn)] + [p_e(Zn)]^2.d[p_e(S_2)] \quad \text{——— } 2.3$$

and since $p_e(Zn) + p_e(S_2)$ is a minimum

$$d[p_e(S_2)] + d[p_e(Zn)] = 0 \quad \text{——— } 2.4$$

Combining equations 2.3 and 2.4 leads to the result that

$$p_e(Zn) = 2p_e(S_2) \quad \text{——— } 2.5$$

A similar result will also be proved for $p(Zn)$ and $p(S_2)$ where $p(Zn)$, $p(S_2)$ represent the actual pressures of zinc and sulphur gases present in the system. In view of this, calculations will only be made for $p(Zn)$ and $p_e(Zn)$, it being understood that exactly the same relationships must exist between $p(S_2)$ and $p_e(S_2)$ and between the sum total pressures were they also to be calculated.

2.7.2 Determination of $p_e(Zn)$

In order to determine $p_e(Zn)$ as a function of temperature it is necessary to know the equilibrium constant K (equation 2.2) as a function of temperature. This information was obtained from the graph of log K against 1/T given by Goldfinger and Jeunehomme[27]. However, it was more convenient to express the data in the form of the empirical relationship given by the following equation:-

$$\log K = A + \frac{B}{T} \qquad 2.6$$

The constants A and B were then obtained by fitting equation 2.6 to the data of reference 27.

The resulting equation was:

$$\log K = 18.4(9) - \frac{3.75(4)\times 10^{4}}{T} \qquad 2.7$$

From equations 2.2 and 2.5

$$p_e(Zn) = (2K)^{1/3} \qquad 2.8$$

or

$$\log p_e(Zn) = \frac{\log 2 + \log K}{3}$$

$$= 6.26(3) - \frac{12.5(1)\times 10^{3}}{T} \qquad 2.9$$

2.7.3 Determination of the actual zinc vapour pressure p(Zn)

Let the volume flow rate of argon in the growing tube at temperature T°K be $F_V(T)$c.c. per hour.

Let v_D cm/sec be the average velocity of zinc gas along the growing tube due to diffusion only.

Consider a point downstream from the charge where zinc vapour has reached equilibrium with the argon carrier gas. The volume flow rate of zinc vapour must then be

$$F_V^{Zn}(T) = (F_V(T) + 3600Av_D)\text{c.c./hr.} \qquad 2.10$$

where A is the tube cross sectional area in cm^2.

Let the mass loss rate of zinc sulphide from the charge be $\dot{m}_{ZnS}$ grams/hour.

For continuity, the mass transport rate of zinc sulphide along the tube must also be $\dot{m}_{ZnS}$ gm/hr. before the onset of condensation.

.'. Molar flux of zinc sulphide along the tube

$$J_M = \frac{\dot{m}_{ZnS}}{3600AM_{ZnS}} \text{ moles/cm}^2\text{sec} \qquad 2.11$$

where M_{ZnS} is the gram molecular weight of zinc sulphide

$M_{ZnS} = 97.446$ gm

$A \simeq 9.6$ cm^2

$\dot{m}_{ZnS} > 0.4$ gm/hr and typically $\dot{m}_{ZnS} = 2$ gm/hr.

$$\therefore \quad \text{Molar flux } J_M > 10^{-7} \text{ moles/cm}^2\text{sec} \qquad 2.12$$

$$\text{and typically } J_M = 6 \times 10^{-7} \text{ moles/cm}^2\text{sec} \qquad 2.13$$

It was thought highly unlikely that the molar flux due to diffusion would be significant in comparison with the molar flux of material transported by the argon flow for any flow rate used in practice. To test this assumption the molar flux in the experiments performed by Samelson(8) was estimated from the details given. The geometry, temperature gradients and evaporation temperatures of his syetem were the same as used in the present case. Transport was by diffusion since a pure sealed tube system was used.

Maximum possible molar flux $< 4.3 \times 10^{-8}$ moles/cm^2sec.

since any greater flux would have led to the charge being completely evaporated before the end of the run.

$\therefore$ Molar flux with no inert ambient atmosphere

$$< 4.3 \times 10^{-8} \text{ moles/cm}^2\text{sec.}$$

Assuming that the diffusion flux is proportional to the mean free path of molecules in the vapour, then

$J_M \propto \frac{1}{p}$ where p atm. is the total ambient pressure.

With no ambient atmosphere $p = p(Zn) + p(S_2) \simeq 10^{-2}$ atm at the temperature of interest.

$\therefore$ Expected diffusion flux in 1 atm. of argon is of the order of 4×10^{-10} moles/cm^{2}sec (or less).

The diffusion flux is therefore likely to be negligible in this case compared with the zinc sulphide transported by the argon carrier itself.

Neglecting diffusion therefore, equation 2.10 becomes

$$F_V^{Zn}(T) = F_V(T) \qquad\text{————————————} \quad 2.14$$

Thus, the volume flow rate of the evaporated zinc sulphide vapours is defined solely by the volume flow rate of argon.

The volume flow rate of argon is measured on the flow meter at room temperature (300°K) whereas $F_V(T)$ is the volume flow rate at T°K. Since the whole system is at 1 atmosphere pressure

$$F_V(T) = \frac{T}{300} \cdot F_V(300) \text{ c.c./hr.} \qquad\text{————————} \quad 2.15$$

where $F_V(300)$ is the measured volume flow rate

By calibration $F_V(300) = 3900F$ c.c./hr. ———————— 2.16

where F is the argon flow as measured in divisions on the flow meter.

$\therefore F_V(T) = 13$ F.T. c.c./hr. ——— 2.17

The temperature range between evaporation and crystallisation points was roughly 1600°K to 1300°K. The pressure of the zinc and sulphur vapours was of the order of 10^{-2} atmospheres. These vapours, being dilute, were therefore treated as approximating to ideal gases in the temperature range mentioned and the equation

$$\frac{p(Zn).V(Zn)}{T} = \text{constant} = K_1 \qquad 2.18$$

was used to describe their behaviour. From equations 2.14 and 2.17 the molar volume of zinc vapour is given by

$$V(Zn) = \frac{13T.F.M_{Zn}}{\dot{m}_{Zn}} \text{ c.c./mole} \qquad 2.18(a)$$

Since, by equation 2.1, the molar evaporation rates of ZnS and Zn are equal, we may replace M_{Zn}, $\dot{m}_{Zn}$ in equation 2.18(a) by M_{ZnS}, $\dot{m}_{ZnS}$ respectively.

$\therefore$ from equation 2.18

$$p(Zn) = \frac{K_1 \dot{m}_{ZnS} T}{13F.T.M_{ZnS}}$$

$$= \frac{K_2 \dot{m}_{ZnS}}{F} \text{ atm.} \qquad 2.19$$

$$\text{where } K_2 = \frac{K_1}{13 \; M_{ZnS}} \qquad 2.20$$

Equation 2.19 applies only in the region of no evaporation or condensation i.e., between the charge and the crystals and shows that p(Zn) is independent of temperature in this region. K_1 and

K_2 account for the conversion factors involved in using convenient units for $\dot{m}_{ZnS}$, F and p(Zn). K_1 also includes a factor for the lowering of p(Zn) due to any interaction of zinc vapour molecules with other gaseous molecules present.

2.7.4 Theoretical calculation of the evaporation rate of zinc sulphide.

Material is removed from the zinc sulphide charge by the continuous stream of argon which carries evaporated zinc sulphide out of the evaporation zone. The actual pressure of say, zinc vapour above the charge p(Zn) is therefore less than its equilibrium value. Undoubtedly vapour has to diffuse from the immediate vicinity of the charge into the main stream of argon in order to be transported. However, it is difficult to see how any diffusion theory could be applied to determine the evaporation rate of a charge since no information is available regarding concentration gradients or states of turbulence in the argon in the region of the charge. As a substitute, the zinc pressure over the charge will be assumed to be uniform and equal to the zinc pressure downstream from the charge which has already been defined by equation 2.19.

Applying the Hertz - Knudsen - Langmuir (H.K.L.) equation we obtain the evaporation and recondensation rates at the charge.

Condensation flux $J^{Zn}_{cond} = \dfrac{\alpha_{Zn} p(Zn)}{(2\pi M_{Zn} RT)^{\frac{1}{2}}}$ moles/cm^{2}sec ____ 2.21

where α_{Zn} is the condensation coefficient for zinc

M_{Zn} is the gram molecular weight of zinc vapour

p(Zn) is expressed in dynes/cm^2

R is expressed in ergs/mole.°K

Similarly evaporation flux

$$J^{Zn}_{evap.} = \frac{\beta_{Zn}p_e(Zn)}{(2\pi M_{Zn}RT)^{\frac{1}{2}}} \text{ moles/cm}^2\text{sec} \qquad 2.22$$

.˙. Mass loss of zinc per second

$$\dot{m}_{Zn} = M_{Zn}.A_{eff}(J^{Zn}_{evap} - J^{Zn}_{cond})$$

$$= \frac{M_{Zn}.A_{eff}[\beta_{Zn}p_e(Zn) - \alpha_{Zn}p(Zn)]}{(2\pi M_{Zn}RT)^{\frac{1}{2}}} \text{ g/sec} \qquad 2.23$$

Here A_{eff}cm^2 is the effective area over which evaporation takes place and is the area of the charge surface reduced by a suitable factor to take account of the fact that zinc vapour has to diffuse into the main stream of argon.

For stoichiometric evaporation

$$\frac{\dot{m}_{Zn}}{\dot{m}_{ZnS}}.\frac{M_{ZnS}}{M_{Zn}} = \frac{\dot{m}_{S_2}}{\dot{m}_{ZnS}}.\frac{2M_{ZnS}}{M_{S_2}} = 1 \qquad 2.24$$

i.e. $$\dot{m}_{ZnS} = \frac{M_{ZnS}}{M_{Zn}}.\dot{m}_{Zn}$$

$$= \frac{[\beta_{Zn}p_e(Zn) - \alpha_{Zn}p(Zn)]}{(2\pi M_{Zn}RT)^{\frac{1}{2}}} A_{eff}.M_{ZnS}$$

$$= \frac{2[\beta_{S_2}p_e(S_2) - \alpha_{Zn}p(S_2)]}{(2\pi M_{S_2}RT)^{\frac{1}{2}}} A_{eff}.M_{ZnS} \qquad 2.25$$

$$\therefore [\beta_{Zn}p_e(Zn) - \alpha_{Zn}p(Zn)] = 2\sqrt{\frac{M_{Zn}}{M_{S_2}}}.[\beta_{S_2}p_e(S_2) - \alpha_{S_2}p(S_2)] \quad \text{—— } 2.26$$

$M_{S_2} = 64.01 \qquad M_{Zn} = 65.38$

$$\therefore \sqrt{\frac{M_{Zn}}{M_{S_2}}} = 1.0107 \simeq 1$$

Since the error in subsequent calculations will be greater than 1%, $\sqrt{\frac{M_{Zn}}{M_{S_2}}}$ is taken as 1 and equation 2.26 can be re-written

$$[\alpha_{Zn}p(Zn) - 2\alpha_{S_2}p(S_2)] = [\beta_{Zn}p_e(Zn) - 2\beta_{S_2}p_e(S_2)]$$
$$= \text{Constant} \quad \text{—— } 2.27$$

since $p_e(Zn)$, $p_e(S_2)$ are fixed quantities at any given temperature.

Now $\frac{p(S_2)}{p(Zn)}$ is finite for all p(Zn) since both species are always present together.

$\therefore p(S_2) \rightarrow 0$ as $p(Zn) \rightarrow 0$

$\therefore$ from equation 2.27

$$[\alpha_{Zn}p(Zn) - 2\alpha_{S_2}p(S_2)] \rightarrow 0 \text{ as } p(Zn) \rightarrow 0$$

Hence $[\alpha_{Zn}p(Zn) - 2\alpha_{S_2}p(S_2)] \equiv 0$

$$\equiv [\beta_{Zn}p_e(Zn) - 2\beta_{S_2}p_e(S_2)] \quad \text{—— } 2.28$$

for all $p(Zn)$, $p(S_2)$, since α, $\beta < 1$

$$\therefore \frac{p_e(Zn)}{p_e(S_2)} \equiv \frac{2\beta_{S_2}}{\beta_{Zn}} \equiv 2$$

i.e. $\beta_{Zn} = \beta_{S_2}$ —— 2.29

and $\frac{p(Zn)}{p(S_2)} \equiv \frac{2\alpha_{S_2}}{\alpha_{Zn}} \equiv 2$

since $p(Zn) \rightarrow p_e(Zn)$ and $p(S_2) \rightarrow p_e(S_2)$ when $\dot{m}_{ZnS} \rightarrow 0$

and α_{S_2}, α_{Zn} are constants.

i.e. $\alpha_{Zn} = \alpha_{S_2}$ ——— 2.30

The results given by equations 2.29, 2.30 depend only on the assumption of stoichiometric evaporation. If the solid is in thermodynamic equilibrium with its vapour then there are equal numbers of zinc and sulphur atoms in the vapour phase [since $p_e(Zn) = 2p_e(S_2)$] and the vapour phase is therefore stoichiometric. In the present case zinc and sulphur are removed from the charge locality by argon in the proportions present over the charge. Replacement is by evaporation such that the mass evaporation rates are in the ratio $\frac{p_e(Zn)}{p_e(S_2)} \cdot \sqrt{\frac{M_{Zn}}{M_{S_2}}}$ i.e. approximately 2:1. Thus replacement is stoichiometric within 1% and so loss must also be stoichiometric within the same limits in the steady state. Deviations from stoichiometry are never very great and reduce progressively the nearer $p(Zn)$ approaches to $p_e(Zn)$.

Restating equation 2.25

$$\dot{m}_{ZnS} = \frac{[\beta_{Zn}p_e(Zn) - \alpha_{Zn}p(Zn)]}{(2\pi M_{Zn}RT)^{\frac{1}{2}}} A_{eff}M_{ZnS} \qquad 2.25$$

$$= \frac{\beta[p_e(Zn) - p(Zn)]}{(2\pi M_{Zn}RT)^{\frac{1}{2}}} A_{eff} \cdot M_{ZnS} \qquad 2.25(a)$$

since $\dot{m}_{ZnS} \rightarrow 0$ as $p(Zn) \rightarrow p_e(Zn)$ and $\beta_{Zn} = \beta_{S_2} = \beta$

$$\therefore \dot{m}_{ZnS} = \frac{M_{ZnS}}{(2\pi M_{Zn}R)^{\frac{1}{2}}} (\beta A_{eff}) \cdot \frac{[p_e(Zn) - p(Zn)]}{T^{\frac{1}{2}}} \qquad 2.31$$

$$\therefore \dot{m}_{ZnS} = K_3 \quad (\beta A_{eff}) \frac{[p_e(Zn) - p(Zn)]}{T^{\frac{1}{2}}} \qquad 2.32$$

where $\dot{m}_{ZnS}$ is expressed in g/hr.

A_{eff} in cm^2

p in atmospheres

T in °K

K_3 takes account of the change in units from equation 2.25 and $K_3 = 1.965 \times 10^6$

Now the effective area for evaporation must depend on the size and shape of the charge.

Suppose all charges have a similar shape. Then to a first approximation $A_{eff} = AM^{2/3}$ $\qquad$ 2.33

where A is a constant

and M is the charge weight in g.

Then $\dot{m}_{ZnS} = K_3 \ \beta AM^{2/3} \frac{[p_e(Zn) - p(Zn)]}{T^{\frac{1}{2}}}$

$$= K_4 M^{2/3} \frac{[p_e(Zn) - p(Zn)]}{T^{\frac{1}{2}}} \qquad 2.34$$

where $K_4 = K_3 \beta A$ $\qquad$ 2.35

Substituting equation 2.19 into 2.34

$$\dot{m}_{ZnS} = K_4 M^{2/3} \frac{[p_e(Zn) - \frac{K_2 \dot{m}_{ZnS}}{F}]}{T^{\frac{1}{2}}} \qquad 2.36$$

$$\therefore \quad \dot{m}_{ZnS} \left\{ \frac{FT^{\frac{1}{2}}}{K_4 M^{\frac{2}{3}}} + K_2 \right\} = F.p_e(Zn)$$

$$\text{i.e. } \frac{p_e(Zn)}{\left(\frac{\dot{m}_{ZnS}}{F}\right)} = \frac{1}{K_4} \cdot \frac{FT^{\frac{1}{2}}}{M^{\frac{2}{3}}} + K_2 \qquad 2.37$$

Figure 2.12 is a graph of $\frac{p_e(Zn)}{\left(\frac{\dot{m}_{ZnS}}{F}\right)}$ against $\frac{F.T.}{M^{\frac{2}{3}}}$ using the values of F, T, M, $\dot{m}_{ZnS}$ obtained from the crystal growing runs for which the full set of data was available. The agreement with a straight line law is remarkable when possible sources of error are considered. Since in most cases M did not vary greatly during a crystal growing run, the values of M and $\dot{m}_{ZnS}$ used to draw figure 2.12 were the average values for each run. To have considered the time variation of $\dot{m}_{ZnS}$ during a run would have led to excessive complexity which would not have been justified considering the approximate nature of the calculations.

The values of K_2 and K_4 were estimated from figure 2.12. Their values were

$$K_2 = (3.5 \pm 0.5) \times 10^{-2}$$

$$K_4 = (8.6 \pm 0.4) \times 10^{2}$$

using equations 2.33 and 2.35 we find

$$\beta \quad A_{eff} = \frac{K_4}{K_3} . M^{\frac{2}{3}}$$

$$\simeq 4.4 \times 10^{-4} M^{\frac{2}{3}}$$

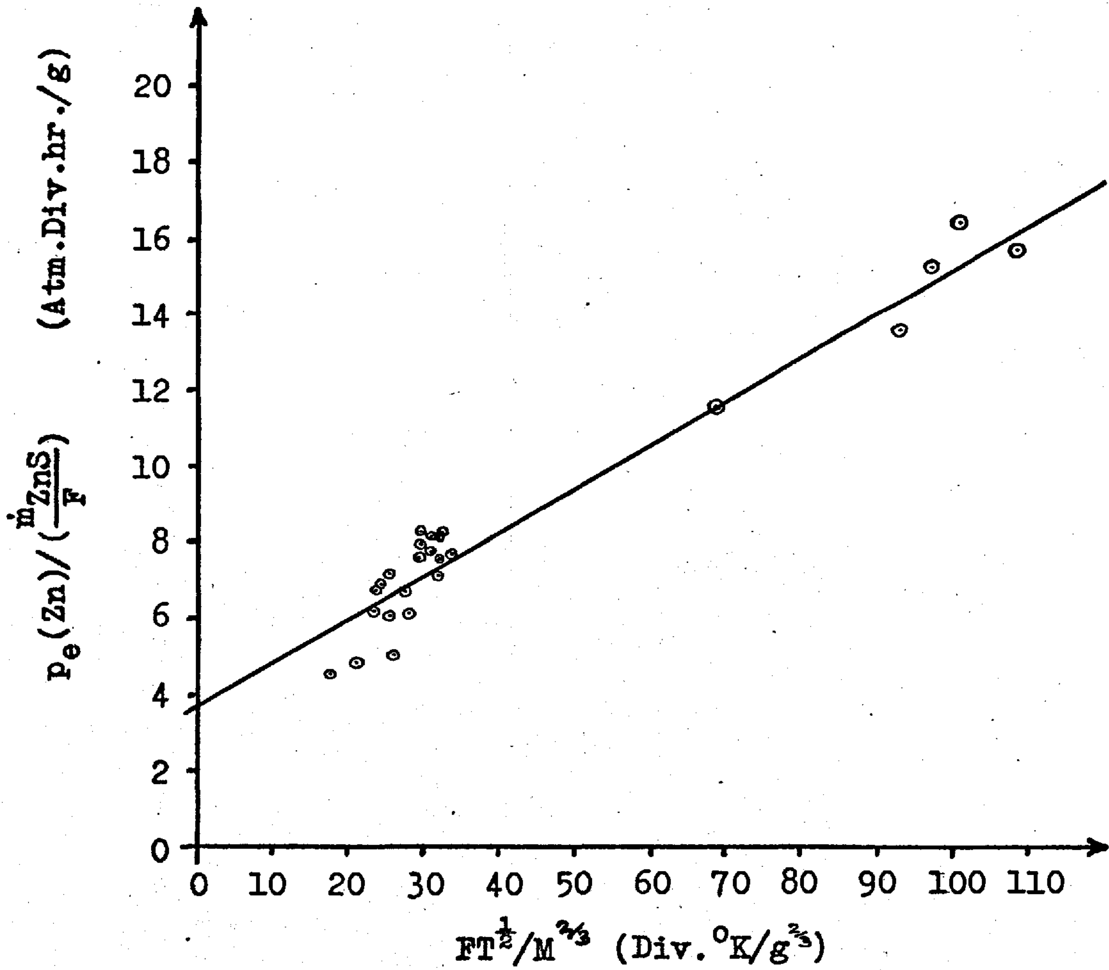

Figure 2.12 $\frac{p_e(Zn)}{\left(\frac{\dot{m}_{ZnS}}{F}\right)}$ versus $\left(\frac{FT^{\frac{1}{2}}}{M^{2/3}}\right)$

i.e. for a typical mass of charge M = 32 g.

$$\beta A_{eff} \simeq 44 \times 10^{-4} cm^2$$

A typical 32 g. charge measures 2 cm. diameter x 6.5 cm. long. Charge area is therefore about 44 cm^2. Since β is generally of the order of 1 for a polycrystalline surface it follows that A_{eff} is of the order of 10^{-4} times the actual charge area.

Argon therefore has a large effect on the rate of evaporation of the charge (c.f. the high argon pressures used in the melt growth of zinc sulphide to prevent sublimation). Since argon cannot suppress the vapourization of zinc sulphide by chemical means, it must act in a purely physical way to prevent zinc and sulphur vapours leaving the vicinity of the charge. In other words, the vapourization of zinc sulphide in the presence of 1 atm. of argon is diffusion limited.

To summarise, it appears that the predominant rate limiting factor for the evaporation of the zinc sulphide charge is the diffusion barrier presented by the argon to the zinc and sulphur vapour, and that this is manifested in the equations as a much reduced effective charge surface area.

2.7.5. Theory of condensation and crystal growth.

Crystal growth theory divides naturally into two parts. On the one hand there is the question of how the material is delivered to the crystal for growth. On the other hand there is the problem of how the atoms so delivered give up energy and become arranged on the appropriate lattice sites. No effort was made to investigate this latter problem experimentally so

discussion will be limited to a brief review of some past work in this direction.

It is possible, however, to discuss how material arrives at the crystals on the basis of experimental results.

2.7.5.1. Condensation theory

It is proposed that argon limits the rate at which material can condense out of the gas stream in exactly the same way as it limits the evaporation of the charge.

By analogy with equation 2.32 for evaporation

$$\frac{\partial(\dot{m}^{cond}_{ZnS})}{\partial x} = K_3 \frac{\partial(\alpha A_{eff})}{\partial x} \frac{[p(Zn) - p_e(Zn)]}{T^{\frac{1}{2}}} \qquad 2.38$$

where $\frac{\partial(\dot{m}^{cond}_{ZnS})}{\partial x}$ is the nett mass condensation rate of zinc sulphide per unit length of growing tube.

The definition of αA_{eff} for condensation is slightly different from that for βA_{eff} for evaporation. In the case of evaporation we were dealing with polycrystalline surfaces where atoms were not mobile. For condensation the situation is different. A properly flame polished tube has a low density of sites capable of impeding the motion of atoms. The same applies to a singular crystal surface. The condensing atoms are therefore highly mobile and may easily re-evaporate before being trapped at one of these sites. This means that α may be much less than 1 and will certainly be variable along the length of the growing tube. A_{eff} then represents the total area available

for condensation and α represents the proportion of that area effective in trapping material. The effect of diffusion limitation is contained in the value of A_{eff} and therefore it is expected that A_{eff} will be roughly 10^{-4} times the available area as for evaporation.

Let $$\sigma = \frac{p(Zn) - p_e(Zn)}{p_e(Zn)} \qquad 2.39$$

where σ is the supersaturation of the vapour.

(It is easily shown that $\sigma_{Zn} = \sigma_{S_2} = \sigma_{ZnS}$)

Substituting equation 2.39 into equation 2.38

$$\frac{\partial(\dot{m}^{cond}_{ZnS})}{\partial x} = \frac{K_3\sigma}{T^{\frac{1}{2}}} \cdot p_e(Zn) \cdot \frac{\partial(\alpha A_{eff})}{\partial x} \qquad 2.40$$

Equation 2.19 is now modified to allow for condensation:

$$p(Zn) = K_2 \frac{\dot{m}_{ZnS} - \int_x \frac{\partial(\dot{m}^{cond}_{ZnS})}{\partial x} \cdot dx}{F} \qquad 2.41$$

from which

$$\frac{\partial p(Zn)}{\partial x} = - \frac{K_2}{F} \cdot \frac{\partial(\dot{m}^{cond}_{ZnS})}{\partial x} \qquad 2.42$$

Also from equation 2.39

$$p_e(Zn) \cdot \frac{\partial(\sigma)}{\partial x} = \frac{\partial p(Zn)}{\partial x} - (\sigma + 1) \cdot \frac{\partial[p_e(Zn)]}{\partial x} \qquad 2.43$$

and from equation 2.9

$$\frac{\partial[p_e(Zn)]}{\partial x} = 2.88 \times 10^4 \cdot \frac{G(x)}{T^2} \cdot p_e(Zn) \qquad 2.44$$

where G(x) is the temperature gradient function.

Combining equations 2.40 to 2.44

$$\frac{\partial(\dot{m}_{ZnS}^{cond})}{\partial x} = -\frac{F}{K_2}\left\{\frac{2.88 \times 10^4(\sigma + 1)G(x)}{T^2} + \frac{\partial(\sigma)}{\partial x}\right\} p_e(Zn)$$

$$= \frac{K_3\sigma}{T^{\frac{1}{2}}} \cdot \frac{\partial(\alpha A_{eff})}{\partial x} \cdot p_e(Zn) \qquad 2.45$$

For no condensation:-

$$\frac{\partial(\sigma)}{\partial x} = -\frac{2.88 \times 10^4(\sigma + 1)G(x)}{T^2}$$

$$\simeq 1.6 \times 10^{-1}(\sigma + 1) \qquad 2.46$$

For $G(x) \simeq -12°C/cm.$ and $T = 1473°K$ when $\sigma = 0$.

Figure 2.13 shows how supersaturation varies as a function of distance along the growing tube when no condensation is taking place. The origin of x is taken for the point at which the vapour is just saturated i.e. $x = 0$ at $\sigma = 0$.

Figure 2.14(a) is a contour map of $\frac{\partial(\dot{m}_{ZnS}^{cond})}{\partial x}$ as a function of σ plotted for various temperatures and typical F = 8 and G = 12. The diagram is divided into 4 regions, A,B,C, amd D with respect to the 1300°C contour. The BC boundary is the line of $\frac{\partial(\sigma)}{\partial x} = 0$ as defined by equation 2.45.

The AD boundary is the line defining the maximum possible condensation rate, which occurs when $\alpha = 1$ and A_{eff} represents the whole tube surface area. The boundary AB is the locus of the intersection of boundaries AD and BC for different temperatures. This can be found by plotting the $\frac{\partial(\alpha A_{eff})}{\partial x}$ required for $\frac{\partial(\sigma)}{\partial x} = 0$ to apply [Figure 2.14(b)] and finding

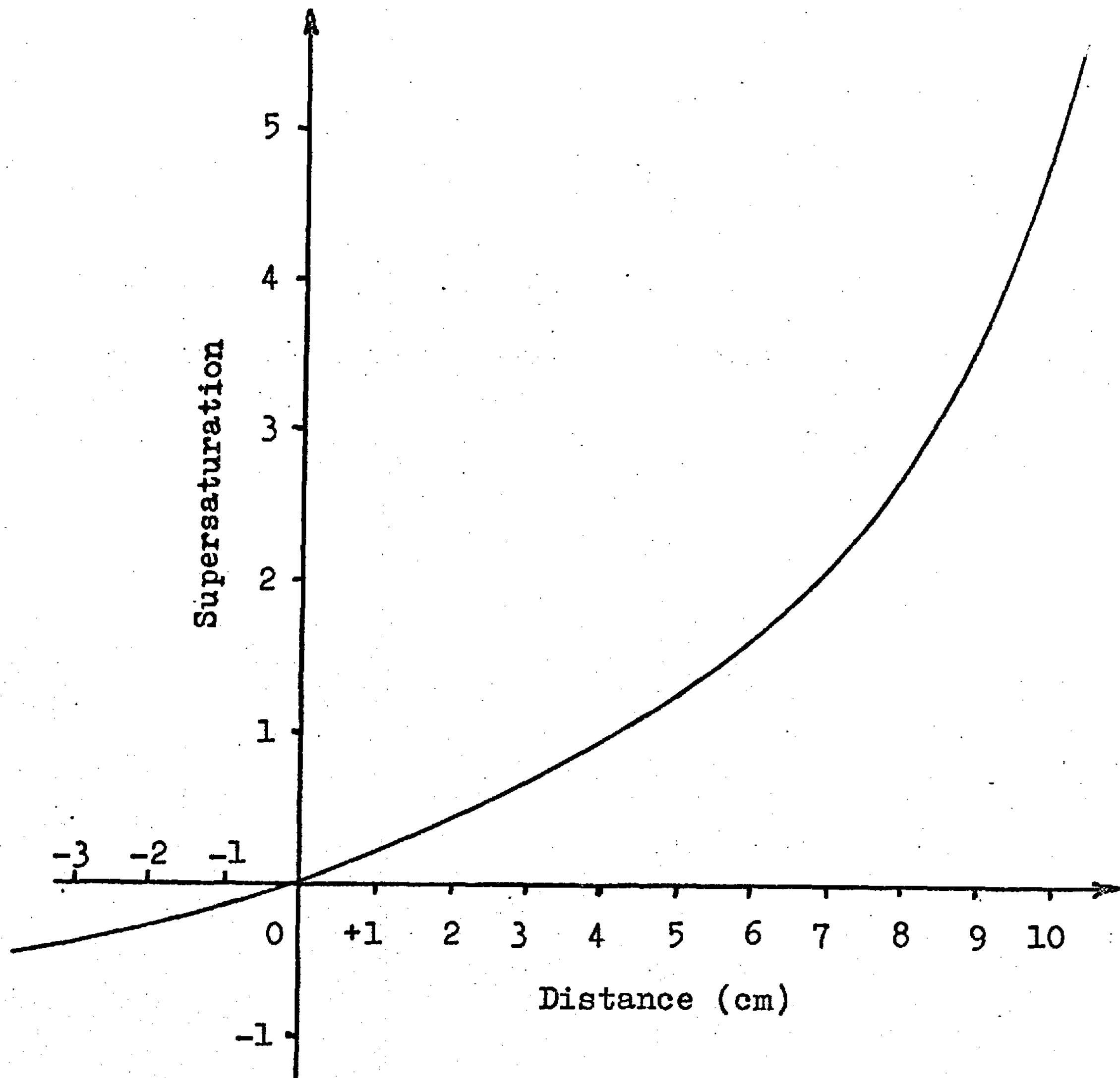

Figure 2.13 Supersaturation versus distance for no condensation

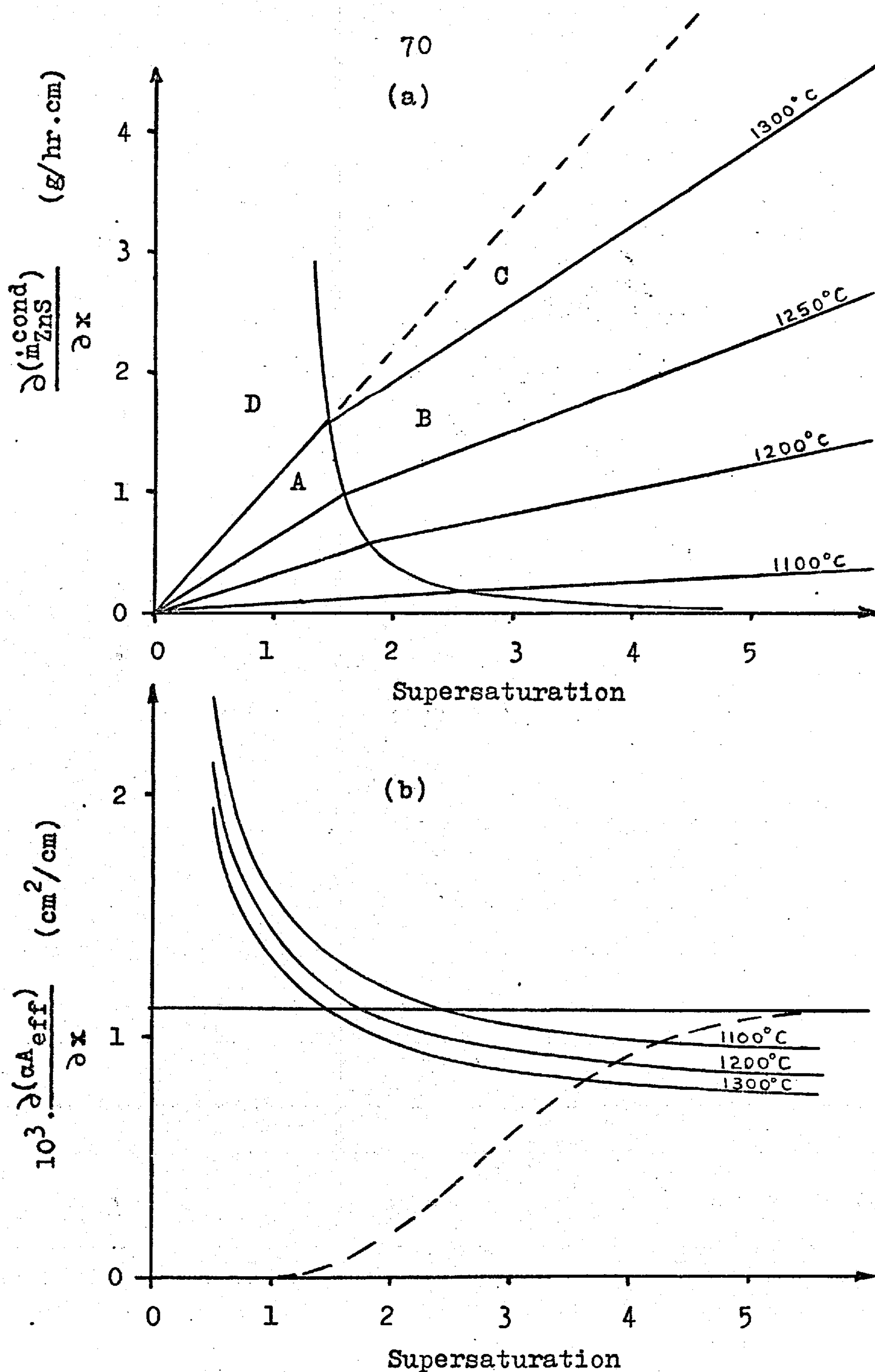

Figure 2.14 Mass condensation rate and effective condensation area versus supersaturation.

the intersections of these curves with $\frac{\partial(A_{eff})}{\partial x}$ for the tube surface. The horizontal line plotted in Figure 2.14(b) to represent the effective tube area per unit length is 10^{-4} x (actual area per unit length). Figure 2.14 (b) and equation 2.45 show that the $\frac{\partial(\alpha A_{eff})}{\partial x}$ required for $\frac{\partial(\sigma)}{\partial x} = 0$ tends to a limiting minimum for $\sigma \longrightarrow \infty$. This minimum is of the order of the

(tube surface area per unit length)x 10^{-4}

for the temperature of interest. This further justifies the assumption that the same factor relating A_{eff} to the actual area can be used for both evaporation and condensation. Similar regions and boundary lines are drawn for other temperatures. The region type is always defined relative to the contour corresponding to the temperature under consideration.

Using equation 2.45 it is easy to characterize the four regions and their boundaries.

Region A is characterized by $\frac{\partial(\sigma)}{\partial x} > 0$ since the whole region lies below the locus of $\frac{\partial(\sigma)}{\partial x} = 0$. Condensation in this region must therefore always be accompanied by an increasing σ.

Region B is similar to A except that it is bounded by the line $\frac{\partial(\sigma)}{\partial x} = 0$ therefore $\frac{\partial(\sigma)}{\partial x} \geqslant 0$ in region B.

Region C is above the $\frac{\partial(\sigma)}{\partial x} = 0$ line and therefore $\frac{\partial(\sigma)}{\partial x} < 0$.

Condensation must therefore be accompanied by a decrease in σ

in region C.

Region D is a forbidden region since it corresponds to a condensation rate greater than that allowed by the available surface area. Condensation in region D must therefore be by spontaneous solidification in the bulk of the gas and therefore corresponds to powder formation.

For a flame polished tube α will be much less than unity for low σ since very few nucleation sites trap material when there is a low supersaturation. As the supersaturation rises more sites become available so α increases. The dotted curve in the figure 2.14(b) shows a possible locus for $\frac{\partial(\alpha A_{eff})}{\partial x}$ for a flame polished tube. Combining this curve with figure 2.14(a) results in the condensation contours labelled 1,2,3, and 4 and shown in figure 2.15. These are the contours which would be followed in practice for a tube with the dotted characteristic of figure 2.14(b). The condensation locus must always lie on one of the numbered contours of figure 2.15 since equation 2.45 must be satisfied. The line PQ defines the locus of the intersections of the numbered contours with the $\frac{\partial(\sigma)}{\partial x} = 0$ lines for varying temperatures. At the boundary PQ the numbered contours pass from a type B region to a type C region.

We consider now the variation of $\frac{\partial(\dot{m}_{ZnS}^{cond})}{\partial x}$ along a growing tube. A typical normal condensation locus is plotted as the solid arrowed line in figure 2.15. Condensation begins at low σ and high T in a type B region. σ therefore increases and

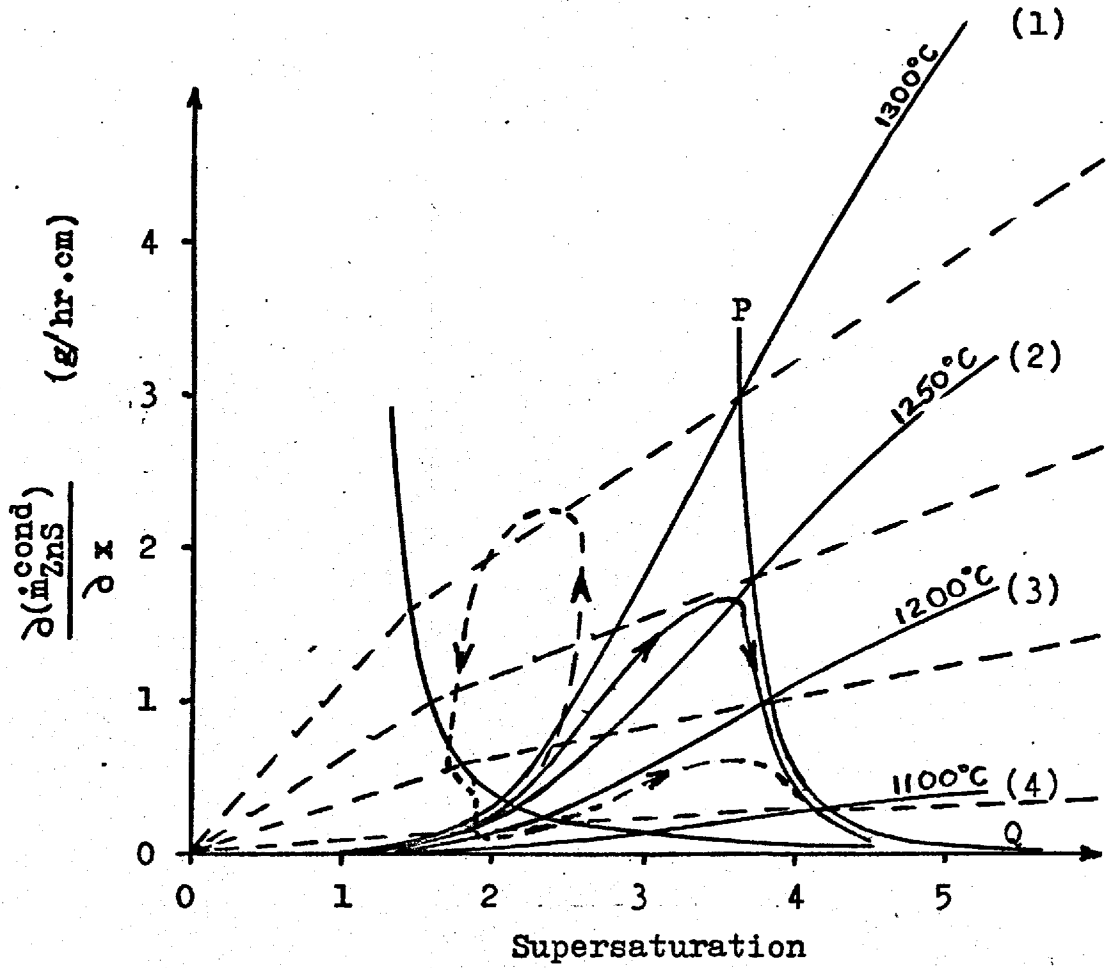

Figure 2.15 Condensation contours and loci.

the condensation locus moves up and across the numbered contours so as always to lie on the one appropriate to the temperature at the given point in the tube. When the locus approaches the PQ boundary $\frac{\partial(\sigma)}{\partial x} \rightarrow 0$. If PQ is reached the locus must move vertically downwards as $\frac{\partial(\sigma)}{\partial x} = 0$ and T is decreasing. This has the effect of moving the locus off PQ back into a type B region. If PQ is crossed then the locus enters a type C region and σ must decrease. The locus is therefore returned to PQ and thence to the type B region. Hence the condensation locus can never actually cross PQ but follows it closely in a downward direction. σ must therefore increase indefinitely as the temperature decreases. This must cause condensation to jump to a type D region eventually and powder formation should always be observed at the lower temperatures. The mass of powder formed is bound to be small, however, as figure 2.15 shows that $\frac{\partial(\dot{m}_{ZnS}^{cond})}{\partial x}$ falls to very low values at low temperature. In fact, a powder deposit was always found in the cooler parts of the tube, though it was not very thick for the reasons already given.

The dotted arrowed curve in figure 2.15 shows the locus of condensation for partially flame polished tube. Condensation begins as before, but the vapour soon enters a region where $\frac{\partial(\dot{\alpha}A_{eff})}{\partial x}$ increases at constant σ. Since the contour is in a type B region σ continues to increase slowly but $\frac{\partial(\dot{m}_{ZnS}^{cond})}{\partial x}$ increases very rapidly until the contour eventually enters a

type C region. σ then decreases and the contour follows a path of maximum condensation as the temperature decreases until it reaches the AB boundary. It then follows this boundary in the same way as the normal condensation contour follows PQ. If the vapour then encounters another properly flame polished region the locus drops rapidly to the appropriate numbered contour and then follows a normal condensation locus at lower temperature. Again σ eventually increases indefinitely. It is obvious from the above that an unflame-polished region robs subsequent regions of material and so prevents proper crystal growth.

Figure 2.15 demonstrates qualitatively that the mass condensation rate must pass through a maximum and that super-saturation must always increase eventually as temperature decreases. The only thing which prevents figure 2.15 from being used quantitatively is the lack of knowledge of the exact function for $\frac{\partial(\alpha A_{eff})}{\partial x}$ in terms of σ. If this were known an exact condensation locus could be traced out for any given conditions.

Equation 2.45 can be re-written:

$$\frac{\partial(\dot{m}_{ZnS}^{cond})}{\partial x} - \frac{\partial(\dot{m}_{ZnS}^{cond})}{\partial T}.G(x)$$

$$= -\frac{F}{K_2}\left\{\frac{2.88 \times 10^4(\sigma + 1)G(x)}{T^2} + \frac{\partial(\sigma)}{\partial T}.G(x)\right\}p_e(Zn)$$

$$= \frac{K_3}{T^{\frac{1}{2}}}\ \frac{\partial(\alpha A_{eff})}{\partial x}.p_e(Zn) \qquad 2.47$$

Thus the condensation rate per unit length of tube increases with increasing temperature gradient, as does $\frac{\partial(\sigma')}{\partial x}$. It has previously been shown that the condensation rate passes through a maximum as σ' increases. The nett result of increasing the temperature gradient is therefore to produce more condensation over a shorter zone, i.e., to give denser crystal growth. This fact was observed in the crystal growth experiments.

Equation 2.37 shows that an increase in F leads to a decrease in concentration of ZnS. This shifts the origin of x (defined as x = 0 when $\sigma' = 0$) for equation 2.45 to a lower value of temperature. The effect of increasing F is therefore to shift the condensation to lower temperatures. In terms of the contours of figures 2.14, 2.15, increases in F and G have identical effects in shifting the $\frac{\partial(\sigma')}{\partial x} = 0$ lines to higher values of $\frac{\partial(\dot{m}_{ZnS}^{cond})}{\partial x}$ and in moving PQ to the right. However, for increases in G the same temperature contours are crossed at higher σ', whereas for increases in F lower temperature contours are crossed at the same σ' by the condensation locus. Increases in both F and G cause more material to be condensed at higher supersaturation by shifting the boundary PQ to the right. They therefore both encourage the formation of more powder. This

increase in powder formation was observed during sintering charges when large F and G were often used.

So far discussion has been limited to condensation on the walls of the growing tube alone. We now consider condensation in the presence of crystals. The initial condensation rate will still be given by figure 2.15, as small crystals will not affect the area available for condensation. As stated in section 2.6 it was necessary for whiskers to form rapidly if the required platy growth were to be obtained.

The growth rate of whiskers was estimated to be of the order of 1 cm per minute on an average. This gives a volume growth rate of 7.5×10^{-6} cc/hr for a 4 micron diameter whisker. Now the density of zinc sulphide is about 4 g/cc. Therefore the mass condensation rate required per whisker was 3×10^{-5} g/hr. It is estimated from experimental results that whisker growth occurred at about 1150°C. Equation 2.45 gives the maximum condensation rate on the tube walls at 1150°C as 0.17 g/hr.cm. per unit supersaturation. If the whisker density was 10 per cm and the supersaturation between 2 and 3 then whiskers drew material from about 10^{-3} of the tube surface area. Whiskers were often observed to re-evaporate or partially re-evaporate after growth and this was put down to competition from neighbouring nuclei whose collecting areas overlapped those of the whiskers.

Short whiskers were obviously able to lose heat to the walls of the tube by conduction. However, as the whiskers

became longer they would have found it more and more difficult to lose heat by conduction. It is therefore proposed that they lost heat by re-evaporation of mobile material passing up the whisker surface to the growing point. The longer the whisker got, the more material evaporated until eventually so much material re-evaporated that growth virtually stopped. This could explain why whiskers generally grew to a length of 1 to 2 cm then ceased to grow.

All the time material was being supplied to the tip of the whisker along its surface there must have been a tendency for some of this material to condense out and thicken it. This effect was observed in the early stages of growth.

It is an observed fact from the aspect ratio of whiskers and plates that the growth rate perpendicular to the c-axis was about 10^{-3} times growth rate in the c-direction. Since this is so, then material trying to condense on the surface of the whisker could easily have been arriving too fast to be incorporated in the crystallographic faces of the whisker. It would therefore have tended to form a rough surface on the whisker which would have impeded the diffusion of material to the growing tip. This would have caused even more material to be deposited on the whisker surface and the orientation would have been forced to change to accommodate the extra material. Whisker growth would then have ceased, but plate growth would have begun in the direction of the new c-axis.

There would have been a tendency for the plate to grow in the downstream direction from the whisker due to the slight

temperature and supersaturation differentials existing across the whisker. This may be the explanation of why a lot of plates and ribbons were observed to have one straight edge and one ragged one.

Fast plate growth was observed to occur at varying rates up to about 0.5 cm/hr. in the c-direction. Assuming growth at a constant thickness of 10 microns and constant width of 1 cm the maximum condensation rate for the fast grown plates was about 2 x 10^{-3} g/hr. This is a somewhat higher rate than for the whiskers. Nevertheless, it would have been possible for this mass of zinc sulphide to have been condensed entirely on the surface of the plate so long as its length in the c-direction were more than 250 microns, assuming a supersaturation of 2 to 3. This, of course, assumes no re-evaporation. A larger plate than this may, therefore, have been self-supporting in terms of material supply.

Assuming a whisker diameter of 4μm and a plate cross-section of 10μm by 1 cm, it can be seen, from the experimentally determined crystal growth rates, that the mass condensation rate per unit area of cross-section is 100 times greater for a whisker than for a plate. A plate crystal therefore requires a much lower temperature gradient along its length than does a whisker in order to dissipate the heat of condensation by thermal conduction. The heat could therefore be removed from the growing edge by conduction much more easily in the case of a plate. This gives a clue to the limiting factor in the growth of plates. A temperature differential along

the c-axis of the plate must have existed, if heat was lost by conduction, such that the growing edge was hotter than the supporting edge. The growing edge of the plate was therefore hotter than its surroundings since by growing downstream it grew towards a lower temperature region. The longer the plate in the c-direction the greater was the temperature differential between it and its surroundings. Therefore there came a time when growth ceased due to the re-evaporation of all material which might otherwise have reached the growing edge.

From the above discussion it would appear that whisker growth is dependent upon a supply of material from the walls of the growing tube, whereas plate growth need not be. It is to be expected therefore, that whiskers must be established quickly before other nucleation sites become operative if they are to grow successfully. Secondly, the fast growing plates cannot grow unless whiskers have formed but, once established, can continue to grow despite other growth on the walls of the tube around them. These were the exact conditions required in practice for the production of fast-growing plates.

There is plenty of evidence to suggest that argon has a segregating effect on zinc sulphide vapour. Patek[9] noticed it and it was obvious in the present work from the yellow and black bands of condensed material which were found towards the cooler end of the tube. It seems plausible to assume that, because argon impedes the diffusion of zinc and sulphur vapours, it also reduces their ability to recombine since the probability of the

two species meeting is reduced.

Recombination of the zinc and sulphur species could either be at random on the walls of the growing tube, or else it could occur at specific recombination sites. The latter might be expected to produce single crystals and the former a polycrystalline substrate. The critical concentration shown to exist in practice (figure 2.11) must, therefore, be the cross-over point between these two mechanisms of condensation.

The failure of Patek[9] and the success of Greene et al.[15] in growing crystals in an argon atmosphere may be interpreted in terms of this critical concentration. Patek used an evaporation temperature of 1200°C which was too low to give the critical concentration of zinc sulphide vapour. Greene, however, used an evaporation temperature of 1600°C which was far greater than that needed to give the critical concentration. Hence Greene was successful where Patek was not.

2.7.5.2. Mechanisms for the growth of zinc sulphide platelets

The defect structures of zinc sulphide vapour grown whiskers and plates have been investigated with reference to possible growth mechanisms by Tanaka[30] et al. and Fitzgerald[31] et al. Chikawa and Nakayama[32] have made similar investigations on cadmium sulphide.

The crystals investigated by Tanaka were grown by reaction of zinc and sulphur vapours in a closed system at a (comparatively) very low temperature (500°C). Those investigated by Fitzgerald were grown by argon transport but at the rather low

temperature of 1000°C. At that temperature a high degree of stacking disorder was to be expected. The CdS crystals examined by Chikawa were also grown by argon transport. Tanaka found axial screw dislocations in some, but not all, whiskers. He also found whiskers with a bicrystal structure and therefore concluded that at least two mechanisms, disclocation growth and grain boundary growth, were possible for the growth of zinc sulphide whiskers. Fitzgerald et al. examined thin plates with a habit similar to the fast grown plates described in the present work. They noticed the same tendency to have one straight and one ragged edge as observed here. The mechanism that they proposed for the growth of a $(\bar{1}2\bar{1}0)$ ribbon ("a plate thin in the $\langle\bar{1}2\bar{1}0\rangle$ direction and long in the $\langle 10\bar{1}0\rangle$ direction") was that a whisker first grew in the $\langle 10\bar{1}0\rangle$ direction by means of an axial dislocation mechanism. This dislocation was then assumed to dissociate (since no trace of it could be found in any of the plates) into partials which moved out of the crystal leaving an (0001) stacking fault behind. The whisker was then assumed to broaden by means of 2-dimensional nucleation on the $(000\bar{1})$faces.

The more rapid growth on the $(000\bar{1})$ face than on the (0001) face was explained as being due to the "crystallographic polarity of the wurtzite structure." The $(000\bar{1})$ face then developed into the ragged edge due to its rapid growth rate whilst the (0001) face remained smooth. The (0001) stacking fault found where the axial dislocation was expected, divided the crystal in two. Close to this stacking fault was a high

density of stacking faults which Fitzgerald could not explain. Chikawa and Nakayama explained the growth of cadmium sulphide plates on the basis of growth from a whisker containing an unstable combination of 2 dislocations. One of these was assumed to slip out of the edge of the whisker forming a line of dislocation half-loops on which growth continued to form a plate crystal. The dislocation half-loops were assumed to move with the growing edge under the action of their own line tension. Evidence for the existence of dislocation half-loops was found from X-ray diffraction micrographs.

Both Fitzgerald et al. and Chikawa and Nakayama say that the axis of the whisker on which the plate grew was in the $\langle 10\bar{1}0 \rangle$ direction. No such whiskers were found in the present case but this does not prove that they do not exist. However, neither of the above papers shows evidence to prove that they do exist. It seems possible that the high density of stacking faults observed by Fitzgerald was really the outline of a whisker whose orientation was different from that of the plate.

Tanaka reports some whiskers whose axis was in the <0001> direction and Chikawa and Nakayama report the existence of <0001> direction CdS needles.

The evidence shows that dislocations probably play a part in the growth of zinc sulphide plate crystals, but exactly what mechanism is involved has yet to be established.

In summary it may be said that the sequence of growth of plate crystals of zinc sulphide seems well established, but

that the precise mechanism involved in this growth sequence has yet to be elucidated.

CHAPTER 3

MATERIAL CHARACTERISATION

3.1 Introduction

The work described in this chapter deals with the chemical and physical characterisation of the material as far as was possible with the facilities available. Chemical analyses by X-ray fluorescence, emission spectrochemical and electron microprobe techniques were made for both crystals and starting materials. Physical examination was by optical and X-ray methods and included optical transmission spectra at and around the band gap energy.

3.2 Chemical Analyses

Chemical analyses of the zinc sulphide starting materials and crystals were made by the Analytical Services Laboratory at Imperial College. An independent spectrochemical analysis of the Merck starting material was also made by the Analytical Laboratories of Johnson Matthey Chemicals Ltd., Orchard Road, Royston, Herts., who have a reputation for high reliability in the use of this technique. In addition, certain information was given by manufacturers regarding the composition of their materials.

X-ray fluorescence (X.R.F.) and spectrochemical analysis techniques allow most elements to be detected in concentrations below 10 parts per million (p.p.m.). The limits of detection for the electron microprobe are of the order of 100 p.p.m., but accurate concentration profiles can be drawn with this instrum-

where elements are present above the limits of detection.

3.2.1 Starting material

Starting materials were obtained from the following sources:

1. Levy West & Co., Ltd.,
   Harlow,
   Essex.
2. British Drug Houses Ltd., (B.D.H.)
   Poole,
   Dorset.
3. E. Merck, A.G.,
   Darmstadt,
   Germany.

Four analyses were carried out on the starting material at different times and the results compared. One set of X.R.F results was in extreme disagreement with all the other analytical results. In addition this set of results showed the same impurity concentrations in Merck starting material and crystals grown from Levy West material. In view of the different sources of the materials this was considered to be most unlikely to be correct. This set of results was therefore disregarded since there was general agreement between the other results. All impurities detected with the exceptions of chlorine and silicon were near the limits of detection of the various analytical techniques used, so that quantitative estimates of concentration were difficult. Table 3.1 summarises the results of X.R.F. and

TABLE 3.1

Element	Levy West				Merck	B.D.H.
	Batch 1	Batch 2	Batch 3	Sintered charge		
Al	2	2	2	2	2	2
Ag	1	N.D	N.D	N.D	N.D	N.D
Au	–	–	–	–	N.D	–
Bi	–	–	–	–	<1	–
Ca	–	–	–	–	1	–
Cd	✓	?	?	?	<1	?
Cl	700	700	3000	60	<5	40
Cr	–	–	–	–	1	–
Co	N.D	N.D	N.D	N.D	N.D	N.D
Cu	N.D	?	?	?	≤1	N.D
Fe	N.D	?	?	5	5	N.D
In	N.D	N.D	N.D	N.D	N.D	–
Mg	1	1	1	1	1	<1
Mn	N.D	N.D	N.D	N.D	N.D	N.D
Na	–	–	–	–	<1	–
Ni	N.D	N.D	N.D	N.D	N.D	N.D
Pb	N.D	N.D	N.D	N.D	N.D	N.D
Si	10	20	10	10	30	5
Sn	–	N.D	N.D	N.D	N.D	N.D

N.D = None detected

? = doubtful result

✓ = present in unknown quantity

– = no result

emission spectrochemical analyses on all the starting materials used and gives rough estimates of impurity concentrations.

As can be seen, the impurity concentrations were very small in most cases. The results labelled "none detected" were supported by two independent analyses in each case. Most of the impurities detected were elements commonly found in laboratory dust and could easily be accounted for by accidental contamination. This particularly applies to the iron which could have been introduced during pelletising the samples for analysis, since this process involves pressing the material in steel dies. The silicon concentrations were high and liable to be erratic. Silicon is most likely to be introduced during the preparation of zinc sulphide which is usually distilled or fired at some stage in silica vessels. In view of the fact that crystal growth is in a silica tube there is little point in removing silicon from the charge. The most surprising impurity concentrations were those of chlorine, despite all materials being nominally chlorine free. The Levy West batch 3 material was so contaminated that zinc chloride was observed to distil off and condense as a colourless liquid while sintering charges of this material. This high concentration of chlorine probably explains why it was found almost impossible to grow the desired crystals with this material. Table 3.1 illustrates that a great improvement is achieved with regard to the chlorine concentration by charge sintering. However, it also shows that by no means all the chlorine can be removed this way so that it is always desirable

to start with a chlorine free material if possible. The only material found to be effectively chlorine free was Merck. The level of 5 p.p.m. given was sufficiently small to be considered of doubtful significance. In all probability this was introduced into the sample in the laboratory at some stage. The manufacturers claim that chlorine is not involved in the manufacture of their material and that it should be entirely free from chlorine contamination. The Johnson Matthey analysis also reports finding none of the following elements in Merck material:

As, B, Ba, Be, Cs, Ga, Ge, Hf, Hg, Ir, K, Li, Mo,
Nb, Os, P, Pd, Pt, Rb, Re, Rh, Ru, Sb, Se, Sr, Ta,
Te, Ti, Tl, V, W, Zr

although they were specifically sought. It may be concluded therefore that Merck material was probably the best obtained. The B.D.H. material will be seen from Table 3.1 to be second best.

3.2.2. Crystals

X.R.F. and emission spectrochemical analyses of the crystals showed little or no change in impurity concentrations from the starting material. In view of the fact that most elements were at the limits of detection of these methods in the starting material it is not surprising that no changes were detected. Silicon concentration stayed at the same level in crystals as in the starting material. There was an improvement with respect to chlorine for crystalline material obtained from the Levy West batch 3 material.

These analyses did show that no gross incorporation of impurities was taking place during crystal growth. The system was thus proved to be at least moderately clean with no large unwanted sources of impurity. There could well have been advantageous impurity segregation during crystal growth which could not be detected by these analyses. The electron micro-probe was used to scan crystals to find elemental concentration profiles. In fact all elements were below the limit of detection for the probe except the zinc and sulphur themselves. Some crystals examined with the probe had striations at which there was electro-luminescent emission. The scans of these areas revealed that although the zinc concentration was constant across the striations, the sulphur concentration dropped in striations. Assuming that the striations were structural faults (probably stacking faults) the above result appears to show that faulted growth may occur due to some temporary change in chemical composition of the gaseous species in the crystal growth tube. This deviation in composition could cause a drop in sulphur concentration either by creating sulphur vacancies or by substituting for sulphur in the crystal lattice. In either case the disturbance could easily be sufficient to cause temporary structural modification and it is believed that this is far more likely to be the cause of structural faults than temporary variations in the temperature of the growing crystal. The existence of a measurable variation in chemical composition at structural faults is likely to be the cause of electroluminescence at the fault. This is because barriers presented to

electrons by stacking faults alone would be so thin as to be transparent to electrons. On the other hand an impurity profile around the fault could provide a suitably thick region in which recombination could take place.

3.3 X-ray Diffraction Experiments

Debye-Scherrer powder photographs were found to be of little use for the determination of the crystal structure of zinc sulphide crystals owing to phase transitions induced by grinding(33), which is necessary for preparation of the specimen. All X-ray work was therefore concentrated on transmission Laué single crystal photographs, the main purpose of which was to determine the orientation of the crystals. With this in mind Laué photographs were taken of many fast and slowly grown plates and also of several butterfly twins and whiskers. The photographs were interpreted by making gnomonographic projections of the crystals from them, using a specially made Wycoff rule. The c-axis was found to lie in the plane of the plates without exception. Since only two symmetrical Laué pictures are possibl (those in the <10.0> and <11.0> directions) perpendicular to the c-axis, oreintation was greatly simplified. The crystal was simply rotated to give a symmetrical photograph which was then recognised, by comparison with previously indexed ones, to be a <10.0> or <11.0> type. (Figures 3.1 and 3.2 are examples of photographs taken in these two directions.) The angle between the crystal face and the X-ray beam then immediately allowed the face to be identified and indexed.

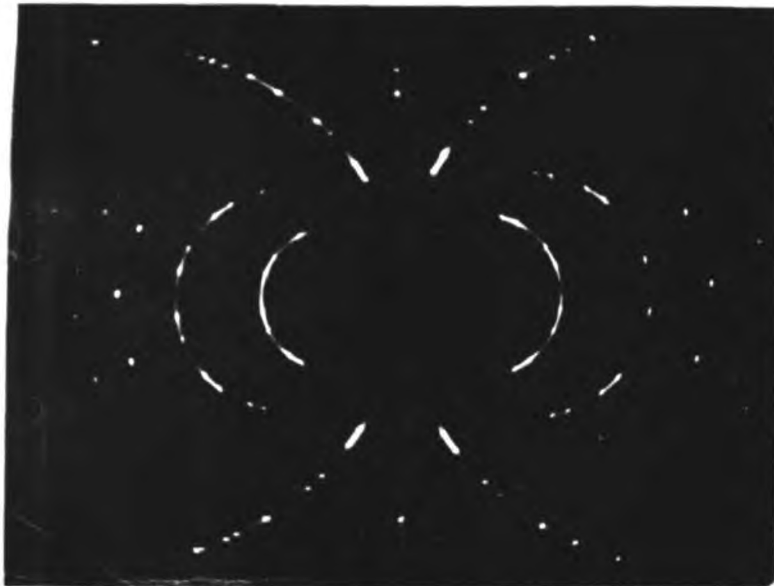

Figure 3.1 Transmission Laue X-ray photograph

< 10.0 > direction

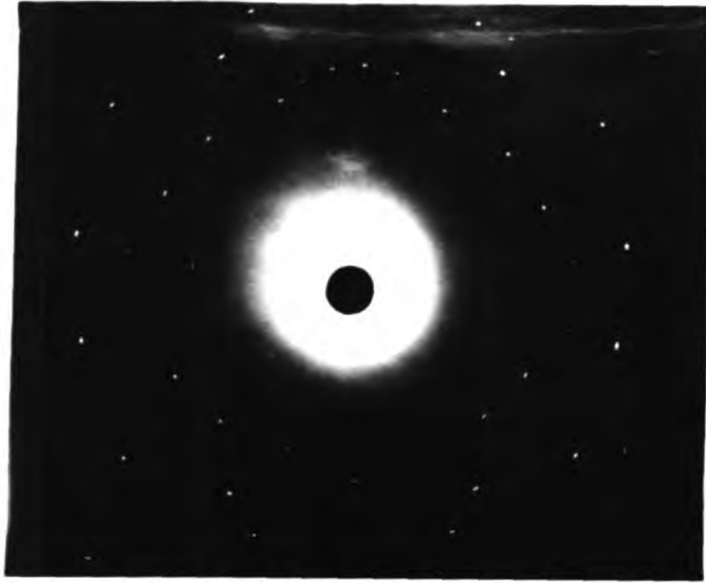

Figure 3.2(a) Transmission Laue X-ray photograph

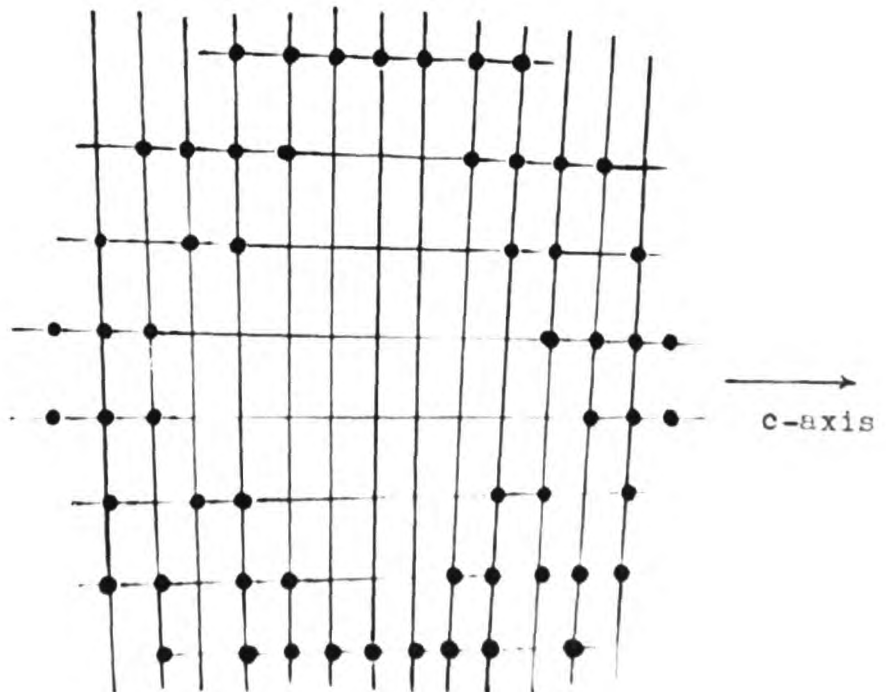

Figure 3.2(b) Gnomonic projection on (11.0) plane derived from the X-ray photograph above.

Slow growing plates were found by this means to have (10.0) and (12.0) type faces whilst fast growing plates were found to have (11.0) faces only. Similarly butterfly twins were found to have two (11.0) type faces. In both these faces the c-axis was found to be at 73° to the twin axis and in the plane of the twin face. All whiskers examined (10 to 40 micron across) had c-axes in the direction of the whisker axes. One whisker in particular had a basic pattern consistent with the c-axis being along the whisker axis but some of the spots were inconsistently intense (Figure 3.3). This was taken as a definite indication that growth on top of the whisker had begun in a different orientation from that of the whisker, but it was unfortunately not found possible to identify this other orientation with certainty.

The well-defined spots in the Laué photographs of the fast grown plates (Figure 3.2(a)) are indicative of structural purity and homogeneity. Where structural quality is poor the spots always appear blurred and streaky (c.f. Figure 3.1). The structural quality of the fast grown plates was therefore superior to that of the slow grown plates. Figure 3.2(b) illustrates the gnomonogram derived from figure 3.2(a). The zonal relationships between the planes are clearly shown by this diagram. The X-ray investigation of the crystals showed that the two sets of perpendicular striations present in some crystal were parallel and perpendicular to the c-axis. This made it easy to determine the direction of the c-axis by visual

Figure 3.3 Transmission Laue X-ray photograph of a whisker

inspection in many instances.

3.4 Optical Examination

Apart from superficial examination with a binocular viewer, a more detailed study of some crystals was made with a Union UMG-Bi polarizing binocular microscope. Structural changes in zinc sulphide are accompanied by changes in birefringence. A crystal viewed under crossed polaroids can be made to appear bright against a dark background. Any structural faults can then show up as dark bands against the light crystal.

Crystals showing no birefringence banding under crossed polaroids therefore have no long range structural faults. It was the case with many of the fast grown plates that the regions of uniform birefringence were much larger than the field of view of the microscope, so that they appeared as uniformly lit areas on a photograph. Such a photograph showing the edge of a crystal with uniform birefringence is shown in Figure 3.4. Obviously such a photograph imparts little useful information since the crystal as a whole is not visible. In general, therefore, microscope photographs were only taken of ribbons where both edges were visible at once although most microscope investigation was in fact devoted to plates.

Figures 3.5(a) and (b) show an unfaulted ribbon under unpolarized light in (a) and crossed polaroids in (b). The existence of one straight and one wavy edge is easily detectable. The "patches" on the crystal were identified as small pieces of other crystals held on by electrostatic attraction.

Figure 3.4 Part of a fast grown plate crystal viewed between crossed polaroids - magnification X50

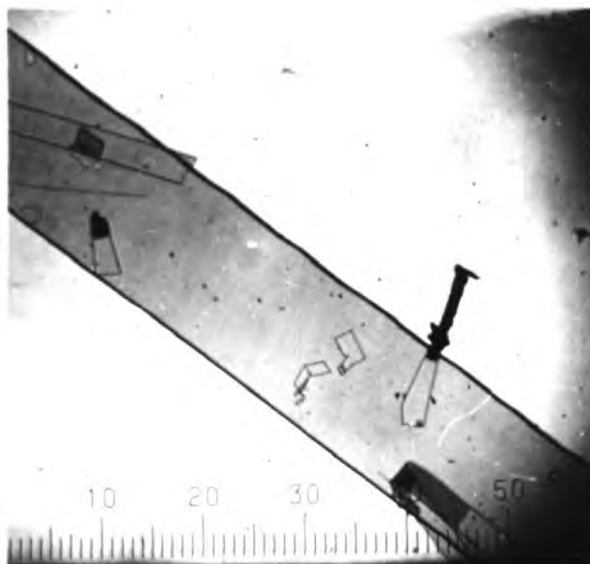

Figure 3.5(a) **Ribbon crystal viewed in unpolarized light (magnification X50)**

Figure 3.5(b) Ribbon crystal viewed between crossed polaroids (magnification X50)

Figure 3.6 shows a ribbon, containing both faulted and unfaulted regions, in unpolarized light. The lines are parallel to the c-axis in this case and correspond to regions where the ribbon surface changes direction. An interesting point to notice is that the c-axis is at 73° to the straight edge of the ribbon as in the butterfly twins. Figure 3.7 shows how a stacking faulted region appears under crossed polaroids. The perfectly straight doublet of dense black lines shows a region of high fault density. On either side of the doublet are very fine black lines parallel to the doublet representing much narrower regions where stacking is at fault. These lines are all perpendicular to the c-axis. The light and dark shading again represents changing surface direction.

The width of the doublet is of the order of 10 microns, i.e., approximately the width of a whisker. It could, therefore, represent the whisker from which the plate grew. The two black lines would then be the faults caused by a change in direction of the c-axis on either side of the whisker.

The above shows how faults could be detected optically. Many of the fast grown plates in fact showed very large areas without a trace of a fault. These could be of the order of a square centimetre, but were typically several millimetres square. This observation, together with the sharp X-ray diffraction spot patterns already described demonstrates the exceptionally good quality of the crystals grown.

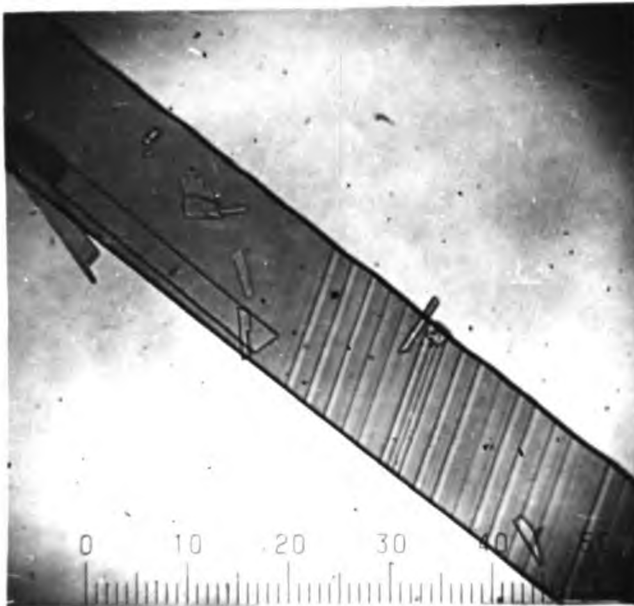

Figure 3.6 Ribbon crystal showing faulted and unfaulted regions (magnification X50)

Figure 3.7 Part of a plate crystal viewed between crossed polaroids, showing both stacking faults and changes in surface direction.

3.5 Spectrometric Observations

In addition to the direct observations so far described a very sensitive indirect method of characterizing a material is to observe its transmission spectrum of electromagnetic radiation at energies of the order of the band gap energy. In this way it is possible to detect the presence of energy levels within the forbidden band gap and so to identify structural and chemical impurities.

The optical band gap of zinc sulphide is about 3.7eV. The wavelength of electromagnetic radiation corresponding to this energy is 3250Å. The part of the spectrum of interest is therefore the visible and ultraviolet region.

A spectrometer using the Ebert configuration and based on a design originally used at Standard Telecommunications Laboratories, Harlow, Essex, was available for measuring the transmission spectrum of crystals. It was unfortunate that the only grating available was designed to work in the infra red region of the spectrum in third order. Owing to the presence of overlapping orders this grating could only be used in first order for the ultraviolet part of the spectrum. The result was that the signal to noise ratio of the output was very poor so that measurements of the absorption of crystals were not very accurate.

3.5.1 Transmission Measurements

Because of the poor signal to noise ratio of the system, transmission measurements were limited to room temperature and

the reference and transmitted intensities were measured consecutively for small ranges of the spectrum at a time. Crystals were mounted electrostatically on black perspex in front of the input slit of the spectrometer. A hole in the perspex under the crystal allowed the light to pass unimpeded to the spectrometer. The input slit was stopped down to make sure that only light passing through the centre of the crystal and the hole in the perspex entered the spectrometer.

Pilkington glass filters were used at the spectrometer input to cut down the band width of the incident light in an effort to increase the signal to noise ratio.

Figure 3.8 shows the transmission of a thin clear plate crystal as a function of energy around the band gap energy. The low energy transmission tends to a limit of approximately 71% due to the high refractive index of zinc sulphide.

The ratio of transmitted to incident power for a parallel sheet is given by[1e].

$$T = \frac{P_t}{P_i} = \frac{(1-R)^2}{\exp(Kd) - R^2\exp(-Kd)} \qquad 3.1$$

$$\text{where } R = \frac{(n-1)^2 + k^2}{(n+1)^2 + k^2} \qquad 3.2$$

n is the real part of the refractive index

k is the extinction coefficient

K is the absorption coefficient

and d is the sample thickness

if interference effects are neglected.

Figure 3.8

Optical Transmission Spectrum of a ZnS Crystal

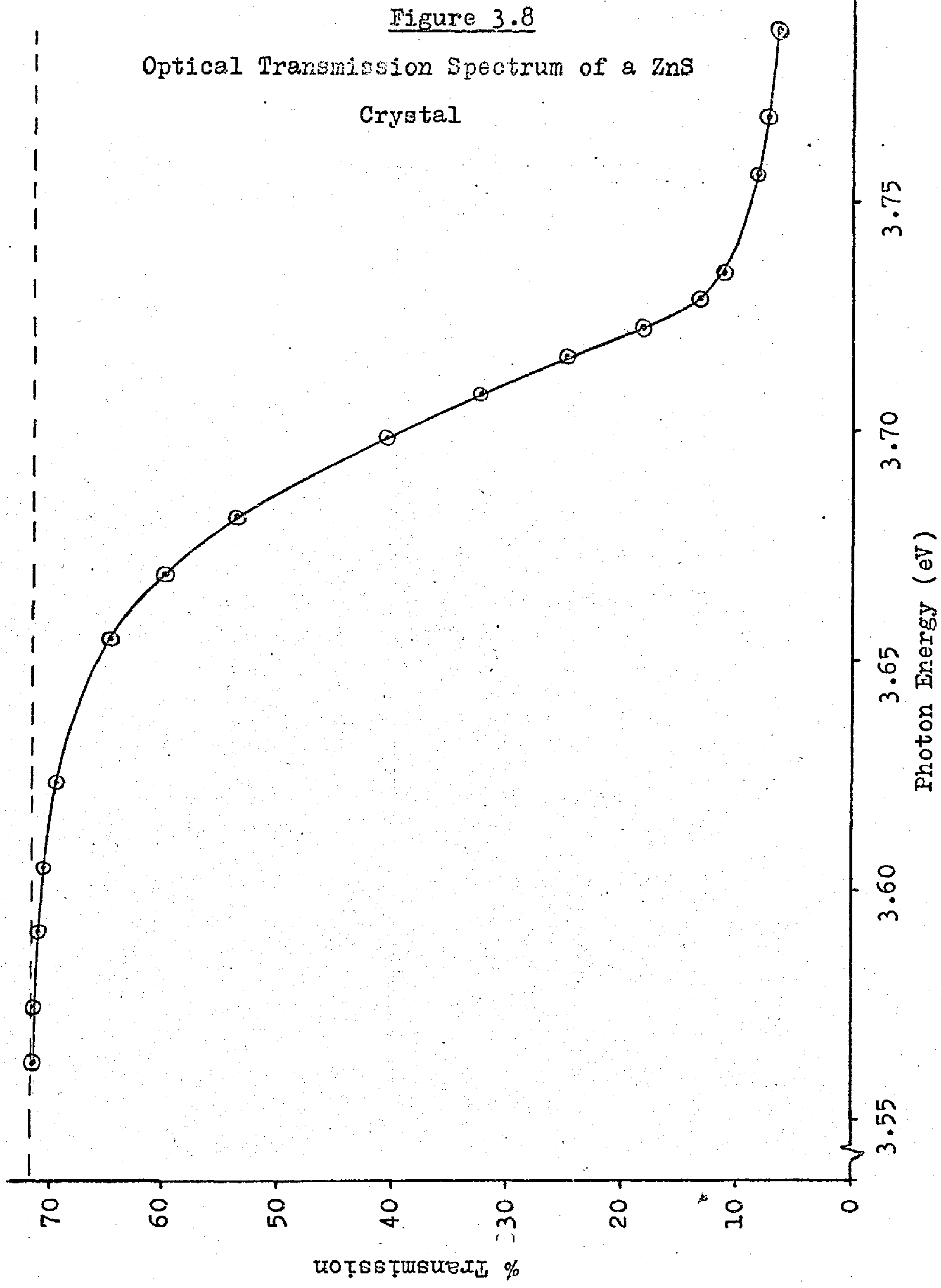

$$\text{Now } K = \frac{4\pi k}{\lambda} \qquad \text{———} 3.3$$

where λ is the wavelength of the incident radiation and $n = 2.37$ for zinc sulphide.

$$\therefore k^2 < \frac{(n-1)^2}{10}$$

if $k < 0.434$

i.e. if $K < 10^5 cm^{-1}$

R is therefore dominated by n for all likely values of K.

$$\therefore R = \left(\frac{1.37}{3.37}\right)^2 = .165$$

$$R^2 = .0272$$

$$(1-R)^2 = .697$$

Thus, from equation 3.1 the maximum transmission is approximately 71% as found experimentally.

Let $\exp(Kd) = x$

Then from equation 3.1

$$x^2T - R^2T - (1-R)^2.x = 0 \qquad \text{———} 3.4$$

$$\text{i.e. } x = \frac{(1-R)^2 + \sqrt{(1-R)^4 + 4R^2T^2}}{2T} \qquad \text{———} 3.5$$

Since $T \leqslant 0.7$

$$4R^2T^2 \leqslant .053$$

and $(1-R)^4 = .486$

$$\therefore \text{ in general } 4R^2T^2 \lesssim \frac{(1-R)^4}{10}$$

near the band gap energy

$$\therefore x = \frac{(1-R)^2\left(1 + \frac{R^2T^2}{(1-R)^4}\right)}{T} \qquad \text{———} 3.6$$

$$\text{or } Kd = \ln(1-R)^2 + \ln\left[1 + \frac{R^2T^2}{(1-R)^4}\right] - \ln T$$

$$= \ln 0.697 + \ln\,(1 + 0.056T^2) - \ln T \qquad \text{———— } 3.7$$

When T approaches its upper limit, 3.7 reduces to

$$Kd = \ln\left(1 + \frac{0.716 - T}{T}\right) \approx \frac{0.716 - T}{T} \qquad \text{———— } 3.8$$

Equation 3.7 was used to derive K from the data of figure 3.8 and the results are plotted as a function of energy in figure 3.9. The thickness of the crystal was measured with a Talyserf to be 4μm.

The high energy levelling off of K in figure 3.9 would appear to be at a rather low value of K ($5\text{x}10^3\text{cm}^{-1}$). However, this is not surprising since the intensity of the absorbed beam at these high absorptions was of a similar magnitude to the intensity of the scattered light from the spectrometer. The background light level therefore masked the effects of a further increase in absorption coefficient.

Determination of the value of K on the low energy side of the absorption edge was limited by the uncertainty in the difference between the actual transmission and the maximum possible transmission due to experimental error. This can be seen from equation 3.8. For this reason, the lowest value of K as shown in figure 3.9 is 75.

The Ebert spectrometer was used to measure the absorption of crystals over the energy range 1.86eV to 3.8eV. Below the band gap energy, the transmission of the crystals was constant and equal to the maximum possible, within the limits of

Figure 3.9

Absorption coefficient of ZnS versus Photon Energy

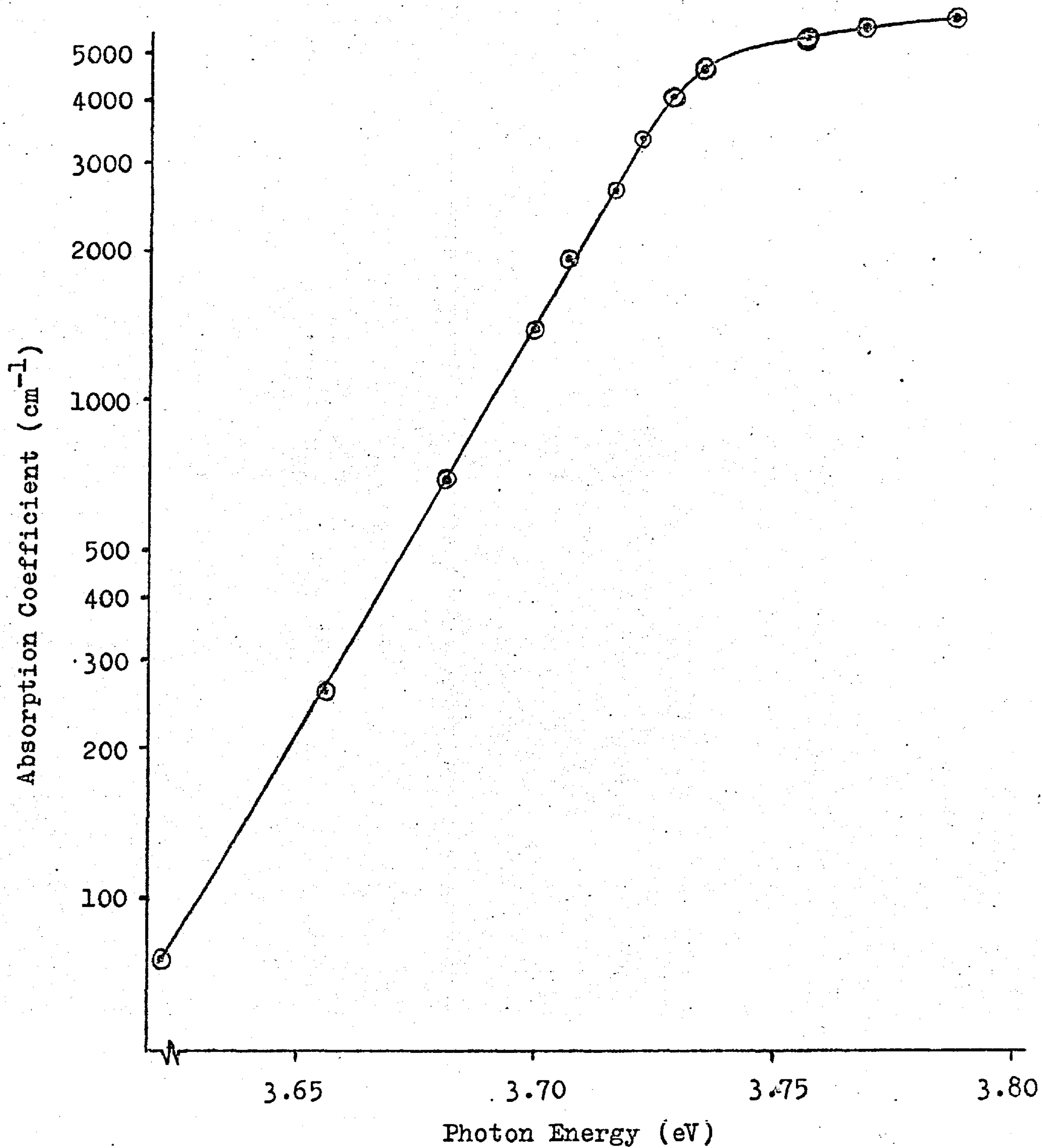

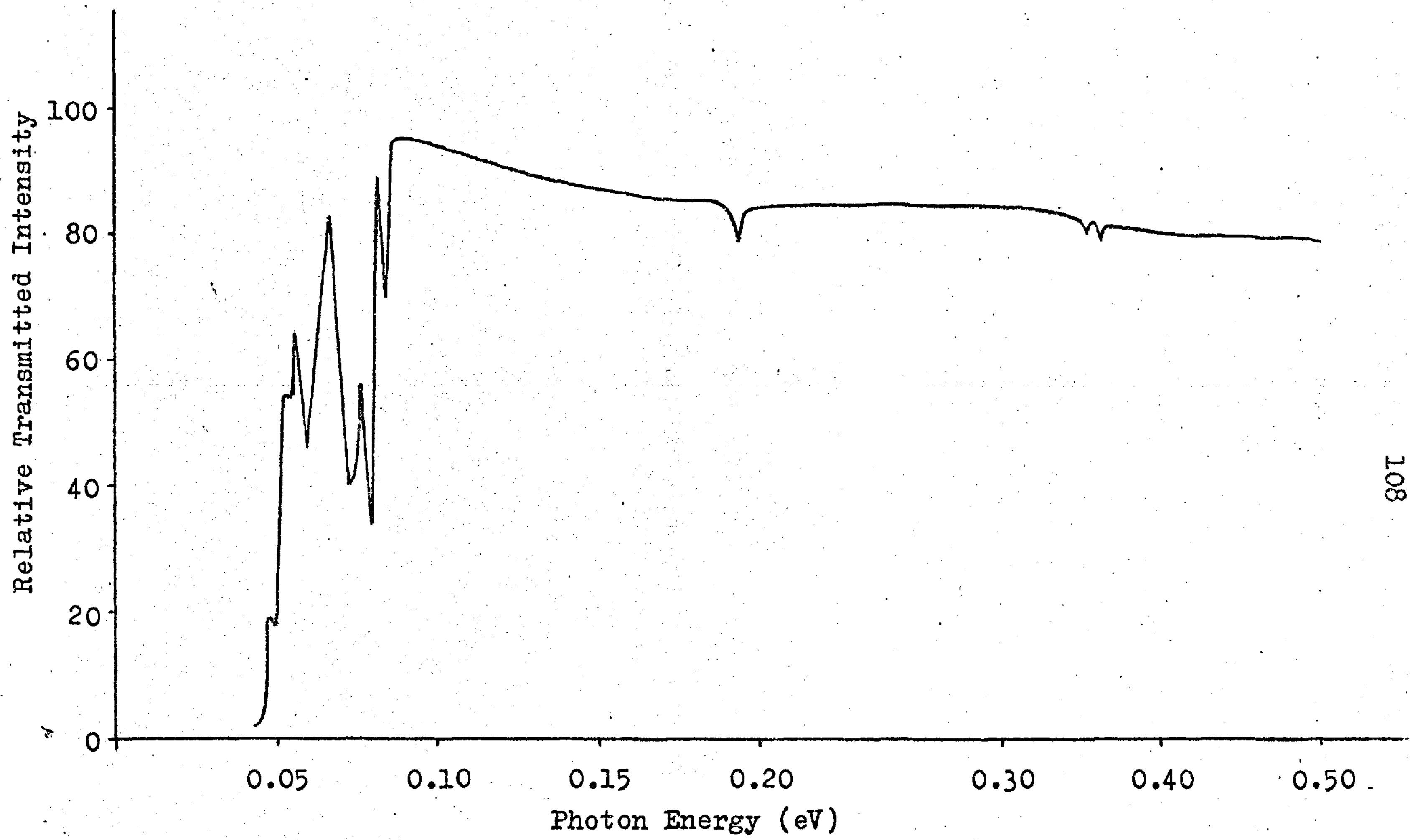

Figure 3.10 Infrared Transmission Spectrum of a ZnS crystal.

experimental error. Since 1.86eV corresponds to about half the band gap energy, this was taken to indicate that the impurity content of the crystals was very small indeed.

Infra red transmission measurements were made by the Analytical Services Laboratory at Imperial College, for energies in the range 0.5eV to 0.05eV. Figure 3.10 shows the results obtained. Two very small absorptions were found at 0.354 and 0.364eV and one small absorption at 0.192eV was also found. Large absorptions around 0.05eV were also found but these are explicable in terms of phonon absorption(34). The small absorption peaks indicate that there may be filled levels just below the conduction band edge(1f), but the small size of the peaks indicates that these levels are few in number.

3.6 General observations

A few concluding observations are now made on the direct physical and chemical characterization of the material. It was found that whiskers could be bent around a radius as small as 4 mm. in some cases without fracture. This represents an elastic strain of 0.5 per cent for 40 micron diameter whiskers which demonstrates their high structural purity. Plates and ribbons were found to cleave easily parallel to the c-axis so bending experiments failed because the direction of the c-axis in these crystals made it virtually impossible to avoid this cleavage. This cleavage plane (10.0) is accepted as normal in ZnS(1g) and does not indicate a faulty structure.

It was observed that the crystals were electrically charged when removed from the growing tube. This charge, in the cases of the highly perfect plates and ribbons, was usually held at least for several weeks with no sign of its leaking away. This suggests that the resistivity of the crystals was very high and therefore that the impurity concentration was relatively low.

Both the starting material charge and the final crystals were irradiated with wide band ultraviolet light. Only the starting charge with the high chlorine content showed any luminescence visible to the naked eye in a dark room; the fluorescence was a bright blue colour. The lack of fluorescence from the crystals indicates either that they contained too low an impurity concentration to show fluorescence or that they contained a "killer" centre in sufficient concentration to prevent luminescence. In view of the chemical analyses results and the fact that the crystals showed no sign of colouration this latter alternative is ruled out.

All observations, therefore, point to high structural and chemical purity.

CHAPTER 4

CONTACTS TO ZINC SULPHIDE

4.1 The Theory of contacts to semiconductor materials

4.1.1 General description of a metal-semiconductor contact

It is found experimentally that there is, in general, only a small potential barrier at the interface between metal electrodes and covalent semiconductors such as silicon and germanium and that this barrier varies little from one metal to another. On the other hand, metal contacts to ionic semiconductors (such as zinc sulphide) are found to present large barriers (in general) to the passage of current carriers and, furthermore, these barriers are found to vary from one metal to another. The reason for this difference appears to lie with surface states. At the surface of a semiconductor the electronic wavefunctions meet an abrupt discontinuity in lattice periodicity. This has the effect of producing localized energy states in the forbidden energy gap. In covalent semiconductors the electronic wavefunctions are long range (by definition) while in ionic semiconductors wavefunctions are highly localized (also by definition). Thus the surface presents a much greater disturbance to the covalent wavefunctions than to the ionic wave functions. The surface states, therefore, extend deep into the forbidden energy gap in silicon and germanium, but remain very close to the band edges in materials such as zinc sulphide. The high densities of surface states in germanium and silicon therefore act as a reservoir of surface charge which electrostatically screens the bulk material from the metal contact. No such screening exists in zinc sulphide. The charge transfer

which must occur when the metal is joined to the semiconductor (to equalize the Fermi levels for thermal equilibrium) therefore causes an accumulation or depletion layer to be formed in materials such as zinc sulphide.

Contacts to zinc sulphide are often described as ohmic. This description is phenomenological and does not indicate what is actually happening at the contact. It merely states that the voltage drop across the contact is negligible in comparison with the voltage drop across the bulk of the material.

From a theoretical point of view it is more satisfactory to describe contacts in terms of what they actually do. We shall therefore refer to contacts as electron injecting, hole injecting, tunnelling, etc. It will be seen that in general a majority carrier injecting contact will be "ohmic".

4.1.2 Carrier concentrations and conductivity in zinc sulphide

It is interesting to note the values of

$$N_c = 2\left(\frac{2\pi m_e kT}{h^2}\right)^{\frac{3}{2}} \quad \text{and}$$

$$N_v = 2\left(\frac{2\pi m_h kT}{h^2}\right)^{\frac{3}{2}} \quad \text{and}$$

$$n_i^{\,2} = N_c N_v \exp\left(\frac{-\mathcal{E}_g}{kT}\right) = n.p \qquad 4.1$$

for zinc sulphide where N_c, N_v are the effective densities of states at the conduction and valence band edges and n_i is the

intrinsic carrier concentration (see for instance, S. Wang, Solid State Electronics, McGraw Hill, page 142). n and p are the specific carrier concentrations in a particular sample and $\mathcal{E}_g$ is the band gap energy. Complete data could not be found for m_e, m_h for the evaluation of N_c and N_v; however, it was considered sufficiently accurate to use the data listed in reference 1h.

The values of N_c and N_v are then:

$$\left.\begin{aligned} N_c &= 7.0 \times 10^{24} m^{-3} \text{ at } 300°K \\ N_c &= 9.1 \times 10^{23} m^{-3} \text{ at } 77°K \end{aligned}\right\} \qquad 4.2$$

$$\left.\begin{aligned} N_v &= 1.5 \times 10^{25} m^{-3} \text{ at } 300°K \\ N_v &= 2.0 \times 10^{24} m^{-3} \text{ at } 77°K \end{aligned}\right\} \qquad 4.3$$

The energy gap of zinc sulphide varies according to the method of measurement. However 3.6 eV seems to be the best available estimate for $\mathcal{E}_g$ at room temperature in connection with electrical measurements[1j].

$$\therefore\ n_i^2 = 5 \times 10^{-11} m^{-6} \text{ at } 300°K \qquad 4.4$$

$$n_i^2 = 5 \times 10^{-188} m^{-6} \text{ at } 77°K \qquad 4.5$$

Equations 4.4 and 4.5 show that the intrinsic carrier concentration in zinc sulphide is negligible under all likely conditions. Even at 600°K, n_i is of the order of $10^{10} m^{-3}$. Also, in view of equations 4.4 and 4.5, equation 4.1 shows that conduction can be by one type of carrier only in a given crystal in

thermal equilibrium. Thus, if electron and hole conduction are to occur simultaneously, then excess carriers must be introduced.

There is little evidence that zinc sulphide can be doped to give it significant p-type conductivity. It appears to be a condition of thermodynamic equilibrium that any acceptor impurity dissolved in zinc sulphide is more than fully compensated by donors. These donors can be either another impurity such as chlorine or aluminium, or else anion vacancies. Georgobiani and Steblin[35] have reported p-n junctions in zinc sulphide, but it seems likely that their p region consisted of a second phase, possibly Cu_2S, precipitated from the zinc sulphide after excess copper had been diffused in at high temperature[1k]. It is also fairly difficult to produce high conductivity n-type zinc sulphide because of its autocompensation tendency. Cation vacancies are produced automatically to compensate for the presence of donors. Nevertheless, 1 to 10 ohm cm room temperature resistivity zinc sulphide has been reported[36].

In view of the above only n-type zinc sulphide will be considered.

A survey of the literature shows the electron mobility in zinc sulphide to be of the order of $0.02 m^2/Vs$ (e.g. references 1j and 1m) or possibly much higher for very pure samples. The conductivity is given by:

$$\sigma = e\mu_e n \qquad (4.6)$$

where μ_e is the mobility of electrons and e is the electronic

charge.

Since $n = N_c \exp\left(-\frac{\mathcal{E}_c - \mathcal{E}_f}{kT}\right)$ ——————— 4.7

where $\mathcal{E}_c$ is the conduction band edge energy and $\mathcal{E}_f$ is the Fermi energy, we may calculate n and $\mathcal{E}_f$ for given values of conductivity, using $\mu_e = 0.02 m^2/Vs$. Table 4.1 is a list of n and $\mathcal{E}_f$ for various conductivities at 77°K and 300°K. The values of $\mathcal{E}_f$ are referred to the conduction band edge. It can be seen that the Fermi level lies relatively close to the conduction band for any significant conductivity and that, even at very low conductivities, it is nowhere near the centre of the band gap.

4.1.3 Metal-zinc sulphide junctions

Bearing Table 4.1 in mind we can now construct band diagrams for possible metal to zinc sulphide junctions. We shall first assume that the zinc sulphide is n-type. Thus a majority carrier injecting contact injects electrons.

Figure 4.1 shows a simple model for such a contact. A metal is chosen so that the metal work function ϕ_m is less than the zinc sulphide work function and preferably less than the electron affinity of zinc sulphide χ_{ZnS}. The zinc sulphide Fermi level is then at a lower energy than that of the metal. When the two materials are brought together the metal contains more electrons at higher energies than does the zinc sulphide. Electrons therefore diffuse into the surface of the zinc sulphide creating an opposing potential barrier ϕ_b as they do so. Nett current flow ceases when the drift current caused by the space charge exactly balances the diffusion current.

TABLE 4.1

σ	n	$\mathcal{E}_f(77°K)$	$\mathcal{E}_f(300°K)$
$(\Omega\,m)^{-1}$	m^{-3}	eV	eV
10^2	3.13×10^{22}	0.0223	0.140
1	3.13×10^{20}	0.0524	0.259
10^{-2}	3.13×10^{18}	0.0829	0.378
10^{-4}	3.13×10^{16}	0.114	0.496
10^{-6}	3.13×10^{14}	0.144	0.615
10^{-8}	3.13×10^{12}	0.175	0.735
10^{-10}	3.13×10^{10}	0.205	0.853
10^{-12}	3.13×10^{8}	0.236	0.972

$\mathcal{E}_f$ is referred to the conduction band edge

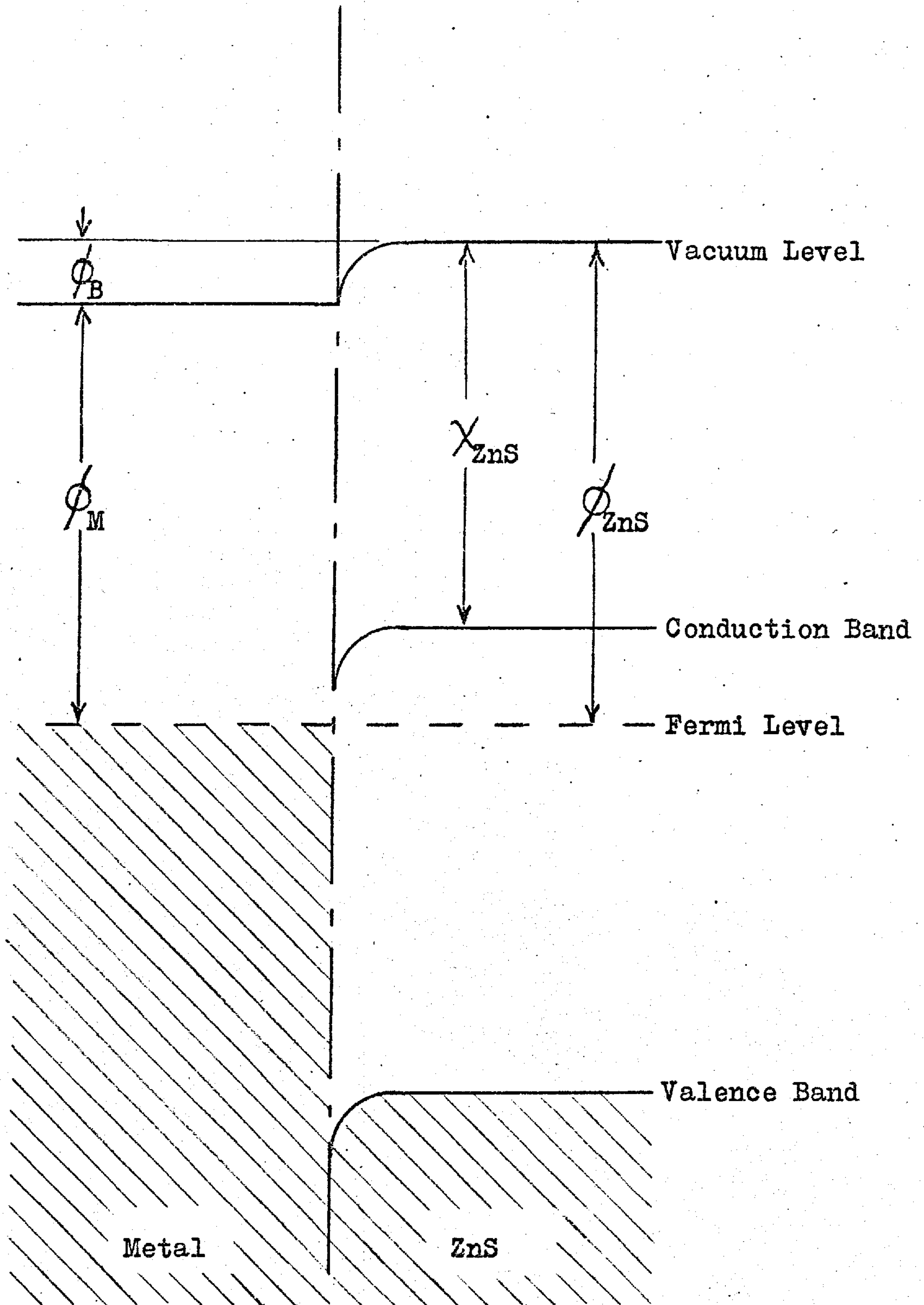

Figure 4.1 Electron Injecting Contact.

Four points may be noted from Figure 4.1:

(i) The potential barrier causes the Fermi level in the zinc sulphide to approach the conduction band at the interface.

(ii) The flow of charge is such as to cause an accumulation of free carriers at the interface.

(iii) The space charge is provided by mobile charges.

(iv) The accumulated charge carriers are the same type as the majority carriers in the bulk of the zinc sulphide.

Such a contact would provide a good source of electrons for conduction. It would also act as a good sink for electrons leaving the zinc sulphide. The differential resistance of such a contact would necessarily be small because of the relatively high majority carrier density at the interface. The contact would therefore be termed "ohmic".

It is unfortunate that this contact cannot exist in practice for zinc sulphide (although it may do for other materials e.g. CdS) since the electron affinity χ_{ZnS} of zinc sulphide is too small to allow the condition that $\phi_m < \chi_{ZnS}$ to be fulfilled*. Indeed, it is unlikely that ϕ_m is smaller than ϕ_{ZnS} for any real crystal.

The electron affinity of cadmium sulphide has been

---

* Certain alkali metals such as sodium or rare earths such as praseodimium have low enough work functions. However, alkali metals are too reactive to make useful contacts and the rare earths are too expensive to be practical.

evaluated by Bujatti[37] and Goodman[38] using both optical and electrical techniques to determine the contact barrier ϕ_b for various different metal contacts. Both agree that χ for CdS $\simeq$ 4 eV. Aven and Mead[36] plotted contact barrier height against the electronegativity of the contact material for both CdS and ZnS and deduced that the electron affinity of zinc sulphide is about 1.1 eV less than that for cadmium sulphide. This puts the value of χ_{ZnS} at about 3eV or just less. Since the work functions of suitable metallic contacts lie between 4 and 5eV the problem is obvious.

Fortunately it appears that the above restrictive condition on ϕ_m is not necessary in practice. Kröger et al.[39] proposed a model to account for the fact that contacts with ohmic characteristics could be made with almost any metal to CdS, provided the crystal was first exposed to electron or ion bombardment. The same model was later used by Blount[40] et al. to explain results for indium-gallium alloy contacts to high resistivity zinc sulphide. Figure 4.2 shows the metal to be used for the contact with ϕ_m = 4.5 eV and high resistivity zinc sulphide (10^{10} Ω m) with χ_{ZnS} = 3eV. Figure 4.2(b) shows the same metal and the zinc sulphide with some of the metal diffused into the surface to dope it to a lower resistivity. Finally, Figure 4.2(c) shows the barrier which is formed by bringing the metal and zinc sulphide together. The Fermi levels are brought to the same potential energy by electrons flowing out of a very narrow region of the heavily doped surface causing a thin depletion

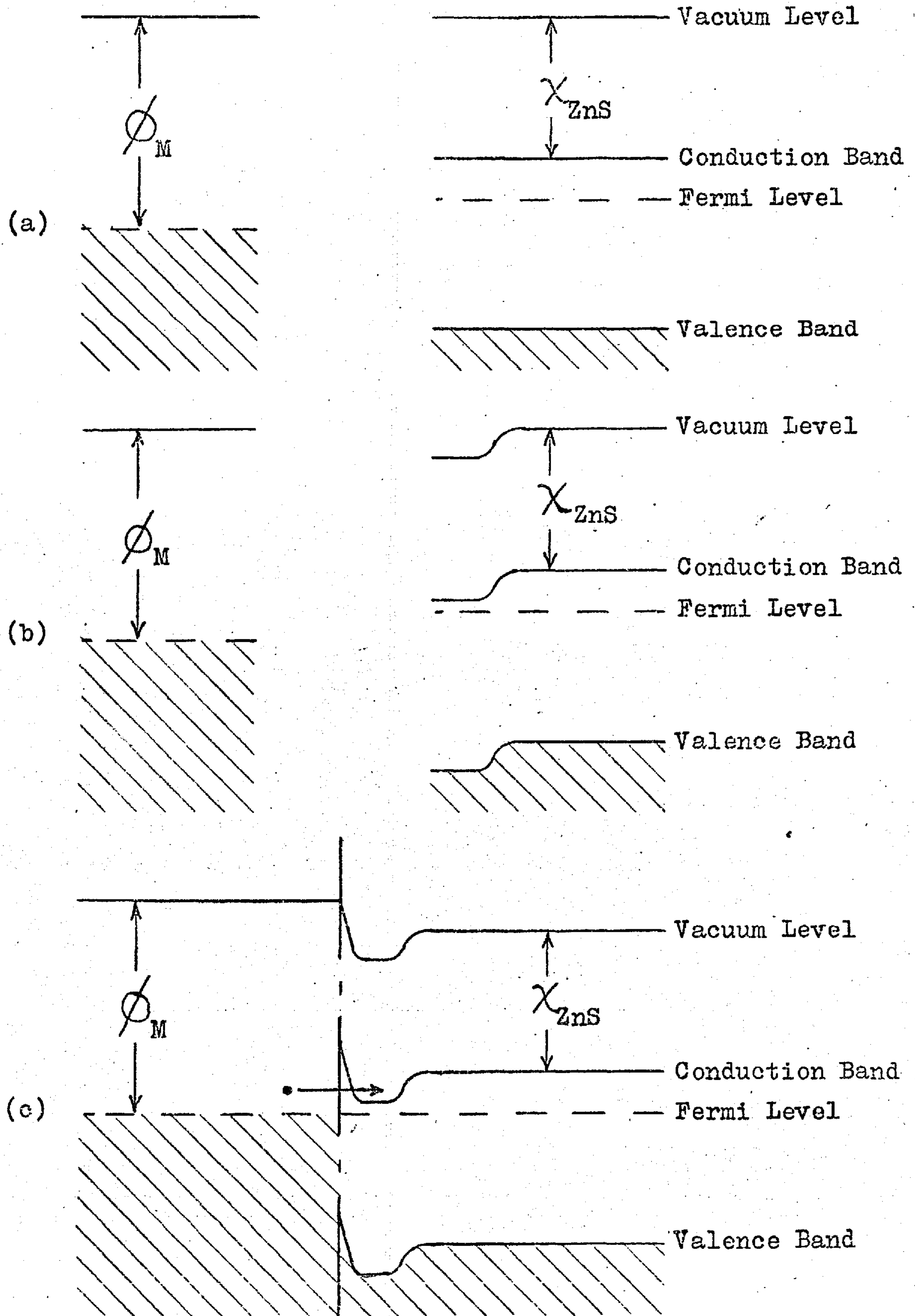

Figure 4.2 Formation of a tunnelling electron injecting contact.

layer to be formed at the surface. The contact acts as an electron injector if the depletion region is thin enough to allow electrons to pass through the barrier by tunnelling or impurity band conduction. We may analyse the shape of the potential barrier in the depletion region if we make some simplifying assumptions. We assume first that the contact metal is diffused into the zinc sulphide to a great enough depth to prevent the two space charge regions (depletion and accumulation) from interacting to a significant degree. The depletion region can then be considered as a normal contact barrier between high conductivity bulk zinc sulphide and the contact metal. Suppose that, in the zinc sulphide there are N_a acceptor states and N_d donor states created mainly by the diffusion of the contact material. Typical donor contact materials Al, Ga, In, produce shallow donor levels[18] with an ionization energy of between 0.01 and 0.02 eV. Since $\mathcal{E}_f$ is much greater than 0.02 eV in the depletion region near the interface, we may safely assume that all the above donors are ionized over the significant part of the barrier. We further assume that no other donor levels contribute significantly to any of the calculations.

Since the material is n-type even at the metal zinc sulphide interface we assume that all acceptors are ionized. The mechanism proposed in reference 40 for the diffusion of the contact material results in an abrupt change in doping levels for good contacts. It is therefore possible to consider the impurity profile in the material to be rectangular in shape;

i.e., there exists a heavily doped, constant impurity concentration, surface layer in the zinc sulphide. This allows us to assume that $N_d - N_a$ is constant in the barrier region.

Figure 4.3 shows the relevant part of the junction with the variables labelled.

The space charge in the depletion region is given by

$$\rho(x) = e(N_d - N_a - n)$$

$$= e\left\{N_1 - n_o \exp\left(-\frac{e\phi_b - eV(x) - \mathcal{E}_{f_o}}{kT}\right)\right\} \qquad 4.8$$

where $N_1 = N_d - N_a$

n_o = bulk equilibrium electron concentration in the heavily doped zinc sulphide.

$\mathcal{E}_{f_o}$, ϕ_b, $V(x)$ are as labelled in Figure 4.3

When $x = x_b$, $\rho = 0$, $eV(x) = e\phi_b - \mathcal{E}_{f_o}$

i.e., $N_1 = n_o$

$$\therefore \rho(x) = eN_1\left\{1 - \exp\left(-\frac{e\phi_b - \mathcal{E}_{f_o} - eV(x)}{kT}\right)\right\} \qquad 4.9$$

But $\exp\left(-\frac{e\phi_b - \mathcal{E}_{f_o} - eV(x)}{kT}\right) \ll 1$

except for $x \simeq x_b$

$\therefore$ $\rho(x) \simeq eN_1$ over practically the whole depletion region.

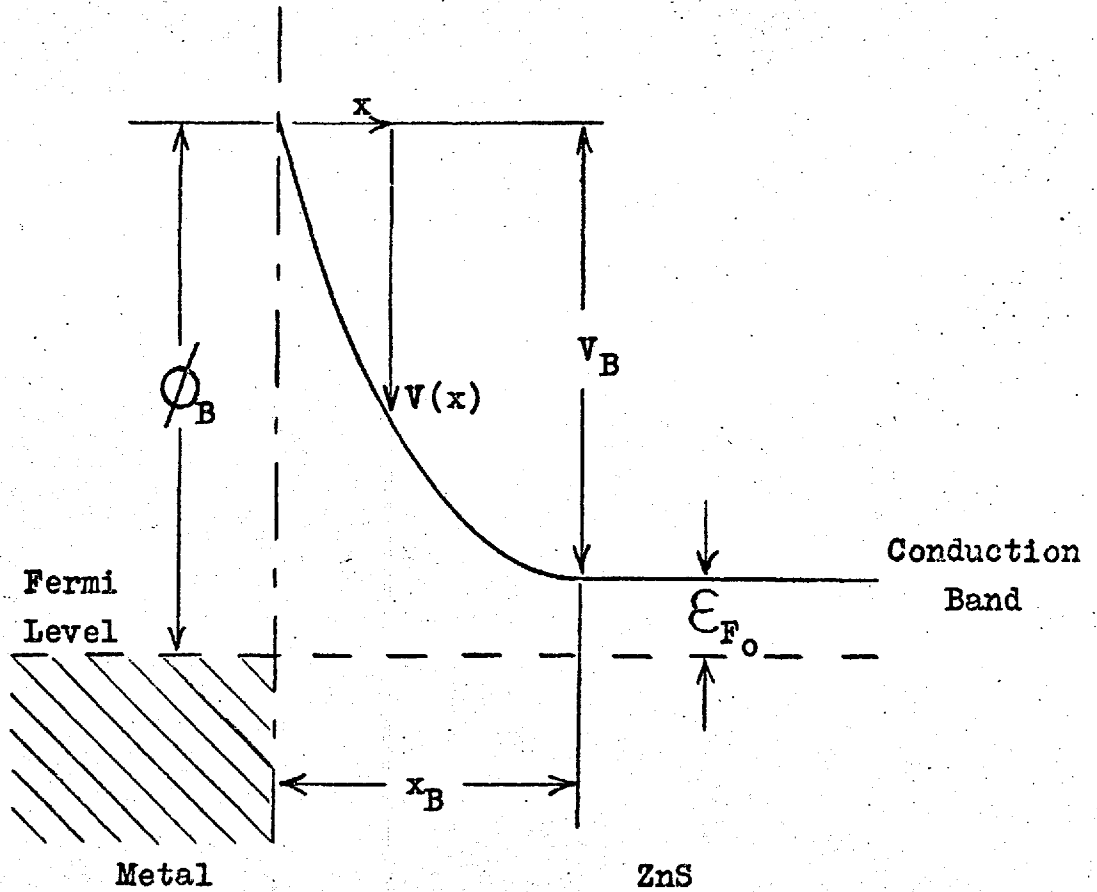

<u>Figure 4.3</u> Depletion layer at a Metal-ZnS interface.

Using Poisson's equation $\frac{\partial^2 V}{\partial x^2} = - \frac{\rho}{\epsilon_r \epsilon_o}$

when ϵ_r is the relative permittivity of zinc sulphide.

$$\frac{\partial^2 V}{\partial x^2} = - \frac{eN_1}{\epsilon_r \epsilon_o} \qquad \text{4.10}$$

Integrating equation 4.10 yields

$$V(x) = - \frac{eN_1}{2\epsilon_r \epsilon_o} x(x - 2x_b) \qquad \text{4.11}$$

Thus $$V_b = \frac{eN_1 x_b{}^2}{2\epsilon_r \epsilon_o} \qquad \text{4.12}$$

We may now eliminate V_b from equation 4.12 and write

$$eV_b = e\phi_m - e\chi - \mathcal{E}_{f_o} = \frac{e^2 N_1 x_b{}^2}{2\,\epsilon_r \epsilon_o} \qquad \text{4.13}$$

$$\text{or } x_b = \sqrt{\frac{2\epsilon_r \epsilon_o\,(e\phi_m - e\chi - \mathcal{E}_{f_o})}{e^2 N_1}} \qquad \text{4.14}$$

Thus x_b is proportional to $\frac{1}{\sqrt{N_1}}$ since we may regard $\mathcal{E}_{f_o}$ as approximately constant over a wide range of N_1.

Putting some numerical values into equation 4.14 we take:

$e\phi_m = 4.5$ eV

$e\chi = 3$ eV

$\mathcal{E}_{f_o} = 0.2$eV (roughly)

$\epsilon_r \epsilon_o \simeq \frac{8.32}{4\pi x 9x10^9} = 7.35 \times 10^{-11}$ farads/metre

$$\text{then } x_b = \frac{3.46 \times 10^4}{\sqrt{N_1}} \text{ m} \qquad \text{———————————— } 4.15$$

where N_1 is expressed in m^{-3}
For x_b to be of the order of 100Å, N_1 must be about 10^{25} m^{-3}. If the proposed mode of operation of the contact is correct then x_b must necessarily be less than or of the order of 100Å. The requirement of high impurity concentration in the barrier region increases the probability of conduction via impurity bands and so aids current conduction through the barrier. In addition the zinc sulphide must become degenerate at x_b since N_1 exceeds N_c.

An impurity concentration of greater than 10^{25} atoms per m^3 corresponds to an average impurity separation of less than 50Å. With this separation between impurity atoms we see that the charge concentration cannot strictly be treated as continuous for barriers as narrow as 100Å. Equation 4.14 is therefore not applicable to very thin barriers and indeed the band diagram of Figure 4.3 loses its meaning when the apparent exhaustion barrier embraces only a few atomic distances. However, we might expect the electron wavefunctions of impurity atoms to overlap for concentrations of greater than 10^{25} m^{-3} bearing in mind the dielectric medium. Therefore the potential barrier as such, must effectively be small or non-existent. All the above considerations lead us to the conclusion that for high enough doping level the exhaustion barrier ceases to exist as a physical impediment to current flow. The contact of Figure 4.2 is therefore

electrically equivalent to that of Figure 4.1. The nature of the accumulation barrier between the highly doped surface layer and the bulk material will be discussed later when the switching properties of the crystals are considered. It will suffice to say here that these barriers have a sharp initial rise of a few kT in energy after which there is a very slow energy rise with distance due to the much reduced free carrier concentration. The final barrier height is decided either by the doping level of the bulk material or by boundary conditions imposed by crystal dimensions whichever is the more stringent requirement.

4.1.4 Hole injecting contacts

The problem of hole injection is rather more difficult than electron injection. At first sight one might suppose that there could be an analogous hole injecting contact to the electron injector shown in Figure 4.1. Figure 4.4 shows how the contact might look in terms of band structure. It can be seen that a suitable metal would have to have a very large work function indeed. Using Table 4.1 as a guide it appears that there would not exist a significant number of holes in the valence band unless the Fermi level were closer than leV to it. If a hole reservoir of any size is to be built up, therefore, the metal work function must be greater than 5.6 eV. No such metal exists. The discussion of a contact such as shown in Figure 4.4 will therefore be taken no further.

It is also easy to see that no hole injecting contact analogous to the electron injector of Figure 4.2 can exist

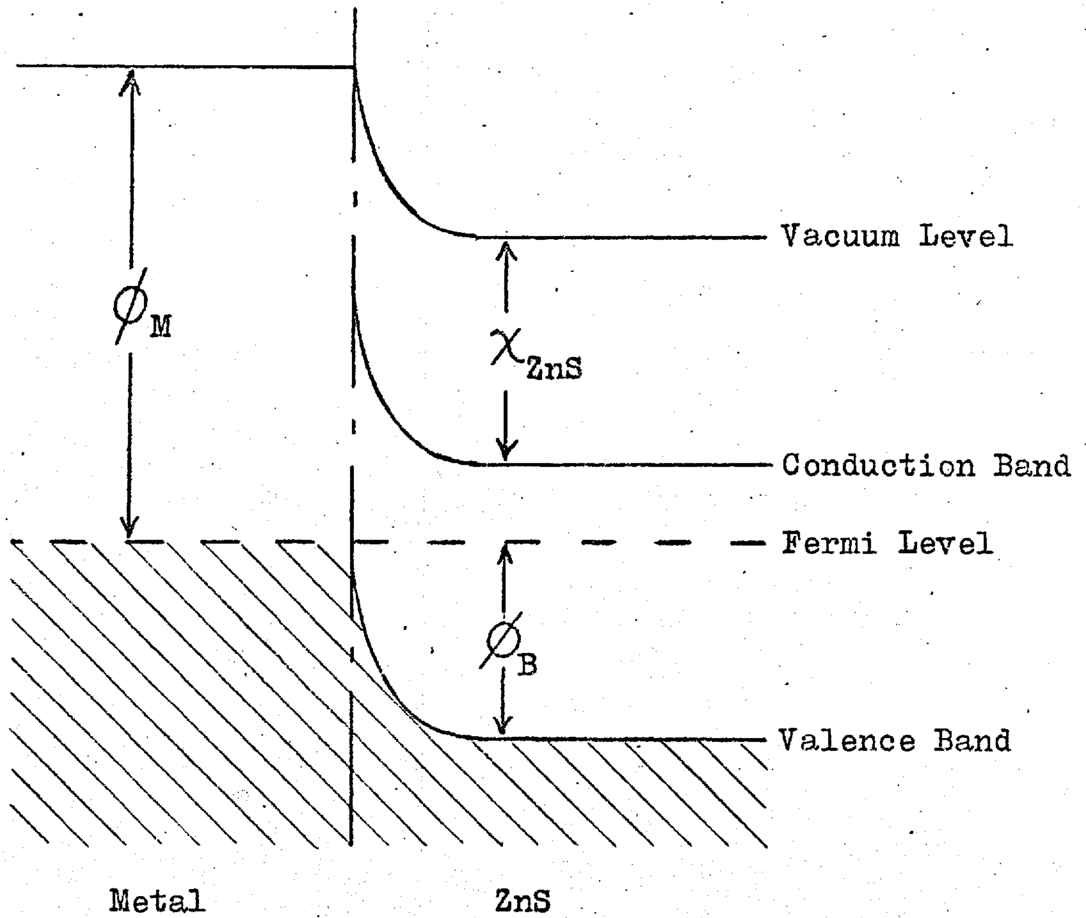

Figure 4.4 Hole Injecting Contact.

either since it is found impossible to dope zinc sulphide p-type to any measurable degree. We are therefore left with only two other possibilities. One is to use some highly p-type semiconducting material and to form a heterejunction. The other is to try to tunnel holes into the valence band through a very wide band gap insulator.

Consider first the heterejunction. A very heavily doped p-type semiconductor is used so that a copious supply of holes is assured. Zinc sulphide is known to be n-type. There are therefore two distinct situations, where the p-type contact has a high or a low work function. Figure 4.5 shows these two possibilities. The low work function p-type semiconductor contact is illustrated in figure 4.5(a). The barrier to hole injection into the valence band is very much greater than the barrier to electron extraction from the conducting band. One would therefore normally expect this contact to extract electrons in preference to injecting holes when biased positively, because of this difference in barrier heights. If, however, virtually no free electrons were present in the zinc sulphide then the contact might be capable of injecting holes at high biasing voltages. The hole current would, however, necessarily be small and the contact resistance high which is just the condition to avoid for efficient injection.

Figure 4.5(b) shows a high work function p-type semiconductor contact. In this case the barrier to electron extraction from the conduction band is formed by the electron depletion

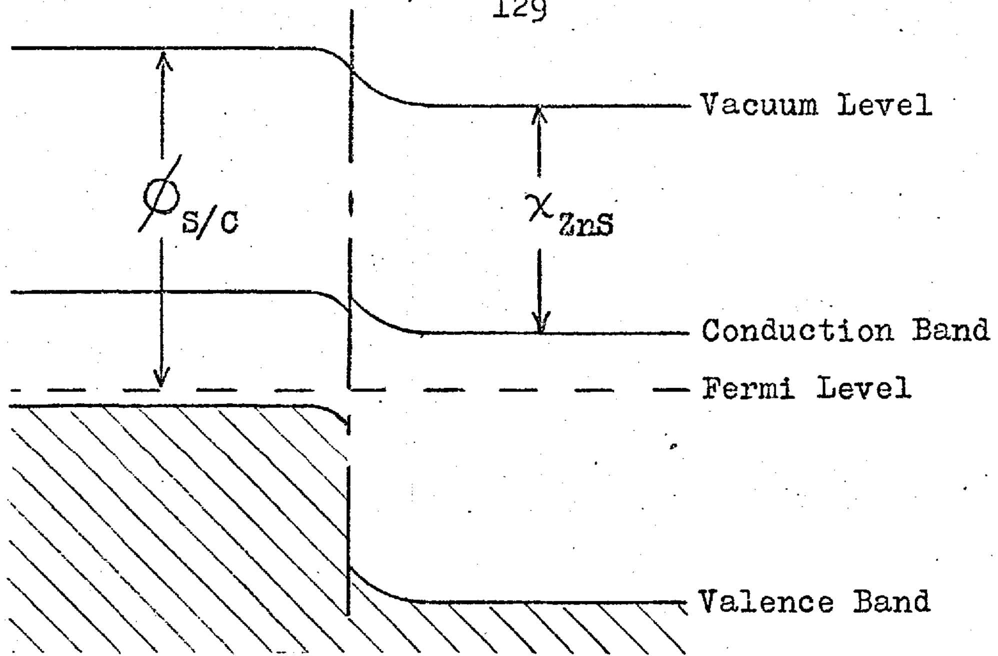

(a)

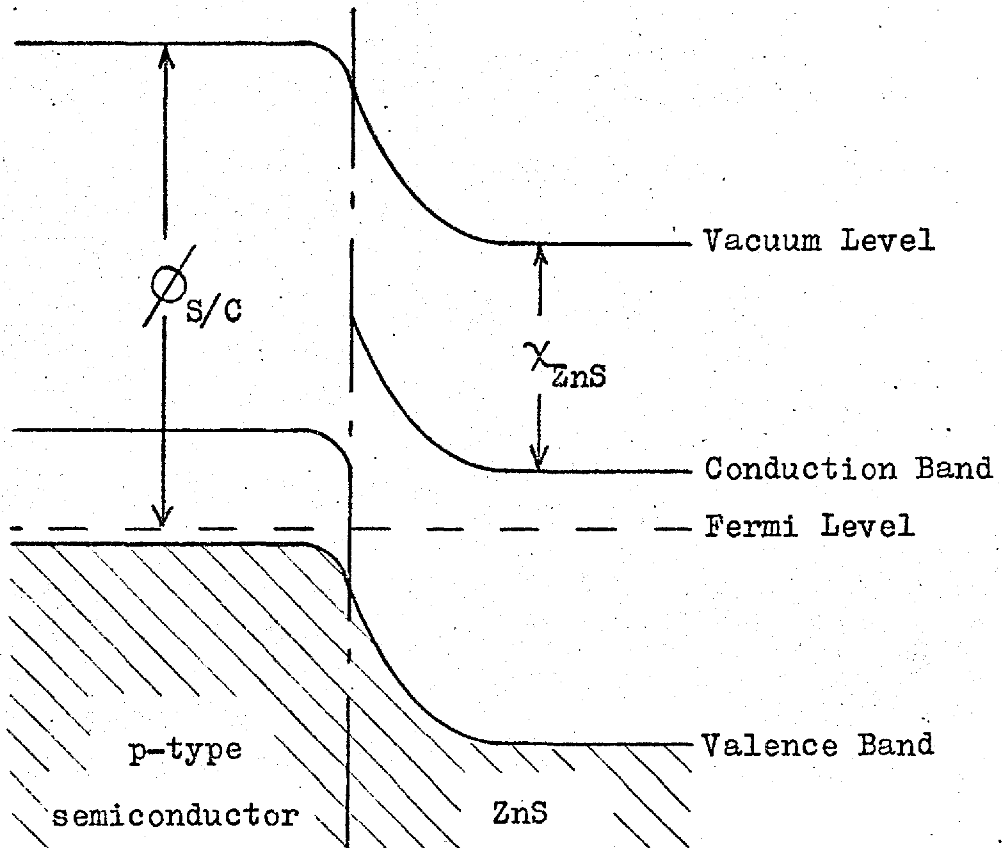

(b)

Figure 4.5 p-n Heterojunctions.

layer in the zinc sulphide. The barrier to hole injection has the same shape and magnitude as the electron extraction barrier but a considerable accumulation of holes exists in the barrier region. No large accumulation of electrons exists so that the probability of holes being injected when the contact is biased positively with respect to the zinc sulphide may be much greater than the probability of electron extraction.

It will be noticed that the p-type semiconductor contacts shown in Figure 4.5 have been drawn with band gaps considerably less than that of zinc sulphide. This is in accordance with what is known to be the case in practice, since only the smaller band gap materials may be made p-type. (The valence band electrons of large band gap ionic semiconductors are very tightly bound so that they are much less likely to be able to make transitions to acceptor levels than are the valence band electrons of small band gap materials, hence the tendency is towards only n-type conduction in the large band gap materials.)

It turns out that a tunnelling contact does not provide the sort of current voltage characteristics required for efficient injection. In practice a tunnelling contact is bound to have a higher resistance than a truly injecting contact, although the ratio of carriers injected to carriers extracted may be much higher for the tunnelling contact. Thus one is led to the conclusion that a truly injecting contact is the best solution where a low resistance contact is required.

It is worthwhile to mention at this point some previous

work on hole injection into zinc sulphide. The most frequently used material for this purpose is cuprous sulphide. Thornton[41] has considered electroluminescence as due to minority carrier injection (possibly from Cu_2S). Georgobiani et al.[35] have prepared what appear to be p-n junctions in zinc sulphide by thermal diffusion of copper. It seems likely that these junctions were, in fact, heterojunctions between Cu_2S and ZnS formed by massive incorporation of copper near the crystal surface. Electroluminescence was obtained at a forward bias of 2.2 volts. The electroluminescent emission included an ultraviolet band with a peak energy of 3.4eV showing that emission must be due to minority carrier injection.

Aven and Cusano[42] prepared Cu_2S-ZnS heterojunctions by immersing the ZnS in a hot solution of Cu^+ ions. They also prepared Cu_2Se-ZnSe heterojunctions which gave results consistent with hole injection. The results of the Cu_2S-ZnS junctions were qualitatively unsatisfactory, apparently because of the non-ohmic behaviour of the indium contact to the ZnS. The crystals used were apparently highly conducting compared with the crystals used in this work and were presumably also comparatively impure as they required purifying before use. The light output was also characteristic of impurity centres associated with copper. No intrinsic ultraviolet output was observed.

Cuprous sulphide appears to be a likely hole injector in view of the above practical results. It can also be justified from a quasi-theoretical point of view. First of all it is

known that Cu_2S is a highly degenerate p-type semiconductor. It therefore contains the required reservoir of holes. Secondly, if one may associate the valence bands of CdS and ZnS with sulphur ions[36] and hence assign the same energy level (referred to free space) to them, then it is logical to argue that the energy level of the valence band in Cu_2S cannot be vastly different from that of CdS and ZnS. The reported band gap for Cu_2S varies between about 0.9eV[43] to 1.8eV[44]. The variation in values is probably linked with the variable composition of cuprous sulphide. The band diagram of the junction Cu_2S-ZnS must therefore appear as in Figure 4.5(b) which, as already described, may inject holes into ZnS.

4.2 Methods of making contacts to zinc sulphide.

Indium contacts were applied to the crystals by a radiation wetting technique[45] but all other contacts were made by vacuum evaporation with one exception. Silver dag paste was sometimes painted directly onto the crystal to form a contact.

4.2.1. Radiation wetted indium contacts

The technique of applying indium contacts by radiation wetting was developed by Barber[45] for contacting to indium antimonide.

Under normal circumstances it is necessary to heat indium to about 500°C in order to get it to wet a crystal surface uniformly. Even if the crystal is cooled rapidly after heating, penetration of indium is bound to be deep. In addition, structural damage may result from the rapid cooling from this

high temperature. The radiation wetting apparatus is designed to allow low temperature wetting of the crystal surface. Figure 4.6(a) is a photograph of the apparatus and figure 4.6(b) shows the essential features diagrammatically. The crystal sits on a large thermal mass heat sink and a small indium dot is placed on its top surface. The assembly is then adjusted by a three-dimensional movement to bring the indium dot centrally under a tungsten wire heater element. The whole system is enclosed in a glass dome which is sealed to the base by a ground glass surface coated with apiezon grease. Hydrogen is flushed through the system for five to ten minutes before use. Exhaust hydrogen is burned as it leaves the system at a small jet. A wire gauze explosion guard is used to cover the whole apparatus in case of accident. After thoroughly flushing with hydrogen, current is fed to the tungsten heater element to make it white hot. The heat melts the indium which rises up into a spherical shape under its own surface tension, reducing its thermal contact with the crystal. At the same time the white hot tungsten heater produces atomic hydrogen which is able to reduce the surface coating of indium oxide at as low a temperature as 200°C. The nett result is that the sphere suddenly becomes unstable and collapses on to the crystal uniformly wetting the surface and at the same time being cooled rapidly by the large thermal mass in contact with the crystal. Evidence supporting the action of atomic hydrogen in reducing indium oxide is given by Barber. Because of the low indium temperature and the very rapid cooling

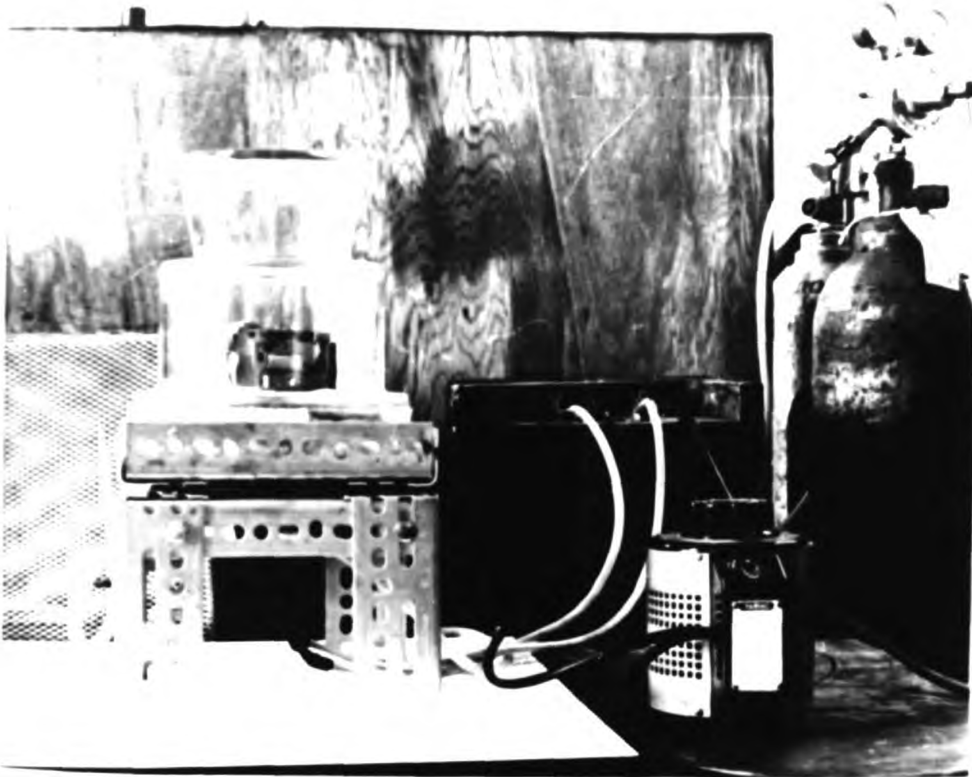

Figure 4.6(a) 'Radiation wetting' apparatus used to make indium contacts to ZnS.

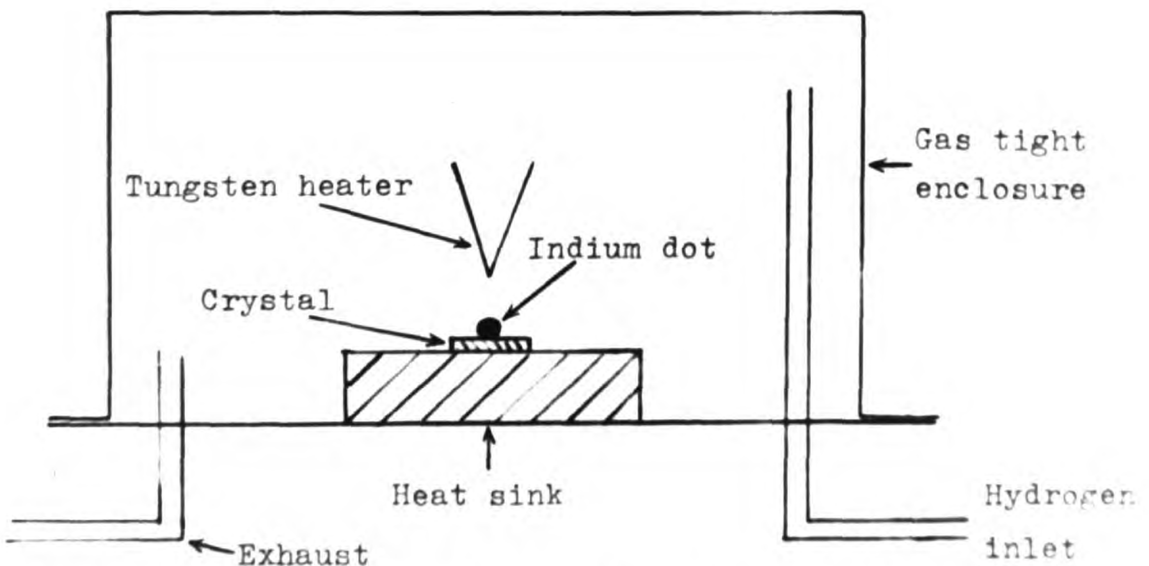

Figure 4.6(b) Diagram of the radiation wetting apparatus.

during wetting a very abrupt junction is made with indium penetration extending to 1 to 3 microns at the most. Diffusion and alloying of the indium contact to the desired depth may then be undertaken at will. In fact, this was not considered necessary as a very thin junction was what was required. Indeed, the unalloyed junctions described by Barber gave ohmic characteristics probably due to the large amount of disorder created by the fast wetting cycle. Since this was exactly the type of junction required here, alloying by further heating was considered undesirable.

Contacts made by radiation wetting to zinc sulphide were examined under a microscope through the other face of the crystal. It was clear that most contacts had wet the crystal satisfactorily since they had a shiny appearance. Small patches which had not been wetted showed up in contrast as dull or black areas. In addition the firm physical bond between crystal and contact indicated efficient wetting. In most cases it was impossible to separate crystal and contact without totally destroying the crystal.

4.2.2. Evaporated contacts

All evaporated contacts were made in an Edwards 12E coating unit. Materials evaporated were gold, silver and cuprous sulphide, all of which were evaporated from tantalum boats.

A molybdenum mask was made with five holes, each 1.5mm square, by a photo reduction and etching technique. This meant that contacts to five crystals could be made in a single

evaporation. A shutter was used to control the evaporation of the contact materials.

The evaporation of cuprous sulphide, kindly supplied by Fass*, needed a certain amount of care as it had a tendency to spit as it was heated up. If, however, it was heated slowly until molten not much was lost from the boat and the molten material could then be used satisfactorily for evaporation. Cuprous sulphide contacts were always coated with a layer of gold as a mechanical protection and for ease of connection(46). Two boats were therefore used so that gold and cuprous sulphide could be evaporated in sequence without having to admit air to the system between the two evaporations.

For the evaporation of silver it was found necessary to use a radiant substrate heater, as the silver films would otherwise curl up the thin zinc sulphide crystals because of the stress in the film. The heater was probably more of an evaporant heater than a substrate heater in practice, as most of the radiant energy would have been absorbed by the deposited silver film rather than the transparent crystal. It was thus rather difficult to estimate the actual temperature at the film caused by the heater. A thermocouple placed in contact with the mask close to a crystal registered about 100°C. This was therefore taken as the best possible estimate of the substrate

---

* Materials Science Section, Electrical Engineering Department, Imperial College, London

temperature. This annealing of the evaporated silver films prevented the tendency of crystals to curl up in practically every case.

The thickness of evaporated contacts is not critical in terms of electrical behaviour as long as a certain minimum thickness is achieved. The thicknesses were not therefore closely controlled, but were rather judged by eye and by experience. Once the appropriate evaporation time for a material was established it was easy to produce similar contacts by evaporating for the same length of time. The evaporation times were generally of the order of one to three minutes for which silver film thicknesses of between 2000Å to 5000Å were obtained.

4.2.3. Silver paste contacts

Some samples were made up with silver paste contacts for comparison of results with evaporated silver contacts. At first a great deal of trouble was encountered with contacts falling off the crystals after they had been used at 77°K. It was found that a much more lasting bond could be made between crystal and paste if the crystal was first wetted with a little amyl acetate. A 0.002" diameter gold wire with a small solidified dot of silver paste on the end was then dipped in fresh paste and applied immediately to the wetted part of the crystal. The amyl acetate caused the silver paste to run slightly and form an intimate contact with the crystal. This method was also used to make contact to evaporated metal electrodes as it avoided the need

to solder on wires and hence the danger of altering the nature of the contact.

4.3 Initial measurements of conduction

For conduction experiments samples were prepared with contacts on opposite faces of plate crystals so that current flow through the crystals was as near normal to the large area faces as possible. Crystals whose surface area was large compared with the contact area were chosen so that the surface leakage paths between contacts were very long in comparison to the conduction path through the crystal. Thus it was hoped to reduce surface leakage to negligible proportions.

4.3.1. Sample mounting

Samples were mounted on transistor headers, one of which is illustrated in Figure 4.7. Gold wires 0.002" diameter were attached to the contacts either by indium soldering or silver paste and the sample connected between the two pegs in the header. Thermal contact between the crystal and header was made with a small dot of silicone grease. Care was taken to avoid the electrical contact areas of the crystal with the grease.

4.3.2 The cryostat

The headers were mounted in a B.O.C. stainless steel optical cryostat and the leads brought out through a ceramic to metal seal. The cryostat was evacuated during use with a one inch bore Edwards rotary and oil diffusion pump set. The cryostat and pumping apparatus is shown in Figure 4.8. The crystal could be observed during experiments through the

Figure 4.7 Transistor header used for mounting samples in the B.O.C. cryostat.

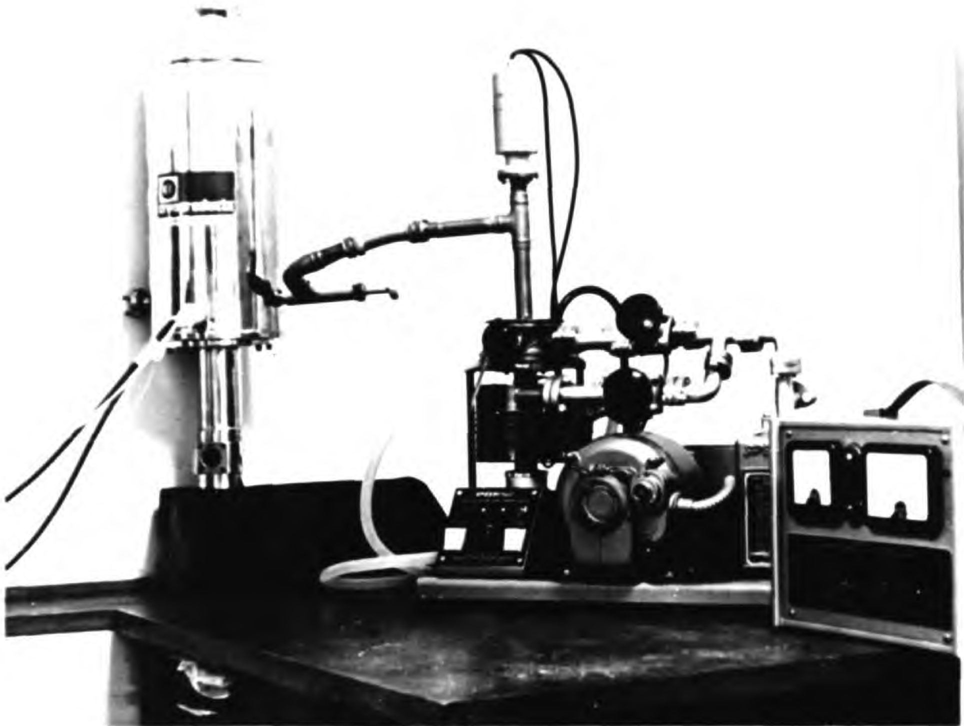

Figure 4.8 B.O.C. cryostat and pumping apparatus.

cryostat window if the top of the transistor header were left off. The cryostat was capable of liquid helium temperatures but in practice was never used below the temperature of liquid nitrogen.

4.3.3 Measuring apparatus and power supply

Early experiments soon established that bias voltages in the region of several hundred volts would be required. A Fluke High Voltage stabilized D.C. supply, type 412B, was therefore used to supply the crystal. A 10MΩ series resistor was used to limit the current in case of breakdown. The power supply was capable of providing a continuously variable output between 0 and ± 2100 volts with a sensitivity of adjustment of 0.1 volts.

The voltage across the crystal was measured with a Philips vibrating reed voltmeter type G.M.6020 whose input impedance was 100MΩ on the ranges used. The crystals could be coupled to a Tektronix 545A oscilloscope via a 0.01μF 500 volt D.C. capacitor when necessary. Initial current measurements were made with a Pye Scalelamp galvanometer which was capable of registering currents down to 2.5×10^{-9}A. Currents greater than 10^{-5}A were measured on a A.V.O. meter.

4.3.4 D.C. results

The In-ZnS-Cu_2S sandwich structures showed neither the hoped-for low resistance nor double injection characteristics. In fact, for voltages in the range 0 to 100 volts the current seemed totally erratic, making random jumps in the direction of both increasing and decreasing current for a constant voltage

applied to the crystal. It was impossible to draw any fixed relationship between current and voltage. Currents were generally in the range of 10^{-8} to 10^{-7} amps for this range of voltage. For voltages greater than 100 volts the current was much less erratic, though random fluctuations still occurred from time to time. A steep rise in average current usually occurred in the voltage range 250 to 500 volts, with currents of 10^{-6} to 10^{-4} amps flowing.

Cooling to liquid nitrogen temperatures had the effect of reducing the current for a given voltage. Indeed, samples appeared to breakdown irretrievably under the application of very high voltages at room temperatures, whereas up to 500 volts could be applied without breakdown at 77°K.

Not only were the samples subject to random changes in conductivity, but it was also quite impossible to reproduce the same average current-voltage characteristics from one voltage cycle to the next in the low voltage range.

The effect of shining ultraviolet light on the sample was to increase its conductivity only while the light was shining. Decay of photo conductivity was very rapid which is not surprising when one considers that fields of between 10^7V/m and 10^8V/m were being applied. These high fields would have ensured that all the photogenerated electrons and holes were rapidly swept out of the crystal.

The results of applying bias of either polarity were qualitatively the same although the average currents with the

indium contact negative tended to be higher than in the reverse direction, as far as the erratic results would allow distinction to be made.

Finally, it was sometimes possible to obtain a meaningful relationship between current and voltage in the voltage range 100 volts to 500 volts for crystals at 77°K. When this was the case the result was a straight line on a logI/logV plot with a slope of about 3. Thus a relation of the form

$$I = AV^3$$

existed in some instances at the higher currents and voltages.

4.3.5 Oscillations

When biased to greater than 100 volts positive or negative the In-ZnS-Cu_2S structures would sometimes burst into spontaneous oscillation. This oscillation would sometimes last several minutes or even half an hour, but very often it would be intermittent lasting only a few seconds in each burst. Oscillations were only observed at liquid nitrogen temperatures and never at room temperatures, probably because of the tendency of the sample to breakdown irretrievably at room temperature under very high biasing voltages.

The frequencies of the oscillations lay within the range 100 to 1000 Hz for all observations made. Amplitudes ranged from 2.5 mV peak to peak to 400 mV peak to peak, amplitude increasing with increasing applied d.c. bias. Insufficient evidence was available to deduce a definite relationship between applied voltage and amplitude of oscillation. No

correlation was evident between applied voltage and oscillation frequency. The waveform of the oscillation was variable. A selection of waveforms is shown in Figure 4.9. The square waveforms of Figure 4.9(a) are two photographs of the waveform produced by a crystal at different times. The output alternated randomly between the large amplitude low frequency wave with the small square wave superimposed and the small amplitude higher frequency wave on its own.

These oscillations were qualitatively the same as some observed by Fass[47] in this laboratory with In-CdS-Cu_2S structures. The frequencies in Fass's experiments were about a factor of 10 greater than here however.

4.3.6 Discussion of results

The high voltages required to pass current through the crystals showed that the contacts could not be injecting. To test which of the contacts was not functioning properly samples were made up with two indium contacts and two cuprous sulphide contacts. Neither produced low resistance characteristics showing that neither was functioning as an efficient carrier. injector. The failure of the indium contact to inject electrons in contrast to the success of the contacts described in reference 40 may be linked with the fact that the crystals used by Blount et al. contained a fairly large quantity of chlorine. Since they were high resistivity crystals they must have been highly compensated, possibly with zinc vacancies. Since trivalent metal dopants occupy zinc sites in the zinc sulphide

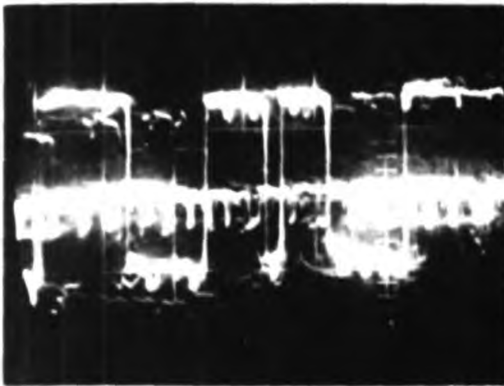

(a) D.C. bias 100V, 2μA.
Vertical scale 5mV/cm.

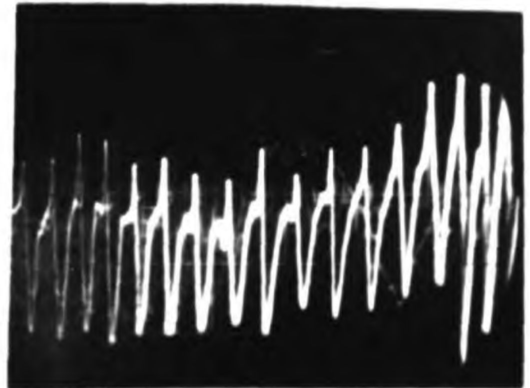

(b) D.C. bias 430V, 85μA
Vertical scale 100mV/cm.

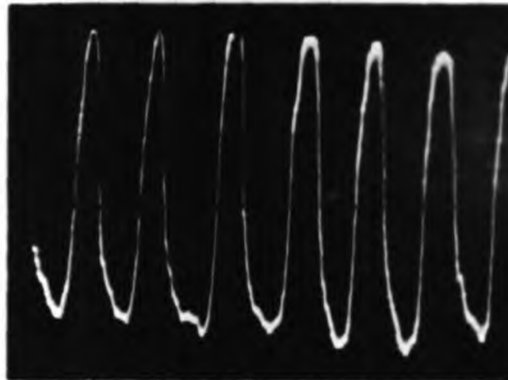

(c) D.C. bias 500V, 165μA.
Vertical scale 50mV/cm.
Horizontal scale 5mS/cm in all cases.

Figure 4.9 Oscillation waveforms produced by In-ZnS-Cu_2S devices.

lattice, it would obviously be relatively easy to dope such compensated crystals heavily with contact material near the surface. This would have the effect of reducing the compensation and the actual donor levels supplying the surface space charge would be mainly associated with chlorine rather than the contact metal. Thus, the production of the injecting contact in reference 40 could have been a result of the chlorine content of the crystals rather than the massive indiffusion of contact material at the surface. More likely it was a combination of both effects. It can now be seen how the absence of chlorine (or similar group VII impurity) might prevent the formation of an injecting contact with indium. If the contact is not injecting then the most likely form for it is still that shown in Figure 4.2(c), but with a much lower surface space charge density. In this case a high resistance contact results.

It is not clear why the Cu_2S contacts would not work as hole injectors. A possible explanation is that the amorphous nature of the Cu_2S film led to the formation of interface states between the zinc sulphide and the Cu_2S. These interface states could have produced an inversion layer at the junction which would have effectively removed the hole reservoir required for injection.

Taking the speed of sound in zinc sulphide to be of the order of 10^3m/s, the "round trip" time for a sound wave travelling between the contacts of a crystal is seen to be of

the order of 10^{-8} to 10^{-7} secs. Clearly, therefore, the observed oscillations could not have been due to any accousto-electric effect. Most probably some periodic change in the electron concentration in the conduction band caused by the ionization and de-ionization of defect centres was the origin of the oscillations. Detailed evaluation of the necessary conditions for oscillation is not possible, but it is believed that the mechanism proposed in Chapter 6 to account for the switching effect in crystals could also account for the oscillations under certain circumstances.

CHAPTER 5

CONDUCTIVITY SWITCHING IN ZINC SULPHIDE

5.1 Introduction

In Chapter 4 the results of experiments using indium and cuprous sulphide as contact materials were described. Owing to the apparent failure of these materials, it was decided to investigate the conduction properties of other metal - ZnS junctions. Silver was chosen as an alternative metal contact because it fulfilled such practical requirements as being non-reactive, easily evaporated and known to produce electronically active centres in ZnS. As a result of these experiments it was found that Ag - ZnS - Ag sandwich structures could be switched between two conductivity states, differing by many orders of magnitude of conductivity, by means of electrical stimulation. The purpose of this chapter is to present the results of experiments conducted on these and related structures, which were aimed at elucidating the switching mechanism involved. A theoretical discussion will then be given in Chapter 6.

5.2 First observations of conductivity switching

Samples similar to those described in section 4.4 were made by the techniques described in section 4.3. In this case both contacts were of silver. Initial observations of the conduction of these structures were made on a Tektronix Transistor Curve Tracer, type 575. A typical room temperature current-voltage trace is shown in Figure 5.1. It can be seen that very little

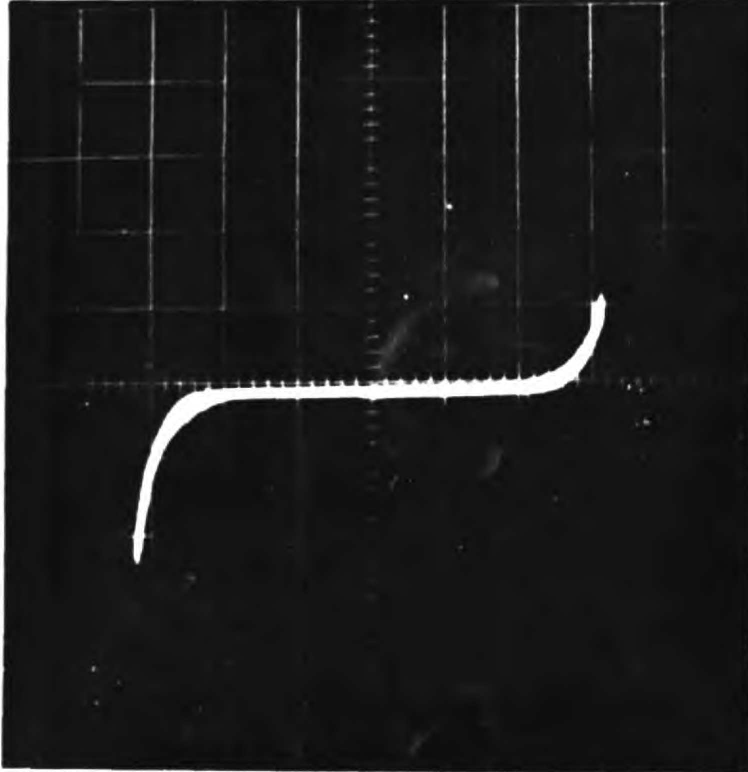

Vertical scale 0.01mA/cm.
Horizontal scale 50V/cm.

Figure 5.1 Room temperature current-voltage characteristic of a switching device before switching.

current flowed until the voltage across the device was of the order of 100 volts. At voltages above the turnover voltage the current flowing increased very rapidly with applied voltage and was limited by the 100kΩ dissipation limiting resistor of the Tektronix curve tracer.

It was found that, if the current in the crystal was increased to about 0.5mA, the characteristic suddenly switched to a straight line through the origin whose slope was of the order of 10^4 ohms. This "high conductivity" characteristic was symmetrical about the origin. If the series resistance of the curve tracer supply was then reduced to about 5Ω the characteristic could be made to switch back to the original non-conducting state by passing a current of between 1mA and 10mA. Figure 5.2 shows the contrast between the two conductivity states by superimposing the two characteristics.

The switching operations between high and low conductivity were repeatable many times, but devices tended to deteriorate after they had been switched about twenty times. A memory effect was observed in that a device in its high conductivity state could be disconnected from the curve tracer for several minutes without returning to its insulating state.

In order to try to prevent the deterioration of devices and, at the same time, further investigate the switching process, the Tetronix curve tracer was replaced by the Fluke 412B power supply with 1MΩ and 10MΩ series resistors and a Vibron 33B

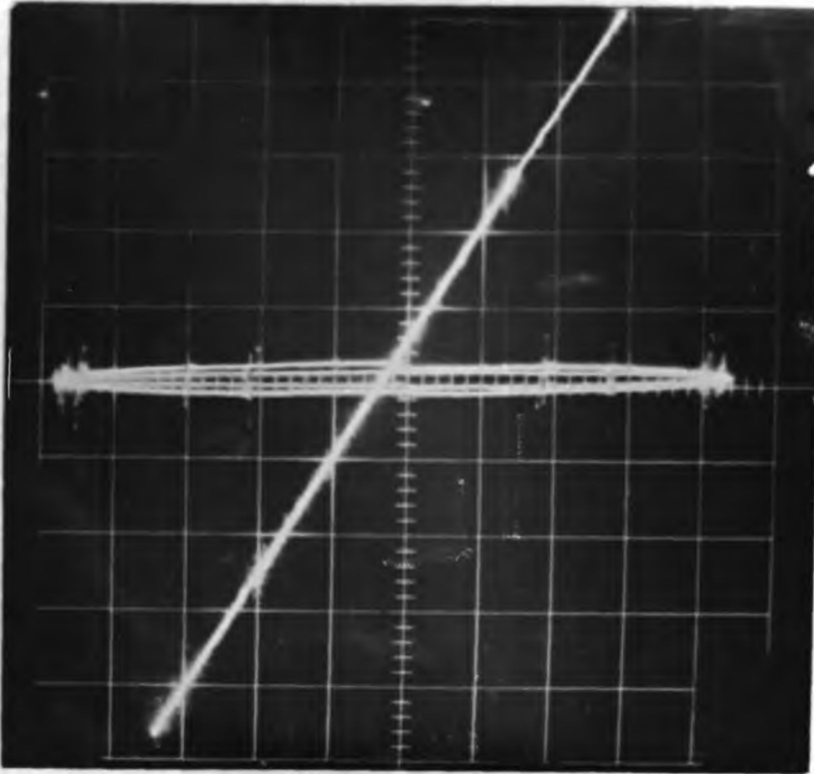

Low resistance state.	High resistance state.
Vertical scale 0.1mA/cm.	Vertical scale 0.02mA/cm.
Horizontal scale 0.5V/cm.	Horizontal scale 50V/cm.

Figure 5.2 Comparison between the high and low resistance states of a switching device at 77°K.

electrometer with a current adaptor box. With this apparatus it was possible to measure and control currents as low as 10^{-12} Amps in the crystals. A Honeywell quarter second chart recorder, type Y153X16 was available when required to record the output of the Vibron. Figure 5.3 illustrates the apparatus used. The circuit diagram of the test rig is shown in Figure 5.4.

Instead of switching the crystals out of the high conductivity state by passing a high current as was done with the curve tracer, they were switched by discharging a small capacitor through them. In this way the possibility of damaging the crystals during switching was reduced since the total energy available in the circuit was limited.

Low temperature measurements could be made using the B.O.C. cryostat shown in Figure 4.8. In addition some crystals were mounted in small sealed transistor cans which could be plugged directly into transistor holders on the end of 50Ω coaxial leads. This method of connection was useful for fast pulse measurements but served equally well for d.c. measurements.

5.3 Definitions of the switched states and criteria for switching.

5.3.1 Definitions

In order to discuss the switching phenomena it is necessary to define what is meant by the "high" and "low" conductivity states. Since practically all crystals investi-

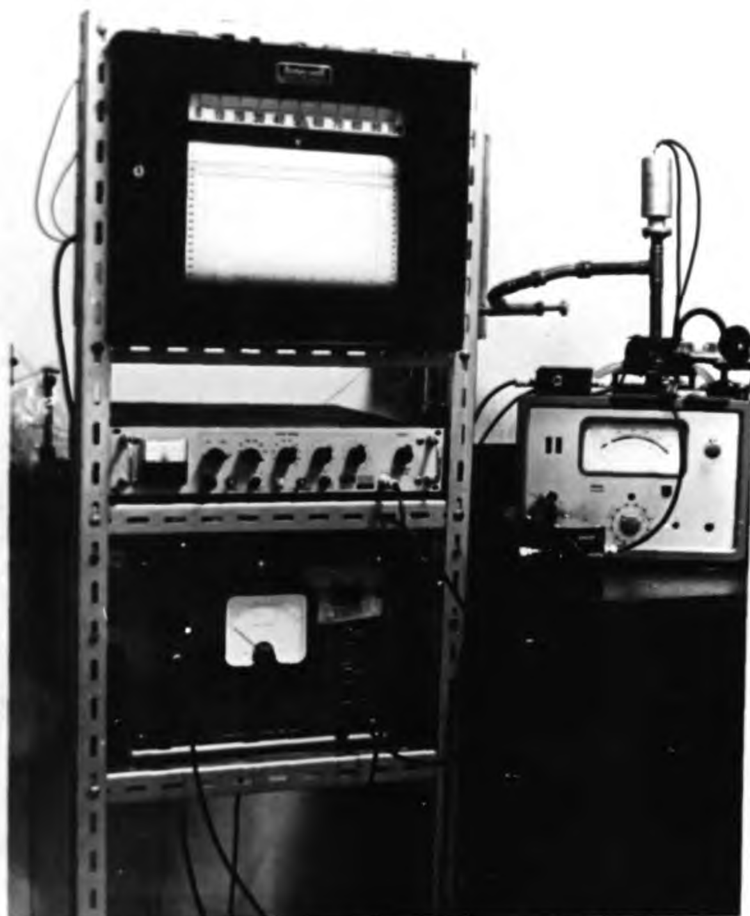

Figure 5.3 Apparatus used for D.C. measurements on switching devices.

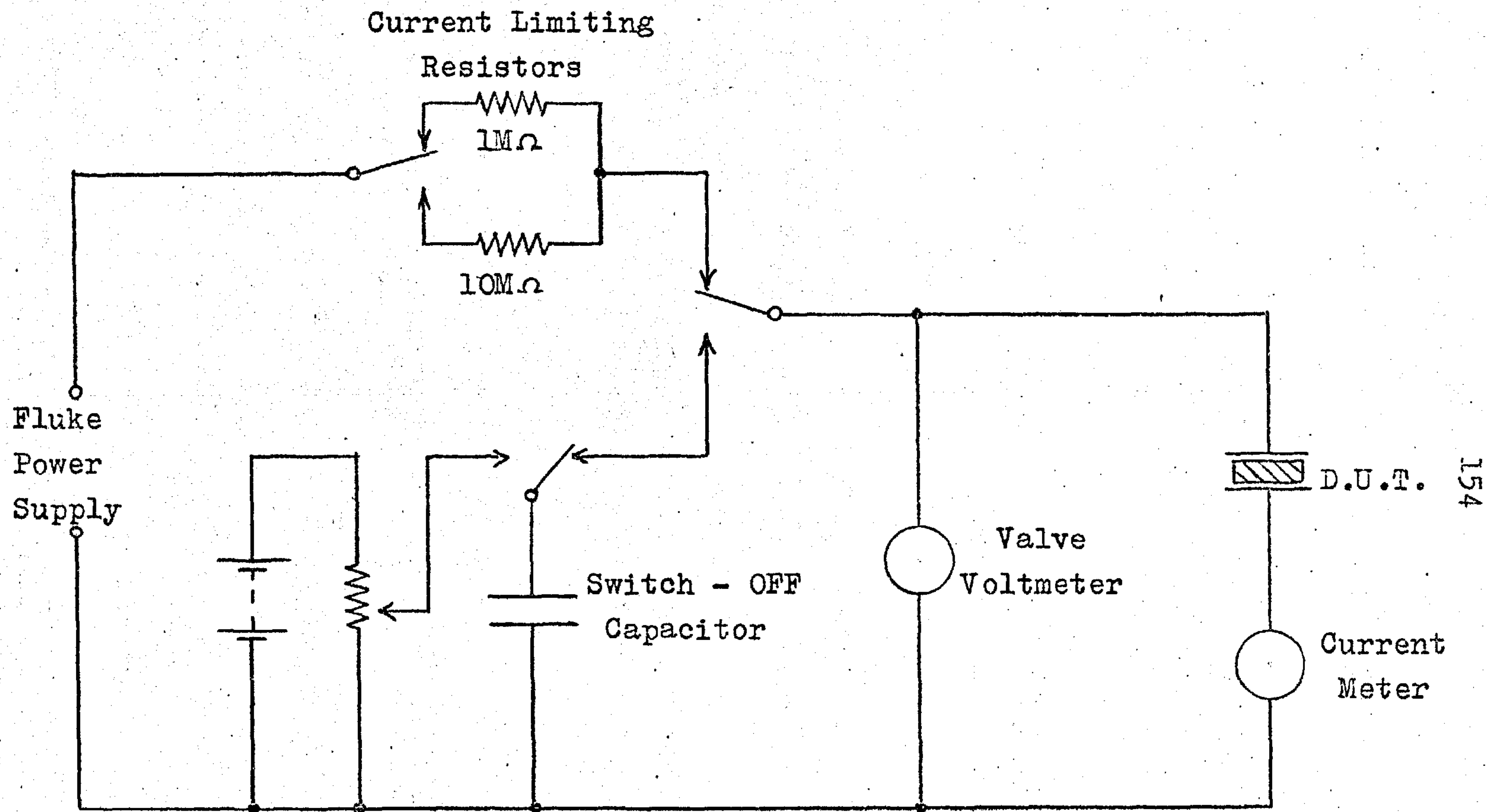

Figure 5.4 Circuit for D.C. Measurements on Switching Devices.

gated were initially in a very low conductivity or insulating state, this was obviously the normal condition of conductivity. However, this low conductivity state was always highly non-linear (i.e. not ohmic), irreproducible and sometimes time dependent.

In contrast the high conductivity or abnormal state of crystals was always symmetrical about the origin, linear, (i.e. ohmic) and very stable and reproducible. For this reason, we take the high conductivity or "ON" state as the reference state and define switching processes in terms of whether or not the crystal is switched ON.

It was found experimentally that typical ON state resistances lay in the range 10kΩ to 20kΩ and that all except two lay in the range 3kΩ to 50kΩ. One of the two exceptions was an abnormally thin crystal whose ON resistance was 700Ω and the other was a crystal with unusual contacts which had an excessively high ON restistance of 100kΩ.

5.3.2. Effect of contact material on conductivity switching

Twenty-six devices were successfully mounted and tested with various contacts, as shown in Table 5.1.

Some crystals failed due to breakage during the electroding and mounting processes and were therefore omitted from Table 5.1. No crystals have been omitted because of electrical failure after mounting.

The ten crystals with two evaporated silver contacts could all be switched repetitively between the two conductivity states

TABLE 5.1

CONTACT SYSTEM	NUMBER OF DEVICES
Two evaporated silver contacts	10
One radiation wetted indium and one evaporated silver contact	3
One evaporated indium and one evaporated silver contact	1
Two radiation wetted indium contacts	6
Two evaporated indium contacts	1
Two silver paste contacts	4
Two graphite paste contacts	1

One failed after a few cycles because too high a current was passed through it and two failed eventually because the connections to the contacts became detached. It was found possible to repair one of the latter which then worked as before. All the other seven showed no sign of electrical failure throughout their testing.

All four of the crystals with one silver and one indium contact could be switched repetitively. Where tests were made it was found that these crystals switched to the ON state at lower applied fields when the silver contact was positive. Only one crystal failed electrically, this failure being caused

by the passage of excess current which burned it out.

All four of the crystals with silver paste electrodes were switched between the two conductivity states reliably and repetitively, one eventually failing because one contact became damaged.

Two out of the seven crystals with two indium contacts were made with the contacts staggered by 1mm as shown in Figure 5.5. These did not exhibit conductivity switching effects, but this may have been because it was impossible to apply fields as high as normally used in switching experiments to these devices. Of the other five indium contacted crystals one had an ohmic characteristic from the start with a resistance of just under 1MΩ*. It was found impossible to switch OFF this ohmic conduction by the methods normally used to switch crystals to the OFF state. Three showed stable current voltage characteristics with the current rising sharply at a threshold voltage which was different for each crystal. The conductivity of these crystals could not be switched but two eventually failed short circuit ($< 1.0\Omega$). One crystal showed normal conductivity switching effects but it was known that silver paste used to make connections to this crystal had

---

* This crystal was in fact one from a batch made with highly chlorinated material. This seems to support the contention of section 4.4.6 that chlorine doping may play a part in obtaining ohmic behaviour from indium contacts to ZnS.

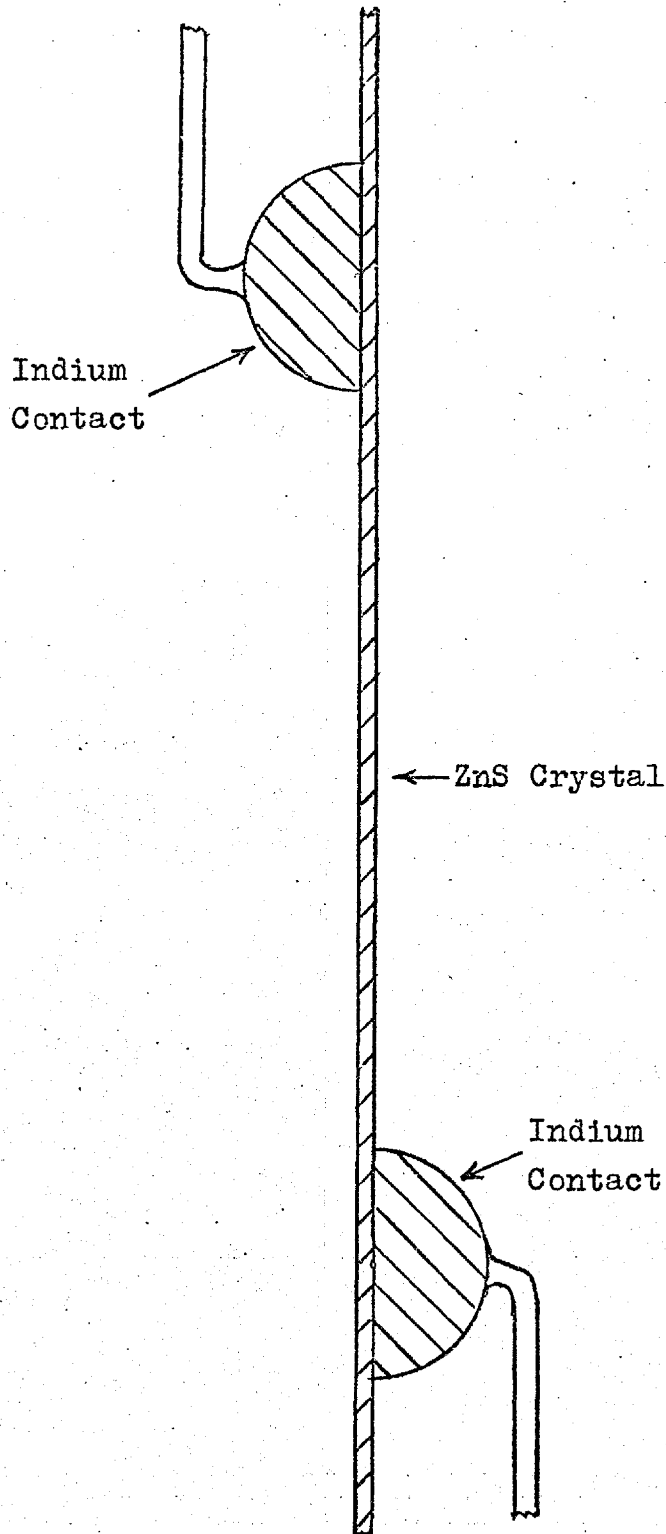

Figure 5.5 Staggered Contact Device.

spread over one contact onto the crystal face. It was therefore possible that the switching effect was a result of the silver paste and not the indium contacts.

The one crystal to which graphite paste contacts were attached showed a marked conductivity switching effect with an ON state resistance of about 100kΩ. This was much higher than usual.

5.3.3. Transition from the OFF to ON state

Since the experiments were done both at room temperature and liquid nitrogen temperatures it was not realized at first that a forming process could be involved with the conductivity switching. This process would normally occur during the first switch ON at room temperature. The importance of such a forming process was tested in some of the later devices by the following procedure. A virgin crystal with contacts attached was mounted on a header and cooled to liquid nitrogen temperature before any electrical signals were applied. An attempt was then made to switch ON the device by applying a high voltage. In a typical case 500 V was applied with no sign of conductivity switching (under normal circumstances this voltage, applied via a 1MΩ series resistor, was quite adequate to ensure that a crystal switched ON.) The crystal was then warmed up to room temperature and 500 V applied again. After two seconds conductivity switching occurred with the device switching ON. It was next switched OFF with a pulse from the capacitor and cooled back to liquid nitrogen temperature.

After this treatment, repeated cycling between ON and OFF states was possible using a switch ON voltage of 400 V and without any further need for warming the crystal. Similar results were obtained with other crystals.

These experiments showed that a permanent change was induced in the crystal by the application of a high field at room temperature, or in other words, that a "forming" process took place. It can be seen that unless forming is carried out, conductivity switching at low temperatures is difficult if not impossible to achieve.

It has already been stated that switching experiments were carried out at both room temperatures and liquid nitrogen temperature. It was found that at room temperature the ON state tended to be unstable and also that intermediate states could be obtained. Most experiments to determine the switching criteria were therefore done at liquid nitrogen temperature where no stability problems were encountered. Minimum fields required to switch ON the crystals were of the order of 10^7 Volts/m., but in some cases it was necessary to apply fields as high as 10^8 Volts/m. In addition to the minimum field requirement, a certain current was also necessary in order to switch a crystal to ON state. This was demonstrated by increasing the current passing through the crystal whilst keeping the voltage across it approximately constant. Approximately 0.3 to 0.5 mA was generally required to induce conductivity switching.

Taking the area of the evaporated silver contacts to be 2.25mm^2, this represents a current density between 130A/m^2 and 220A/m^2,

No conductivity switching would occur unless sufficient current was supplied. On the other hand it was necessary to limit the current flow after switching to prevent the destruction of the devices. Since no constant current high voltage generator was available the Fluke 412B high voltage power supply with a 1MΩ series resistor was used and found to give sufficient voltage drive and adequate current limitation.

It was found that the resistance of the ON state could be controlled by regulating the current drive at switch ON. Greater currents gave lower resistance ON states. However, the apparatus did not permit a quantitative measure of this relationship to be made. There was also a tendency for the ON state resistance to be a time dependent function of switch ON current, resistance falling to some asymptotic value with increasing time. It was therefore necessary to control the switch on condition carefully in order to obtain reproducible ON states. When a consistent switch ON - switch OFF cycle was adopted some devices had ON state resistances which were reproducible to better than 5%.

5.3.4. Transitions from the ON to the OFF state

Experiments were conducted mainly at the temperature of liquid nitrogen because of the instability of the ON state at

room temperature. It has already been stated that the switch OFF operation was best achieved by the discharge of a small capacitor through the ON device. Using this method, it was possible to vary the charge available for the switch OFF process.

The switch OFF pulse was injected into the device from a capacitor via a micro switch and short length of wire approximately $\frac{3}{8}$ inch from the ground plane, followed by about two feet of 50Ω coaxial cable. The total conduction path length from capacitor to coaxial cable was about three inches. It can be shown[48] that this length of wire presents an inductance of approximately 50nH to the discharge of the capacitor.

This has the effect of slowing down the capacitor discharge to the coaxial line giving a pulse length of about 1 nsec for a 2pF capacitor and 8 nsec for 100 pF capacitor.

It was found possible to switch devices OFF with a discharge from any capacitor between 2pF and 100pF charged to a large enough voltage. For a typical device the voltage used was 400V. Thus the maximum charge involved in a typical switch OFF operation must have been less than 800 pC or 5×10^9 electrons.

Switch OFF experiments were also performed with a Hewlett Packard Model 214A pulse generator connected directly to the device via a 50Ω line. In these experiments the pulse length, voltage and repetition rate were varied. In addition different device ON state resistances for the same device were used.

It was found that a pulse voltage of 20V was required to switch OFF a typical device irrespective of the ON state resistance, which varied between 8kΩ and 80kΩ. Pulse voltages less than this threshold would not cause switch OFF to occur. When the pulse voltage was set to the threshold value for switch OFF it was found that a single long pulse of that voltage would not cause switch OFF to occur. However, by decreasing the pulse length it was found that, for short enough pulses, switch OFF would occur. To test whether this was the cumulative effect of a lot of pulses, rather than the shortening of the pulse length, the long pulses were applied many times and found not to cause switch OFF. The shortening of the pulse was therefore the real cause of switch OFF. The range of pulse length used was from 50nsec to 300nsec.

In another experiment a 20 volt pulse of 0.1μ sec. duration would consistently switch OFF a device whereas a 10 volt pulse would not switch it OFF for pulse lengths of 0.1, 1, 10 or 100μ sec. It was therefore not a sufficient condition for switch OFF to supply a given amount of charge in the pulse. In view of the increasing ease of switch OFF with decreasing pulse length it seems likely that the rate at which charge is supplied to the device is an important factor in achieving switch OFF.

5.4 Conduction in the ON state

5.4.1 Linearity

As stated in section 5.3.1 the ON state was recognised by

its comparatively low resistance, linear and symmetrical conduction characteristic. Nothing has been said, however, about the extent of linearity of this characteristic. Measurement was limited to voltages greater than 1mV by instrument sensitivity and by errors due to thermal emfs. At the other end of the scale it was not possible to make measurements above crystal voltages of about 10 volts as there was always a tendency to instability. At high enough voltages devices would switch to the OFF state. Within this range of about four orders of magnitude of device voltage and current the ON state was found to be linear and symmetrical within the limits of experimental errors, which were estimated by replacing the device with a resistor whose value was typical of the ON state resistance of a device (namely 15kΩ). By taking readings of current and voltage in both directions asymmetric errors (e.g. thermal emfs) could be detected. It was found that asymmetric errors amounted to approximately 100μV. The only significant symmetric error was that of reading the meter scale. This was taken to be equal to the value of the smallest division of the meter scale, i.e. $\pm$0.5% of the full scale deflection. Experimental errors were therefore $\pm$0.5% at 1V rising to $\pm$1% at 10mV and $\pm$10% at 1mV.

A typical current voltage characteristic for the ON state is plotted in Figure 5.6.

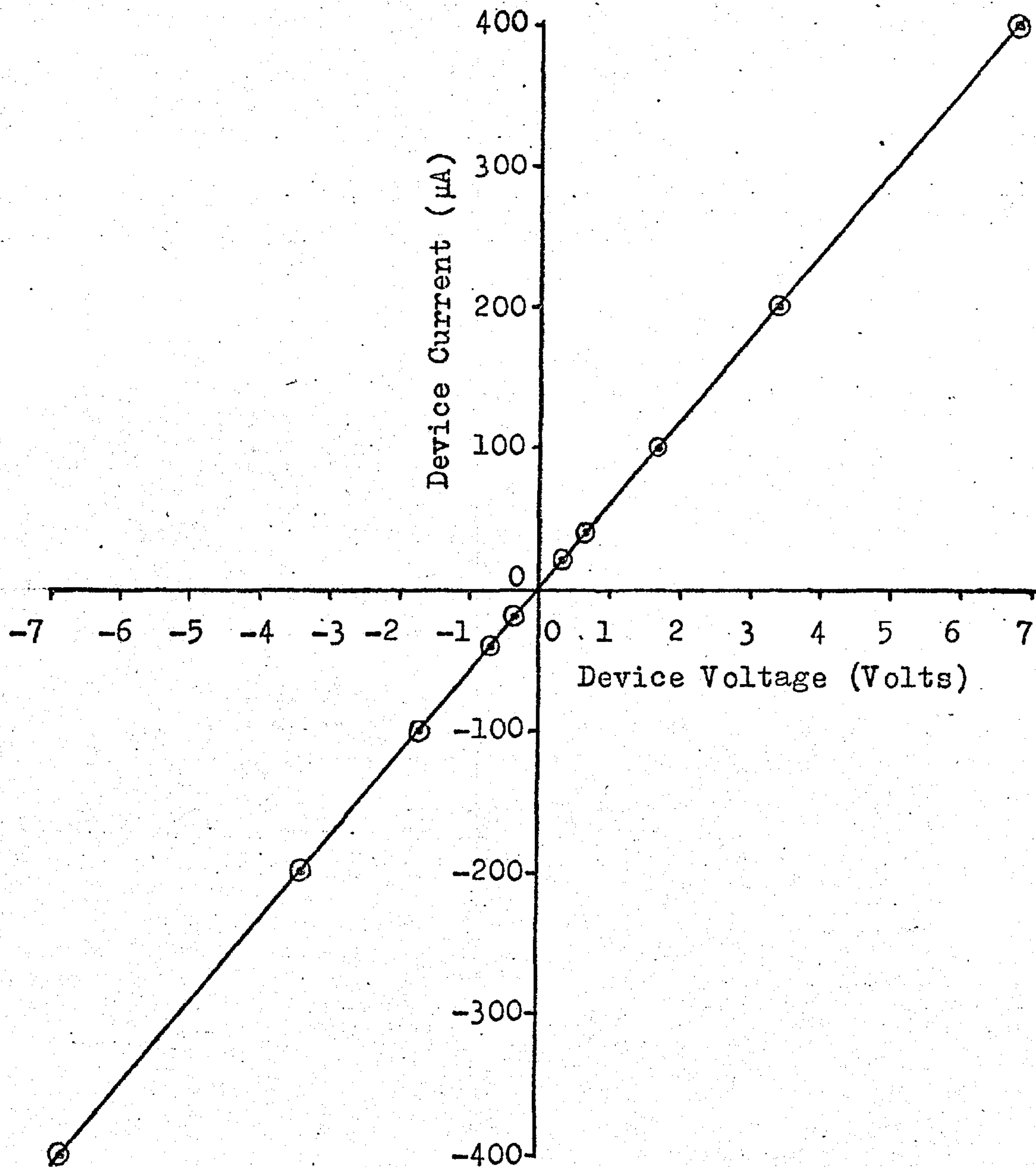

<u>Figure 5.6</u> Current - Voltage Characteristic of the ON State.

5.4.2. Memory

All devices capable of switching exhibited a memory effect at the temperature of liquid nitrogen. If a device was switched to the ON state and the bias removed, the ON state could remain for more than 24 hours. After a period of memory, devices were tested to determine their state by the application of 0.1V via a series resistor. This low voltage was used in order to eliminate the possibility of switching a device back ON with the test voltage, should it happen to have been in the OFF state. No apparent shortening of the memory effect was observed if the device was left short-circuited between tests. It is impossible to make any firm conclusions about the ultimate duration of the memory effect since in all tests there was some reason, other than the decay of the ON state, for the device eventually switching OFF. This was generally some disturbance such as the addition of more liquid nitrogen to the apparatus. It did appear, however, that after 24 hours only a very small disturbance, either electrical or possibly mechanical, was necessary to cause switch OFF to occur.

At room temperature, the memory effect was of much shorter duration generally being of the order of seconds or minutes. It was thus more difficult to maintain the ON state for long at room temperature.

5.4.3. Temperature variation of ON state resistance

To investigate the temperature coefficient of resistance of the ON state devices were switched ON at 77°K and biased

with 1μA from a constant current source. They were then heated at the rate of about 3°K per minute and the voltage across the device was recorded. The temperature was measured with a copper constantan thermocouple in contact with the device can. The thermocouple voltage relative to a reference junction kept in melting ice was measured with a Solartron LM 1450 digital voltmeter. Ten experiments were conducted on four different devices with various ON state resistances. All experiments gave similar results, and Figure 5.7 shows two typical curves for nominal ON resistances of 16kΩ and 30kΩ at 77°K. It can be seen that up to 220°K a very slow rise in apparent resistance takes place. In fact, the rise in device voltage between 77°K and 220°K was approximately the same in all experiments, being roughly 0.3mV. It was therefore concluded that this small change was probably due to thermal emfs in the leads to the device and that no real change in device resistance at all occurred in this temperature range. At 233°K ± 2°K in all cases a sudden increase in device resistance was observed and an apparent instability in the ON state set in. At slightly higher temperatures devices were observed to switch OFF spontaneously although this switch OFF process was not efficient since it was easy to reverse it by the application of voltages of the order of 10 volts across the devices.

The results show that the ON state is apparently stable between 77°K and 233°K and in this range has zero or a very low (< 0.1% per °K) temperature coefficient of resistance.

Figure 5.7 Variation of the ON State Resistance with Temperature.

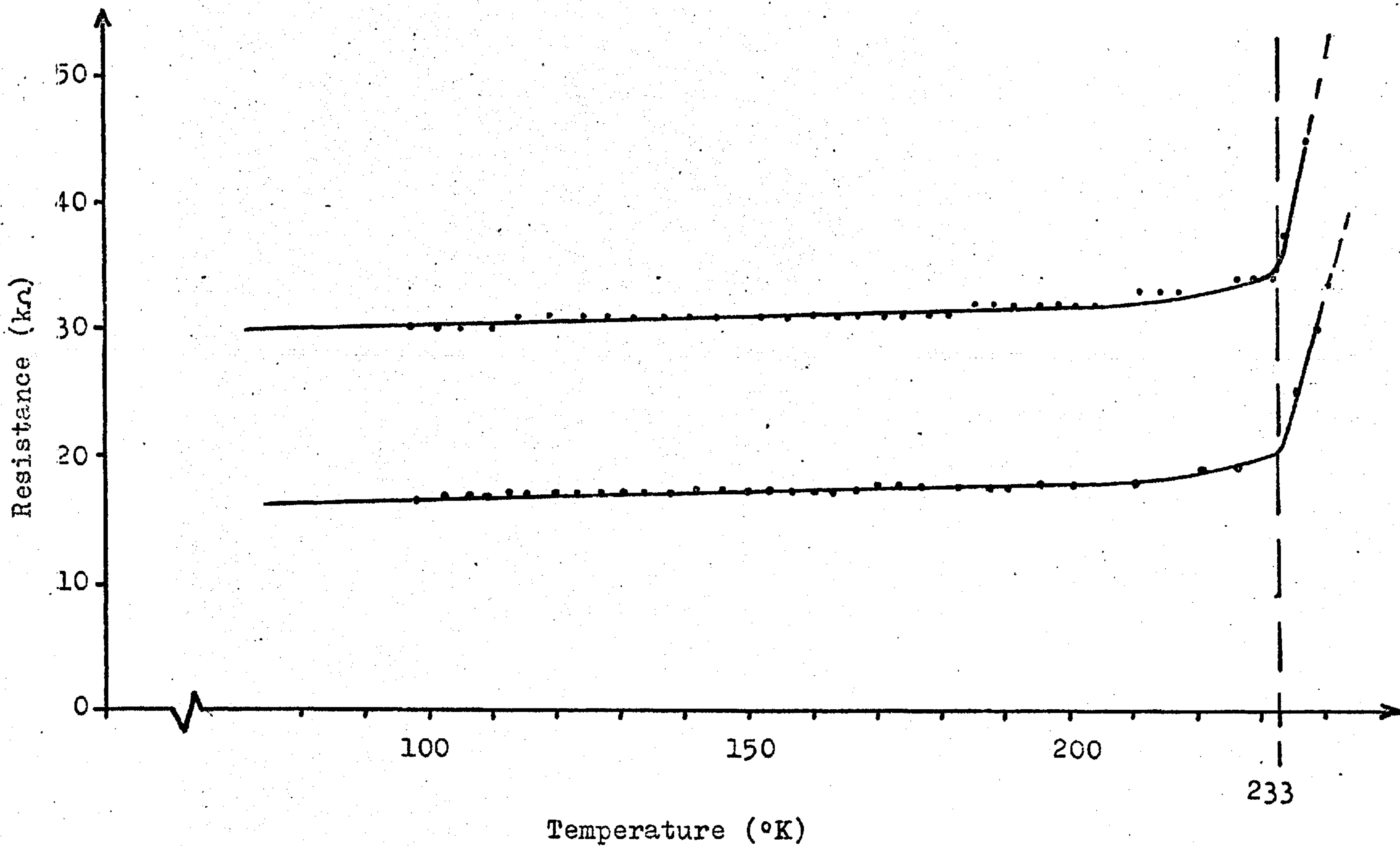

5.4.4. Frequency dependence of the ON state conduction process

The frequency dependence of the ON state resistance at the temperature of liquid nitrogen was measured using a Wayne Kerr Universal Bridge B221 for frequencies of up to 20kHz and a Wayne Kerr radio frequency bridge, type B601, for frequencies of 30kHz to 5 MHz. It was found that the radio frequency bridge introduced an error above frequencies of 1MHz, giving too low a value of resistance. Measurements were therefore made by comparison with the measured value of a 1% tolerance resistor whose d.c. value was equal to that of the d.c. ON state resistance of the device. It was thus possible to eliminate systematic errors introduced by the bridges and so make reliable measurements over the range 10Hz to 5×10^6 Hz, (as well as d.c. measurements). No change in ON state resistance was detected from d.c. to 5MHz for the five devices tested. Random scatter of the data was within $\pm$ 2% of the nominal resistance in cases.

The ON state capacitance was difficult to measure as the ON state resistance acted as a short circuit to it at the lower frequencies. However, measurements of capacitance were made between 10^5Hz and 5×10^6Hz and no variation was detected over this range of frequencies. Random scatter was $\pm$ 10% in this case. The value of capacitance obtained was the same as that of the OFF state immediately prior to switching ON, within 10% for all five devices tested. There was a slight tendency for

the OFF state capacitance to be lower than the ON state capacitance.

Figure 5.8 shows graphs of two typical sets of results from the above measurements. Changing the d.c. bias on devices had no effect on the results obtained.

5.4.5. Effect of optical stimulation on the ON state

Three of the devices with two silver electrodes which were tested in the optical cryostat were irradiated with both broad band and filtered, focussed light from a 25W low pressure mercury arc lamp. When in the OFF state these devices were highly photo conductive (giving more than two orders of magnitude increase in current) for filtered light of approximately band gap energy. However, no change whatsoever was observed in the ON state conductivity no matter what incident light was used and in particular there was no tendency for devices to be switched OFF by the optical excitation.

5.5. Conduction in the OFF state

5.5.1. General description of the OFF state conduction

Current flow in the OFF state was in general a non-linear function of voltage. In addition there was a tendency for the current voltage characteristics to alter at random with an applied voltage across the device. These two factors made the interpretation of the I-V characteristics of the OFF state very difficult. Indeed, only in a very few cases was it possible to obtain plots over a wide enough voltage range to make any reasonable deductions concerning the conduction mechanism

Figure 5.8 ON State Resistance and Capacitance versus Frequency.

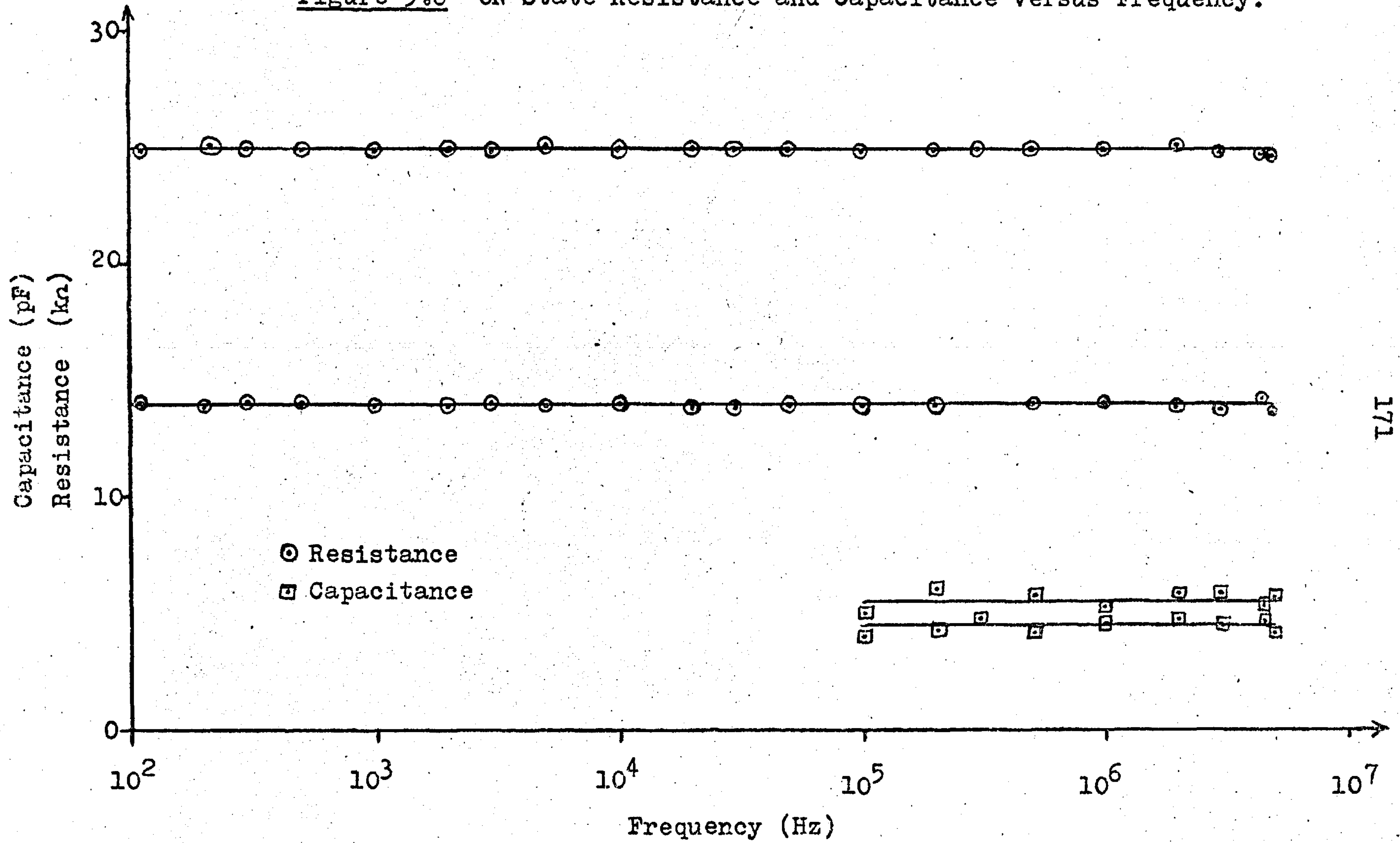

involved. It was almost impossible to make a quantitative comparison between the room temperature and liquid nitrogen temperature conduction curves since the devices would not return to the same characteristic after a cooling and heating cycle, which meant that a continuity of conduction state with changing temperature could not be guaranteed. This did not invalidate the definition of the OFF state given in paragraph 5.3.1 however, since, although the conduction characteristics of the crystal could change, the current was always many orders of magnitude less than the ON state current for a given applied voltage of say 1 volt. All devices were photo conductive in the OFF state when excited with light of band gap energy.

5.5.2 Possible conduction mechanisms and their associated current voltage characteristics.

It is not proposed to give a detailed theoretical analysis of conduction through the crystals at this point. A theoretical discussion of the switching mechanism and associated conduction processes will be given in Chapter 6.

The purpose of this paragraph is to outline some possible conduction mechanisms which may occur so that the reasons for plotting various functions of current against voltage will become clear.

Two convenient reviews of possible non linear conduction mechanisms are given in references 49 and 50 and the reader is referred to these works for further information. Only the results will be quoted here.

Schottky emission of electrons over a barrier gives rise

to a conduction characteristic defined by the following equation:

$$J = AT^2 \exp\left(\frac{\beta V^{\frac{1}{2}} - \phi}{kT}\right) \qquad 5.1$$

where J = current density in amps/metre^2

T = absolute temperature in °K

k = Boltzmann's constant

= 1.38×10^{-23} Joules/°K

$$\beta = e\left(\frac{e}{4\pi\epsilon_r\epsilon_o d}\right)^{\frac{1}{2}} = \text{constant}$$

d = sample thickness in metres

ϕ = barrier height in Joules

V = potential difference across a sample in volts

A = Dushman-Richardson constant

$$= \frac{4\pi emk^2}{h^3} = 1.2 \times 10^6 \text{ Amps/metre}^2/(°K)^2$$

where m is the free electron mass.

If conduction is by Schottky emission then a plot of log I against $V^{\frac{1}{2}}$ yields a straight line from which the constants β and ϕ can be obtained. If the emission is from localised centres within the semiconductor then this is called Poole-Frenkel conduction and a similar relationship exists between log I and $V^{\frac{1}{2}}$. A positive distinction between Schottky and Poole-Frenkel conduction cannot be made by means of the I-V characteristics alone.

Field assisted tunnelling through a thin potential barrier gives rise to a characteristic given by

$$J = BV^n \exp(-\frac{C}{V}) \qquad 5.2$$

where n = 0, 1, 2 or 3[50] and where B and C are constants with the appropriate dimensions. For large enough values of V the exponential term tends to 1 and the conduction characteristic becomes a power law.

A power law conduction characteristic may also be obtained when contacts inject carriers into a sample. If the space charge in the sample due to the injected carriers (both trapped and free) is large, then the potential across the sample is governed by this space charge. The result is that

$$J \propto V^2 \qquad 5.3$$

When all the traps are filled a very rapid increase in current occurs for a small increment of voltage owing to the effective increase in mobility of the carriers. Both space charge limited and tunnelling currents give rise to straight line plots when log I is plotted against log V.

The results of conduction experiments were therefore plotted as log I against log V and log I against $V^{\frac{1}{2}}$ in order to try to identify the mechanism of conduction involved.

5.5.3 Results of the D.C. conduction experiments

Two types of device construction were used in these experiments. The normal type was constructed with contacts directly opposite each other on the two faces of the crystals. The other type (shown in Figure 5.5) was constructed with staggered contacts and was used to show that the conduction observed in normal devices was through the bulk of the material and not due to surface leakage.

Two of the staggered contact type devices were made using radiation wetted indium contacts staggered by about 1mm. At an applied voltage of 300 volts the measured device dark current was of the order of 10^{-13}A. Since this was the limit of detection of the measuring apparatus, no conclusions could be made about the actual magnitude of the current. At 500 volts the device dark current was of the order of 10^{-12} A at room temperature and 10^{-13}A at 77°K.* It will be seen that the above currents were several orders of magnitude less than the current through normal devices at similar applied voltages.

When the devices were illuminated with a low pressure mercury arc lamp the current increased by several orders of magnitude over the dark current. It was then possible to plot conduction characteristics for the devices at both room temperature and 77°K. The results are shown in Figure 5.9. The

---

* It was not considered safe to further increase the voltage across the crystal because of the possibility of electrical discharge which could have caused serious damage to the sensitive measuring apparatus.

Figure 5.9 Current Voltage Characteristics of an Illuminated staggered contact device.

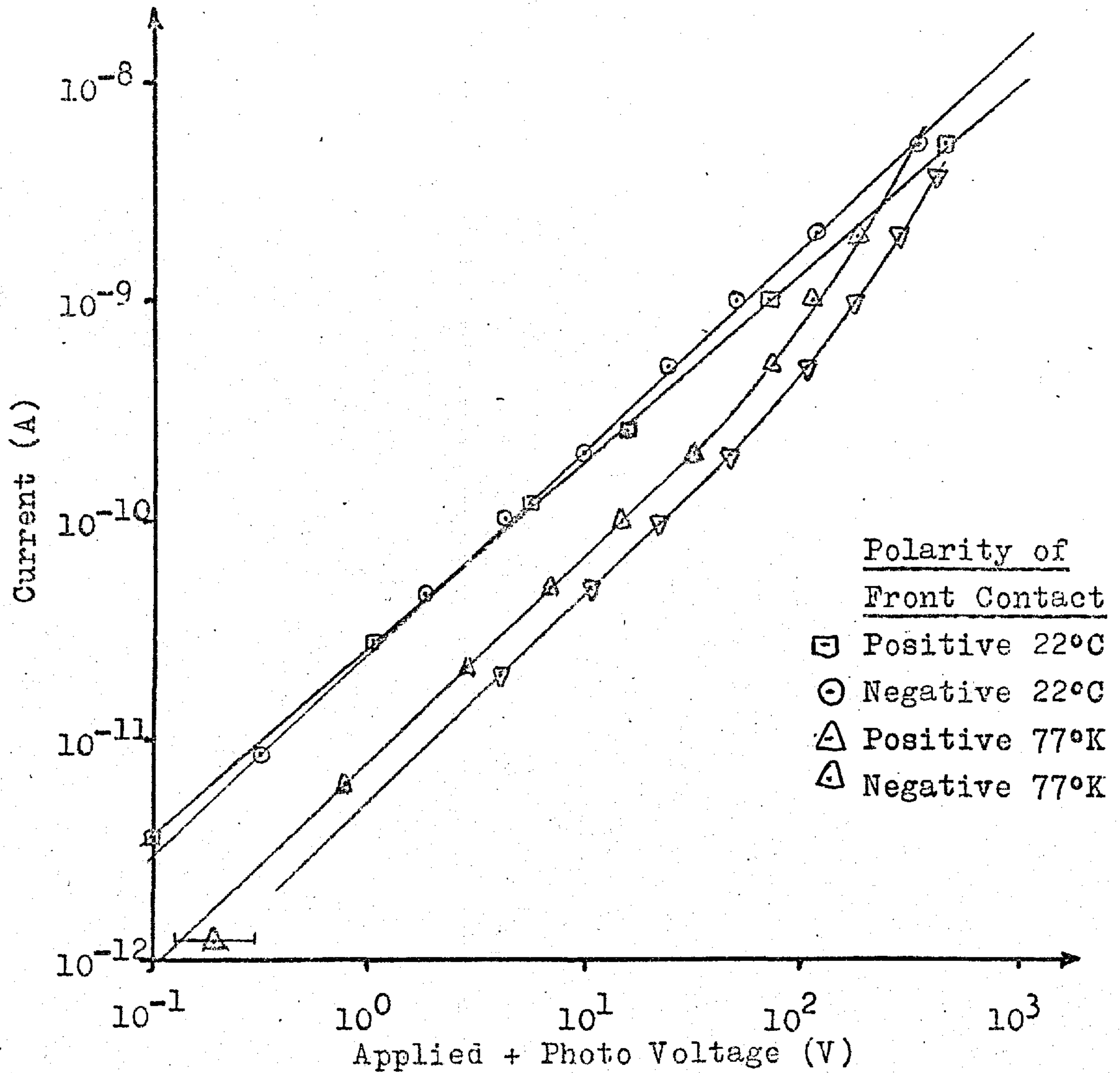

devices exhibited an open circuit photo voltage. This was added to the applied voltage to give the total emf in the circuit in order to plot the curve of Figure 5.9. It can be seen that conduction was nearly ohmic over a large range of voltage in all cases, but that at 77°K a super linear region occurred at high currents.

Because of the similar size of the normal and staggered contact devices, the surface leakage currents must have been of the same order of magnitude in both cases. The experiments with the staggered contact devices therefore show that surface leakage currents can be neglected in comparison with bulk currents in normal devices. The conduction through illuminated devices eliminates the possibility of the devices having been "open circuit" and demonstrates the ability of the radiation wetted indium contacts to extract carriers generated within the bulk of the zinc sulphide.

Most of the normal devices did not conduct stably over a large enough range of voltage for useful deductions to be made from the conduction characteristics. On account of this, only a few "well behaved" results have been plotted and are shown in Figures 5.10 to 5.16 inclusive. Figure 5.10 shows the conduction characteristics of a device with one indium (radiation wetted) and one evaporated silver contact on a log I versus $V^{\frac{1}{2}}$ scale. The room temperature characteristics are clearly straight lines. Figure 5.11 shows a log I versus log V plot of the low temperature characteristics which indicates a power law for

Figure 5.10 OFF State Characteristic.

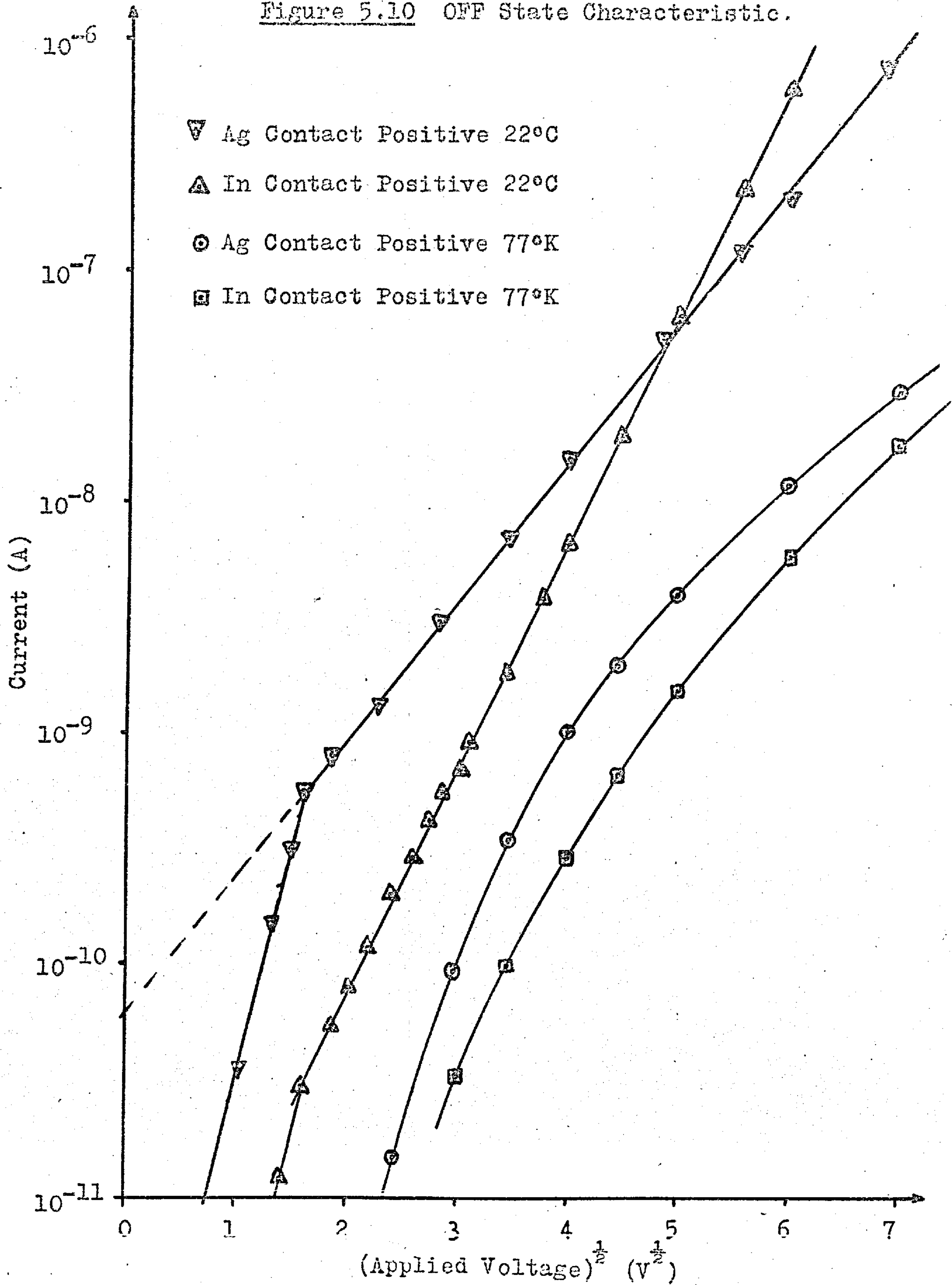

Figure 5.11 OFF State Characteristic.

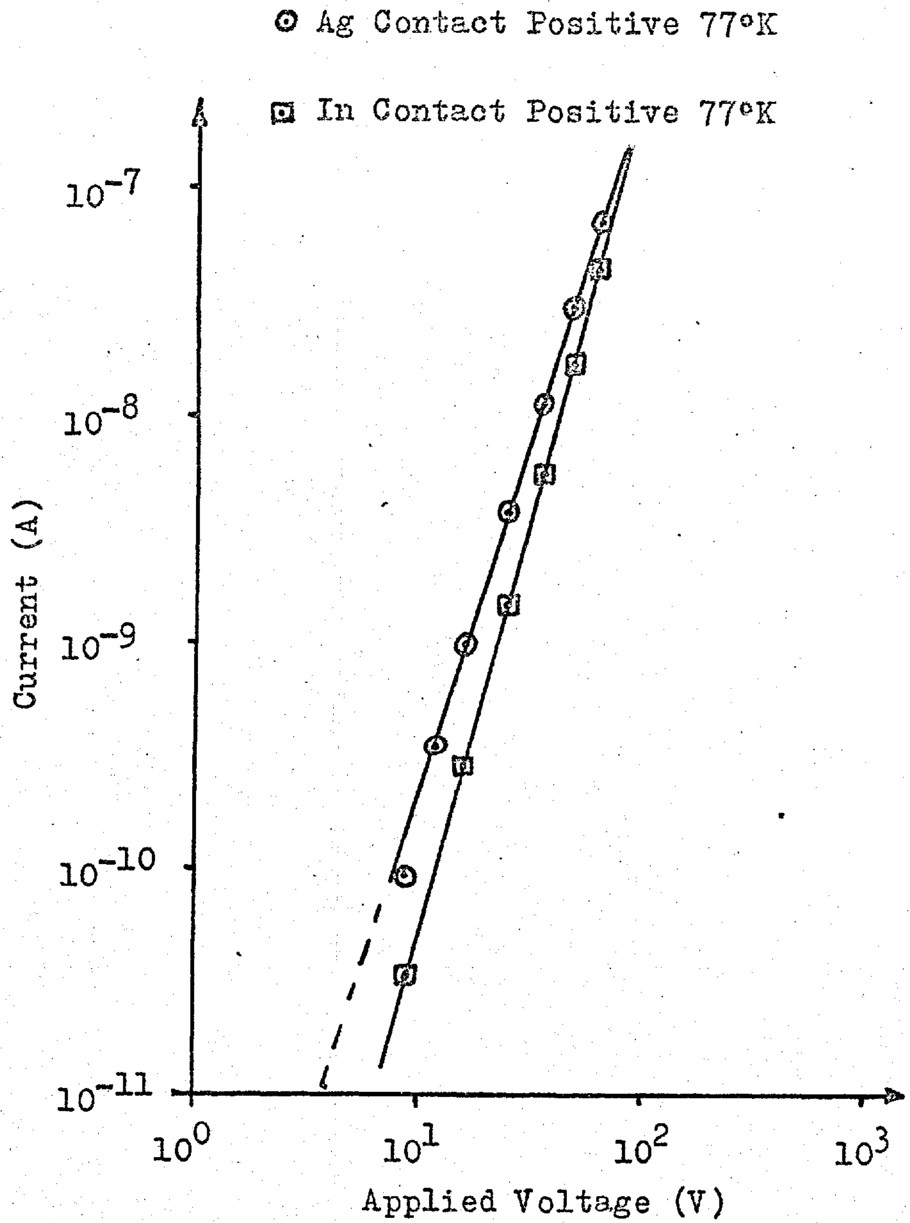

conduction at the lower temperature. Figures 5.12 and 5.13 show the characteristics obtained from three different devices each with two evaporated silver contacts, all plotted on a log I versus $V^{\frac{1}{2}}$ scale. It can be seen that all these plots are straight lines over a large range of current both at room temperature and 77°K. Figure 5.14 shows another characteristic obtained from the device whose characteristics are plotted in Figure 5.13, this time on a log I versus log V scale. In this case the relationship between current and voltage is clearly a power law. Different mechanisms may therefore be responsible for the OFF state conduction of a given device at different times.

Figure 5.15 shows the conduction characteristics for a device with graphite paste electrodes. This too is a straight line on the log I versus $V^{\frac{1}{2}}$ plot.

The room temperature conduction characteristics for two more devices are plotted in Figure 5.16. The lower of these is for a device with two evaporated silver contacts and the upper one is for a device with two silver paste electrodes. Both characteristics are straight lines with the same slope of 1.13. Thus the relationship $I = AV^{1.13}$ holds for both devices. Both curves deviate from the straight line at the same voltage, namely 1 volt. It seems likely therefore, that the same mechanism controls the conduction in both these devices at room temperature.

In interpreting these results we see that at least two

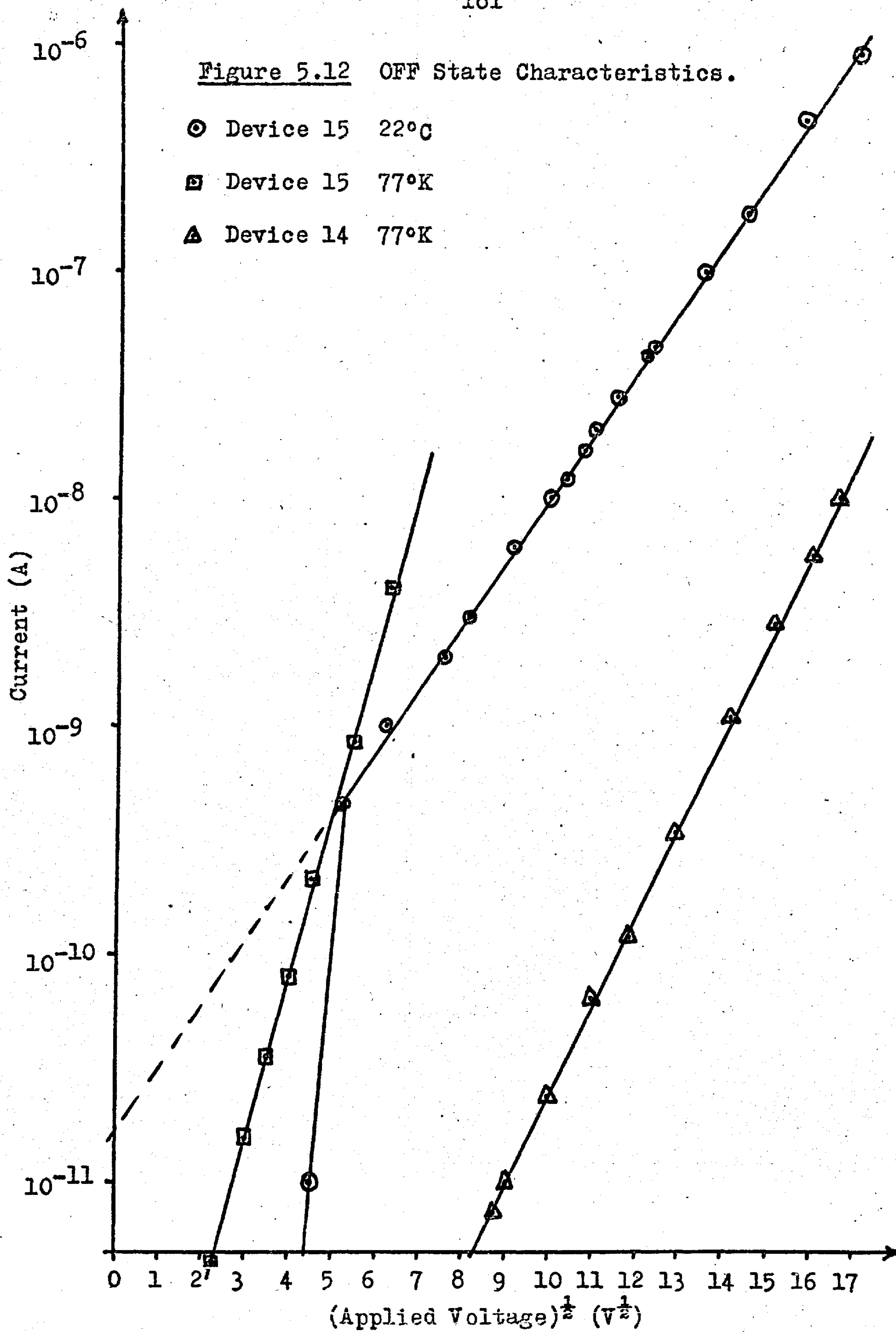
Figure 5.12 OFF State Characteristics.
Device 15 22°C
Device 15 77°K
Device 14 77°K
10-6
10-7
10-8
10-9
10-10
10-11
Current (A)
0 1 2 3 4 5 6 7 8 9 10 11 12 13 14 15 16 17
(Applied Voltage)½ (V½)

Figure 5.13 OFF State Characteristics.

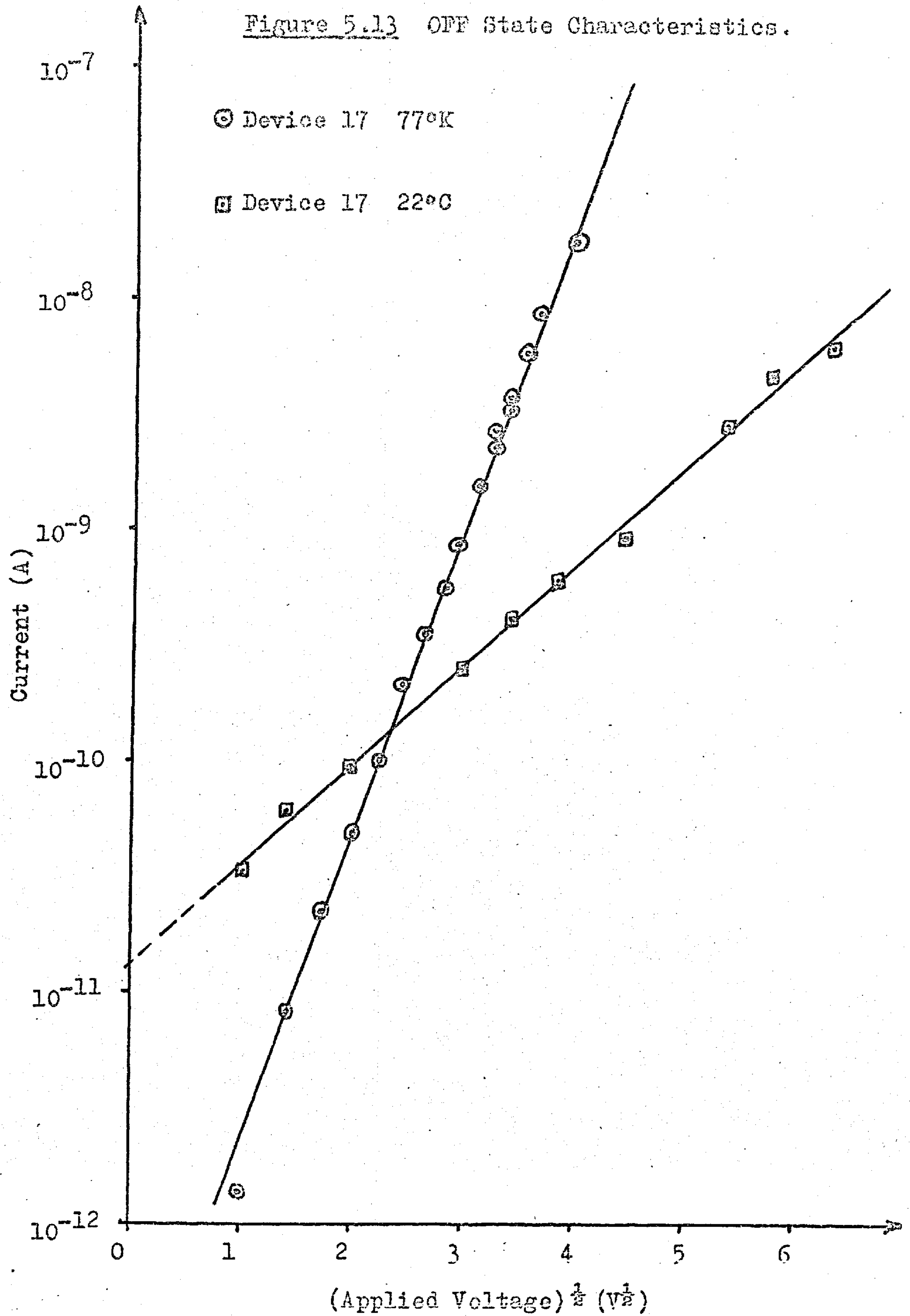

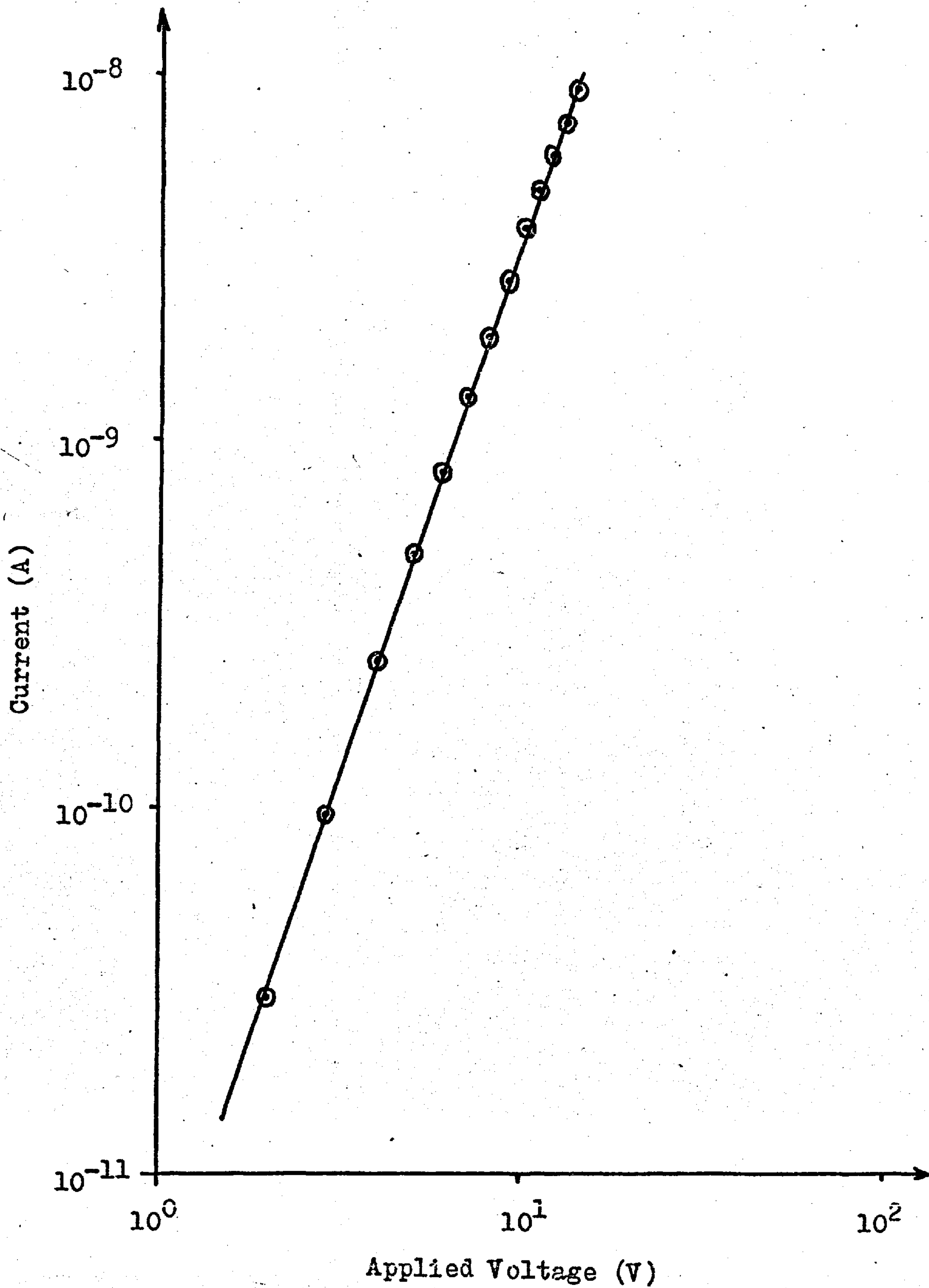

Figure 5.14 OFF State Characteristic.
Device 17 77°K

Figure 5.15 OFF State Characteristic of a Device with Graphite Electrodes 77°K.

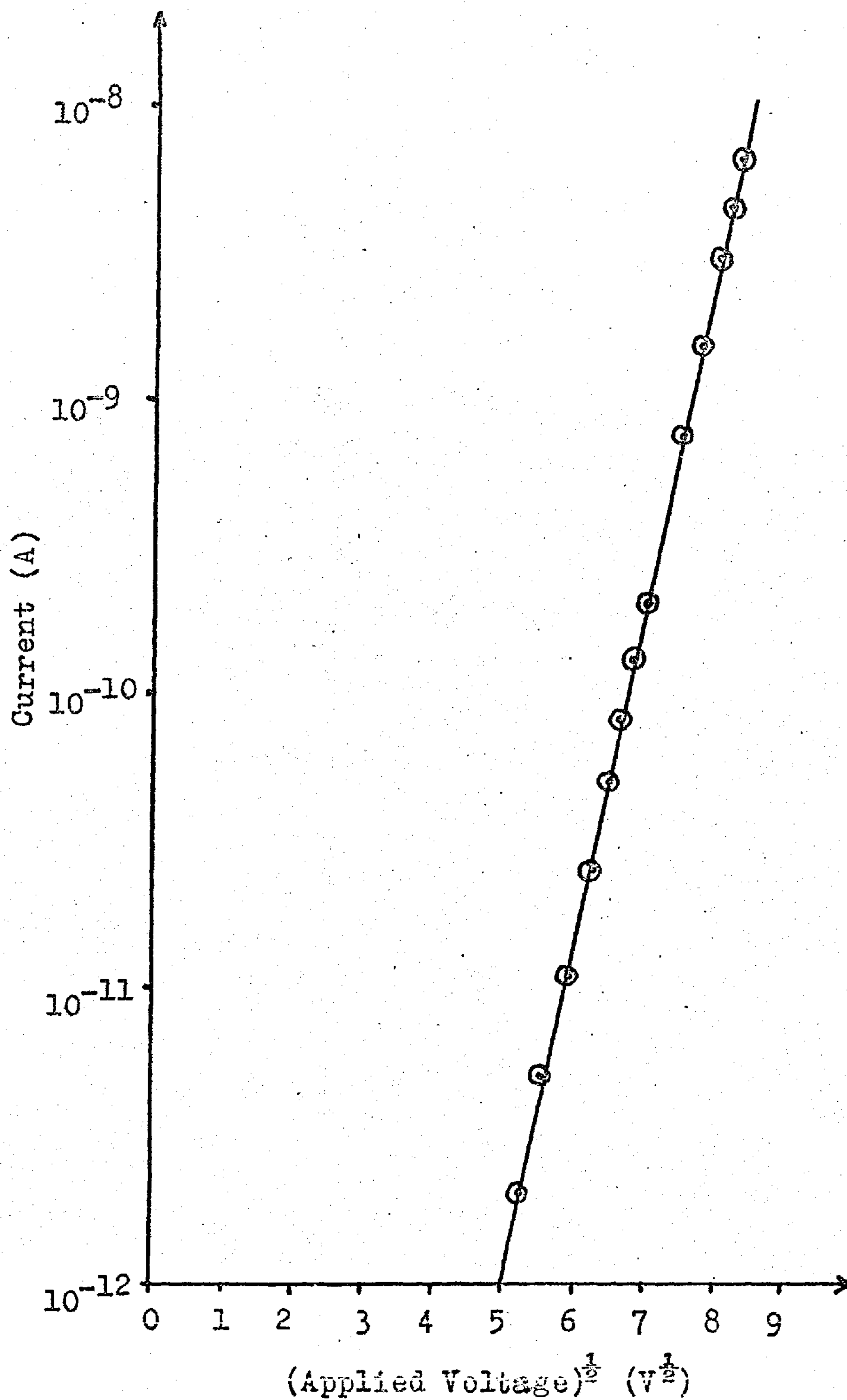

Figure 5.16 OFF State Characteristics 22°C.

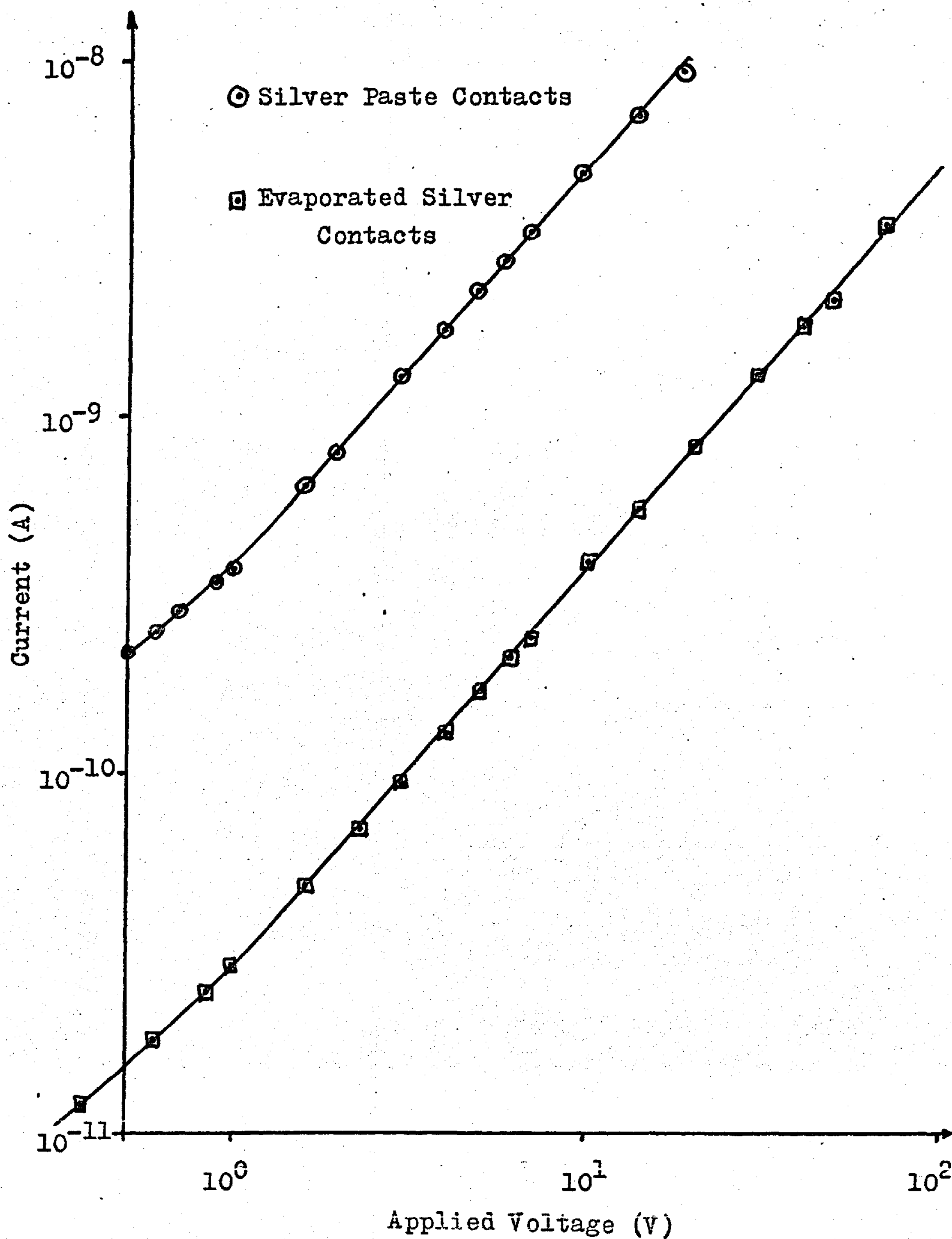

types of conduction characteristic exist in the OFF state, namely,

$$I \ \alpha \ V^{x} \qquad 5.4$$

and $$I \ \alpha \ \exp V^{\frac{1}{2}} \qquad 5.5$$

Experimental values of "x" are given in Table 5.2. This shows that an approximate cube law was followed at 77°K whereas the only available results at room temperature show that conduction was only slightly superlinear (x just greater than one).

TABLE 5.2

GRAPH	CONTACTS	TEMPERATURE	POLARITY	x
5.11	Ag , In	77°K	Ag +	3.25 ± 0.07
5.11	Ag , In	77°K	Ag -	3.45 ± 0.08
5.14	Ag , Ag	77°K	Either	2.95 ± 0.05
5.16	Ag , Ag	Room Temperature	Either	1.13 ± 0.01
5.16	Silver Paste	Room Temperature	Either	1.13 ± 0.01

Very little can be said regarding physical interpretation of this power law dependence of current on voltage. Jonscher[49] states that no satisfactory explanation of this conduction has yet been given. It must therefore suffice to observe a certain consistency between the results for the different devices.

If equation 5.1 is applied to the conduction characteristics which exhibit the dependence given by equation 5.5, then definite quantitative deductions of the value of the energy barrier may be made. The results are given in Table 5.3. These results were derived on the assumption that

(a) the area of current conduction path was approximately equal to the contact area

(b) equation 5.1 correctly described the current flow.

The three room temperature results for devices with a silver contact negative (i.e. electron emission from silver into ZnS) give remarkably consistent values of ϕ . With indium negative at room temperature ϕ is somewhat lower. At 77°K the agreement between the results for devices with a silver contact negative is not quite so good. The high result may however, have been due to the contact not being active over its whole area. It can be seen that the energy barrier for silver contacts was approximately the same multiple of kT at both room temperature and 77°K. Thus the energy barrier was dependent on temperature and a plot of log I against $\frac{1}{T}$ could not be used to provide additional information about the barrier height.

The barrier height obtained for graphite paste contacts is significantly higher than for silver contacts. This may be the true value, or it may be an artificially high value owing to contact inhomogeneity and resultant current "channelling."

According to equation 5.1 it should be possible to deduce the sample thickness from the slope of the graphs if it is

TABLE 5.3

TEMP.	Contacts	Polarity	Intercept	J_o/AT^2	ϕ		Slope	THICKNESS	
			I_o					Calc.	Meas.
^oK			AMPS		kT	eV	Decades/$V^{\frac{1}{2}}$	μm	μm
293	Ag , In	Ag +	6×10^{-11}	3.0×10^{-15}	33.4	0.84	0.60	-	-
293	Ag , In	Ag -	8×10^{-13}	4.0×10^{-17}	37.8	0.96	0.98	-	-
293	Ag , Ag	Either	1.7×10^{-11}	7.3×10^{-17}	37.2	0.94	0.26	0.75	50
77	Ag , Ag	Either	1.2×10^{-13}	7.5×10^{-18}	39.4	0.26	0.71	1.5	50
77	Ag , Ag	Either	2.9×10^{-15}	1.8×10^{-19}	43.2	0.29	0.39	-	-
293	Ag , Ag	Either	1.3×10^{-11}	5.6×10^{-17}	37.4	0.95	0.43	0.28	23
77	Ag , Ag	Either	1.2×10^{-13}	7.5×10^{-18}	39.4	0.26	1.3	0.44	23
77	Graphite	Either	2×10^{-18}	1.2×10^{-22}	48.8	0.32	1.1	-	-

assumed that a uniform field exists in the sample. The values derived from equation 5.1 are shown in Table 5.3 together with the measured crystal thickness for two devices. It can be seen that the calculated values are vastly different from the measured value. In addition the calculated values for 77°K are roughly twice these for room temperature. The only point of agreement is that the calculated thickness of the thicker device is indeed greater than that for the thinner device. This disagreement may indicate that the conduction mechanism is not that implicit in the use of equation 5.1 or that field inhomogeneities in the device cause most of the voltage to be dropped across a very thin region of the crystal. This may be so if the contact region is an exhaustion region with no free carriers in it.

5.5.4 Frequency dependence of the OFF state conductivity

It was not possible to make useful measurements of the in-phase component of the OFF state impedance above about 2kHz as the capacitance of the devices effectively short-circuited this component at higher frequencies. In general the conductance as measured on the Wayne-Kerr bridge was of the same order of magnitude at low frequencies as the d.c. value and it was not possible to establish any definite trends owing to the limited range of measurement frequencies.

5.6 Thermally Stimulated Current (T.S.C.) Measurements

5.6.1 The T.S.C. Method

If a semiconductor or insulator containing trapping states is cooled rapidly from room temperature to some much lower

temperature (say that of liquid nitrogen) electrons (or holes) may be "frozen" into the traps. On slowly reheating these carriers will be released into the conduction (or valence) bands of the material and cause a current to flow in an external circuit. The variation of this current with temperature can be used to identify the energy of the trapping state. Servini[50] discusses this method of thermally stimulated currents in detail and derives an expression for the current flow caused by a single energy trapping state. In deriving such expressions it is necessary to assume a linear rate of increase of temperature. Thus, ideally, experiments should all be done under these conditions.

Experiments were conducted both in the optical cryostat already described (Figure 4.8) and in a simple cryostat normally used for Hall effect measurements and shown in Figure 5.17. This latter cryostat was used for measuring devices when optical excitation was not required as it was much easier and quicker to use. The heater element wound round the outside allowed the device under test to be totally enclosed in a temperature controlled space. A thermocouple was tied to the device case and kept in thermal contact with the device with silicone grease, thus making sure that the measured temperature was that of the device. The heating rate was kept practically constant over the range 100°K to 270°K by using a Solartron P.S.V. AS 1410 power supply to supply a constant current of one amp to the heater. The increasing heat loss as the temperature rose was

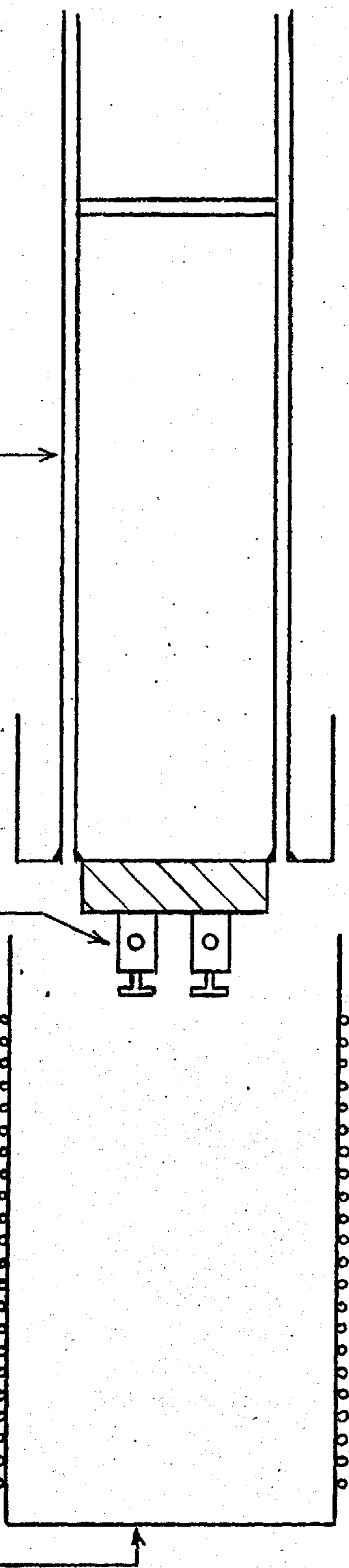

Figure 5.17 Hall Cryostat.

compensated by the rise in power dissipation in the increasing resistance of the heater. The same method was used to maintain the constant heating rate in the optical cryostat where the heater element was wound round the pillar used to support devices. The temperature versus time curves for the two cryostats are shown in Figure 5.18.

Measurements of the charge release from devices were made using the Vibron 33B electrometer with the current adaptor box. The output of the Vibron was fed to the Y input of the Bryans X - Y recorder. The X input was internally switched to the 20 seconds/cm sweep rate.

5.6.2 Results

The results obtained did not show the expected T.S.C. peaks. Instead there was a dramatic release of charge at a temperature of -40°C (±3°C). The rate of charge release at this temperature was too great for the chart recorder pen to follow it. Figure 5.19 shows a typical trace obtained from a device cooled with neither electrical nor optical excitation having been applied before or during cooling. Figure 5.20 shows a similar trace obtained after cooling the device with a bias of 8 volts applied to its terminals. As can be seen the application of a bias during cooling resulted in a background emission superimposed upon the previous discontinuity. This background emission commenced at a temperature just below the discontinuity and the polarity was such that electrons were emitted from the terminal to which they were supplied during cooling.

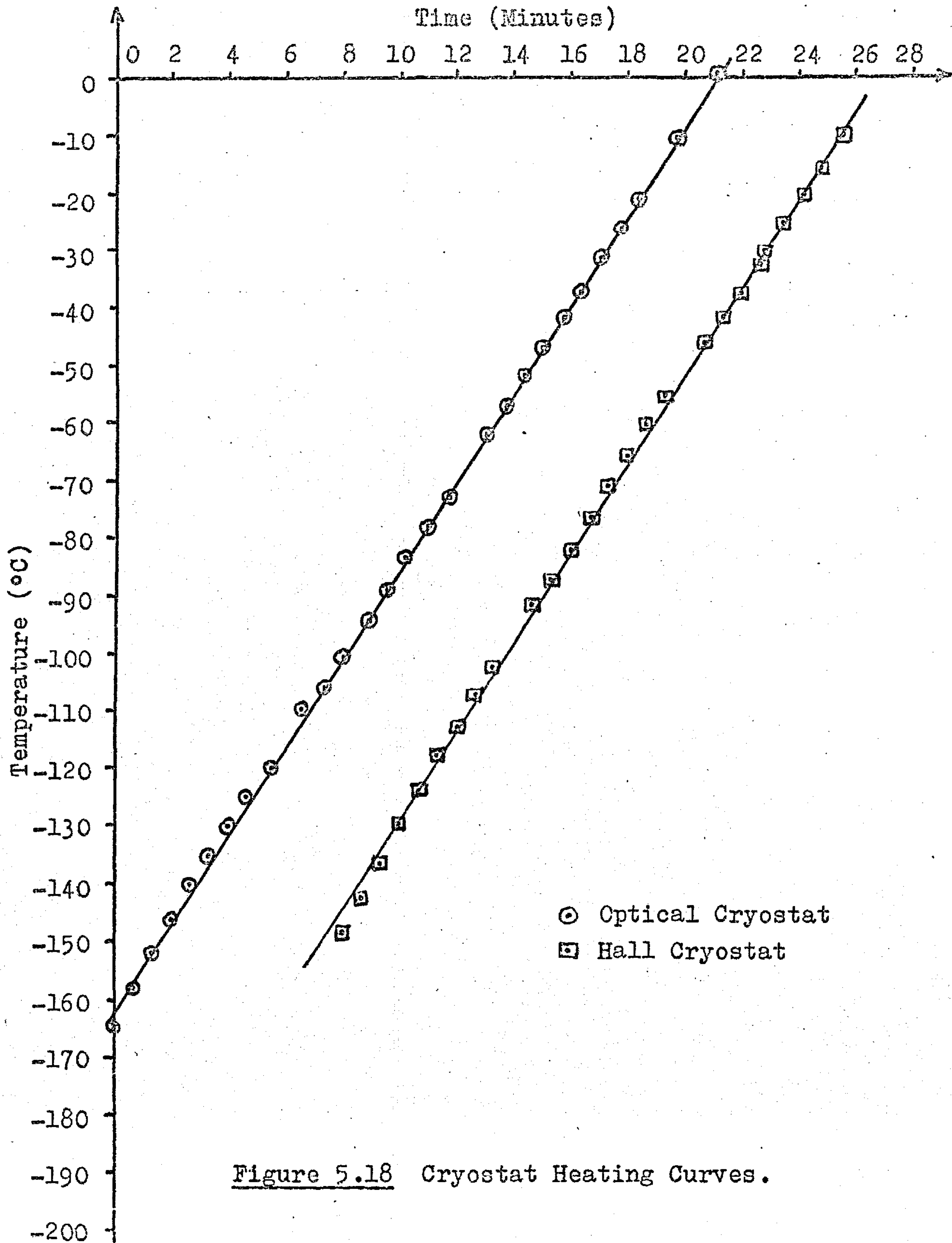

Figure 5.18 Cryostat Heating Curves.

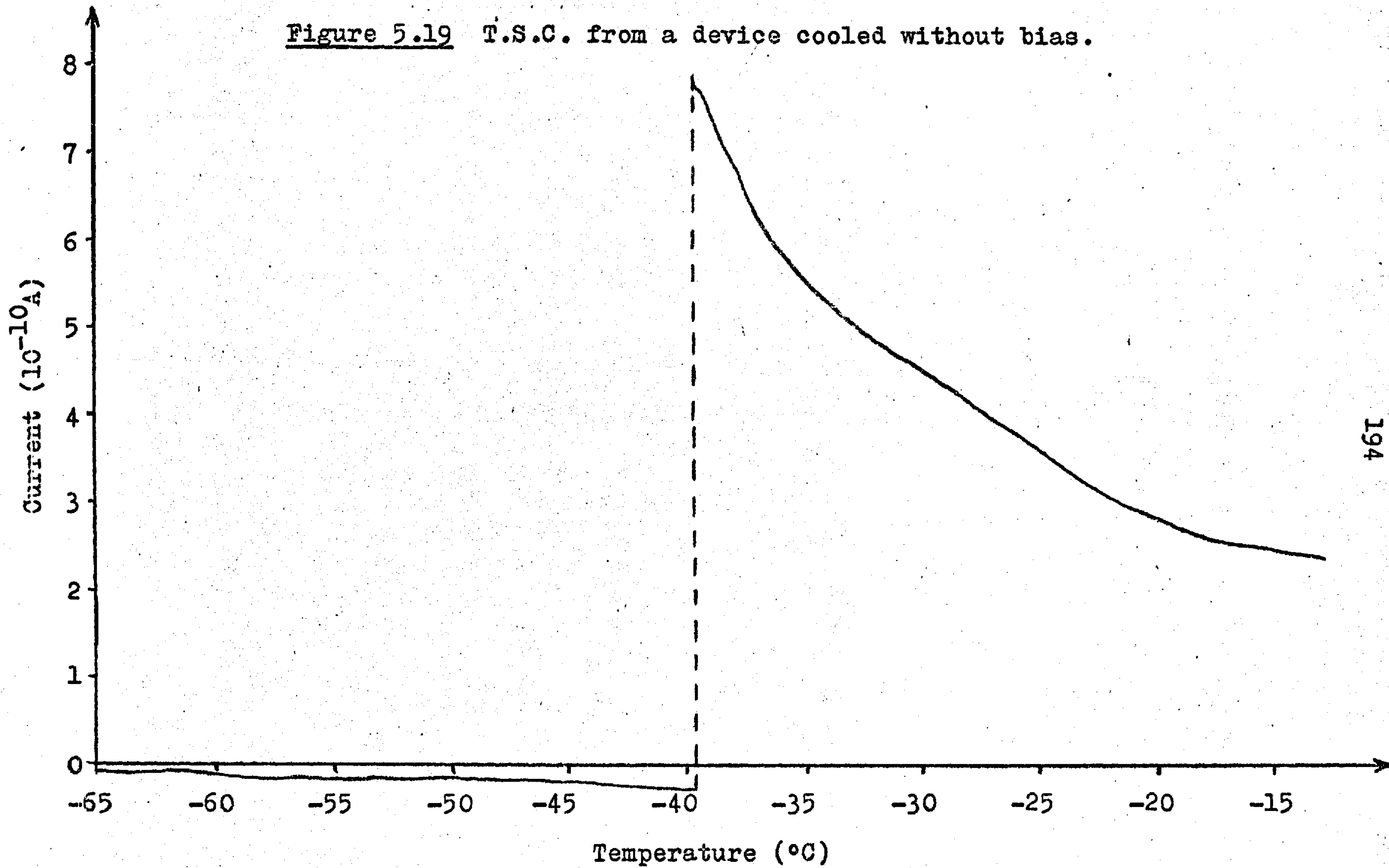

Figure 5.19 T.S.C. from a device cooled without bias.

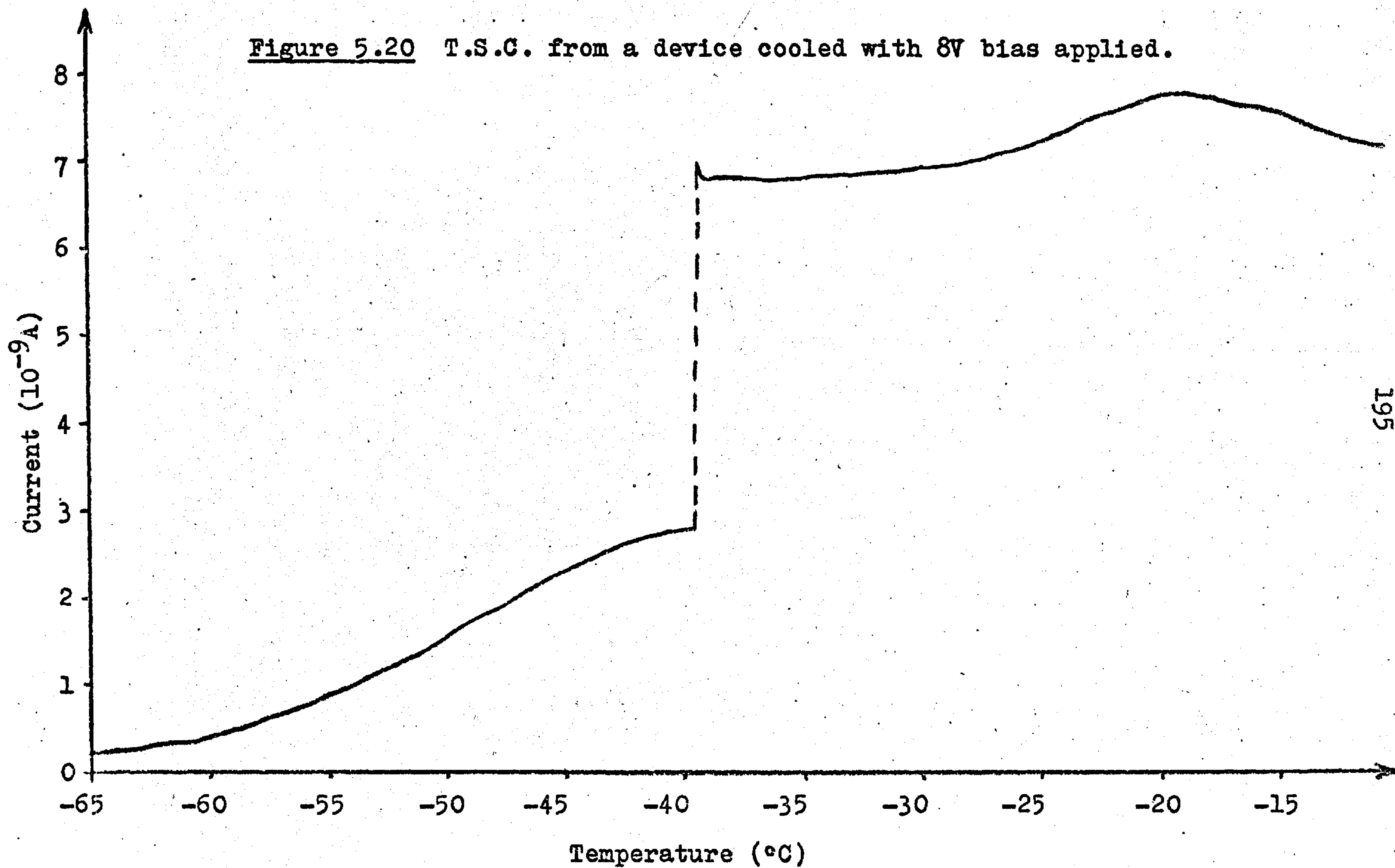

Figure 5.20 T.S.C. from a device cooled with 8V bias applied.

The sudden release of charge at -40°C was present on every heating run and was not quenched after heating and recooling with the device terminals either short-circuited or open circuit.

Figure 5.21 shows the charge emission from a device which was cooled to 77°K, switched to the ON state and then heated at the standard heating rate. The stable trace at the low temperatures shows that the crystal was in the ON state providing a low impedance (and therefore low noise) source to the Vibron. At a temperature of -39°C there was a sudden release of charge. Above this temperature charge release was continuous and variable showing that a temperature of approximately -39°C is a critical point with regard to the switching process. It may be recalled (Figure 5.7) that this temperature was also the point of the onset of rise in the ON state resistance.

No effect on the charge release from crystals was detected when they were optically excited during cooling. This applied whether broad band or narrow band excitation of band gap energy was used.

Seven devices were examined for T.S.C. emission and all showed the unquenchable charge release at -40°C ± 3°C. In particular two devices were tested twenty times each and found to give the same form of charge release at -40°C each time.

Figure 5.21 T.S.C. from a device in the ON state.

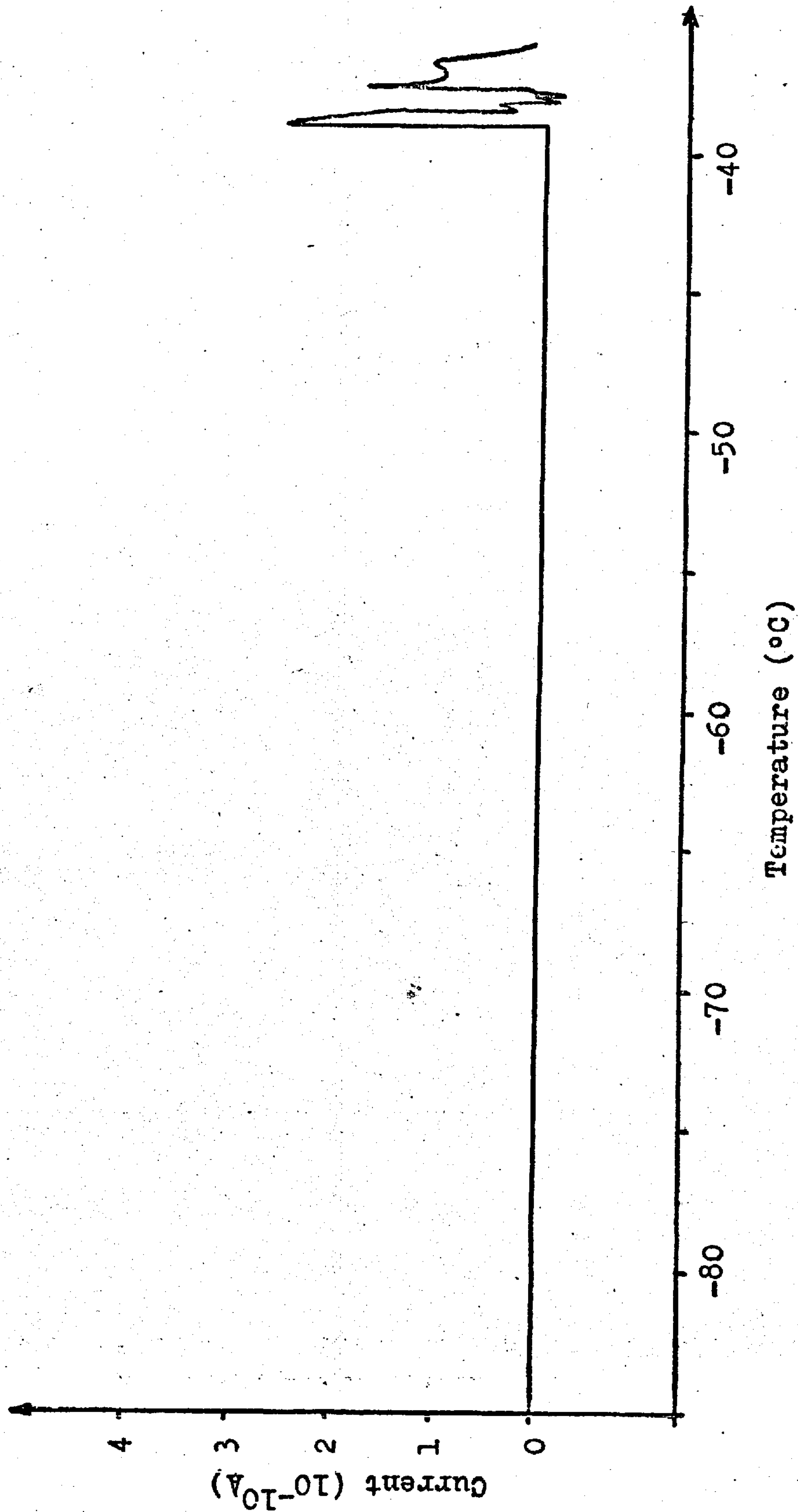

From the results given in this paragraph it is evident that there is an electrically active centre in these devices which is stable below -40°C and unstable above this temperature. The evidence suggests that this centre is involved in the switching process.

CHAPTER 6

Theoretical discussion of conductivity switching

6.1 Review of previous work

In recent years there have been many reports of negative resistance and conductivity switching phenomena in thin insulating films (references 51 to 59 inclusive). There have also been reports of an optically induced conductivity storage effect in CdS single crystals (references 60 and 61).

Four basic mechanisms have been proposed to explain the negative resistance and switching phenomena. These are double carrier injection[54,62], impurity band conduction[51,56], changes in capture cross-section of traps brought about by impact ionization[55] and the formation of conducting filaments between the electrodes[57,59].

Gibbons and Beadle[57] propose that a "metallic bridge" is formed between the electrodes in the conducting state. The results presented in Chapter 5 rule out this explanation for the following reasons:-

(a) The observed temperature coefficient of ON state resistance in the range 77°K to 230°K was far too low to be accounted for by metallic conduction.

(b) The high switch OFF speed suggests an electronic process rather than a mechanical one.

(c) The reproducibility of the ON state resistance for consistent switch ON conditions is inconsistent with the formation of a new metallic channel at every switch ON operation.

(d) The switch OFF time was not shortend noticeably by using higher switch OFF current as was observed by Gibbons and Beadle[57]. The opposite tended to be true.

(e) Several devices were examined under an optical microscope after having been switched many times between the two conductivity states. No sign of macroscopic defects was found.

The filamentary model proposed by Dearnaley[59] is a phenomenological one and is difficult to discuss since it makes no definite proposals for the mechanism by which the filaments are formed or for the mechanism of electrical conduction within such filaments. The only specific proposal is that the filaments rupture when the temperature exceeds some threshold value. The concept of filamentary conduction is not in conflict with the explanation to be given here. Indeed, it is difficult to see how the conduction could be anything other than filamentary in the devices described in this work, since any slight inhomogeneity in the crystals must result in current channelling at the "weak spots" in the crystals. However, the argument that switching to the high resistance state is caused by rupture of filaments due to joule heating is not easily reconcilable with the observation (5.4.3) of the spontaneous switching of the ZnS devices to the high resistance state at temperatures above -40°C.

The double injection theory of Lampert[62] is not directly applicable since it assumes a dynamic equilibrium between the injected carriers and the traps. Thus there can be no memory effect with this model as the trapped charged rapidly decays when the voltage on the device is removed. The linearity of the ON state down to voltages of the order of 1mV also rules out Lampert-type double injection phenomena.

The results of Feldman and Gutierez[55] are, as they state, indicative of a charge multiplication process, since the current increased with increasing film thickness for a given electric field strength. In addition, a sustaining voltage was necessary to maintain the low impedance state. No increase of current with crystal thickness was observed for ZnS and no sustaining voltage was necessary. Thus the mechanism of the conduction observed in reference 55 appears to be different from that observed here in ZnS. A mechanism involving a change in capture cross section may still be applicable although this may operate in a rather different manner from that proposed in reference 55.

Simmons and Verderber[51,52] observed that thin SiO films sandwiched between one gold and one aluminium electrode exhibited voltage controlled negative resistance characteristics as shown in Figure 6.1. In addition they found that a higher resistance conduction state could be induced in their devices if they were switched off very rapidly from any point on the negative resistance part of the characteristic. The original conduction

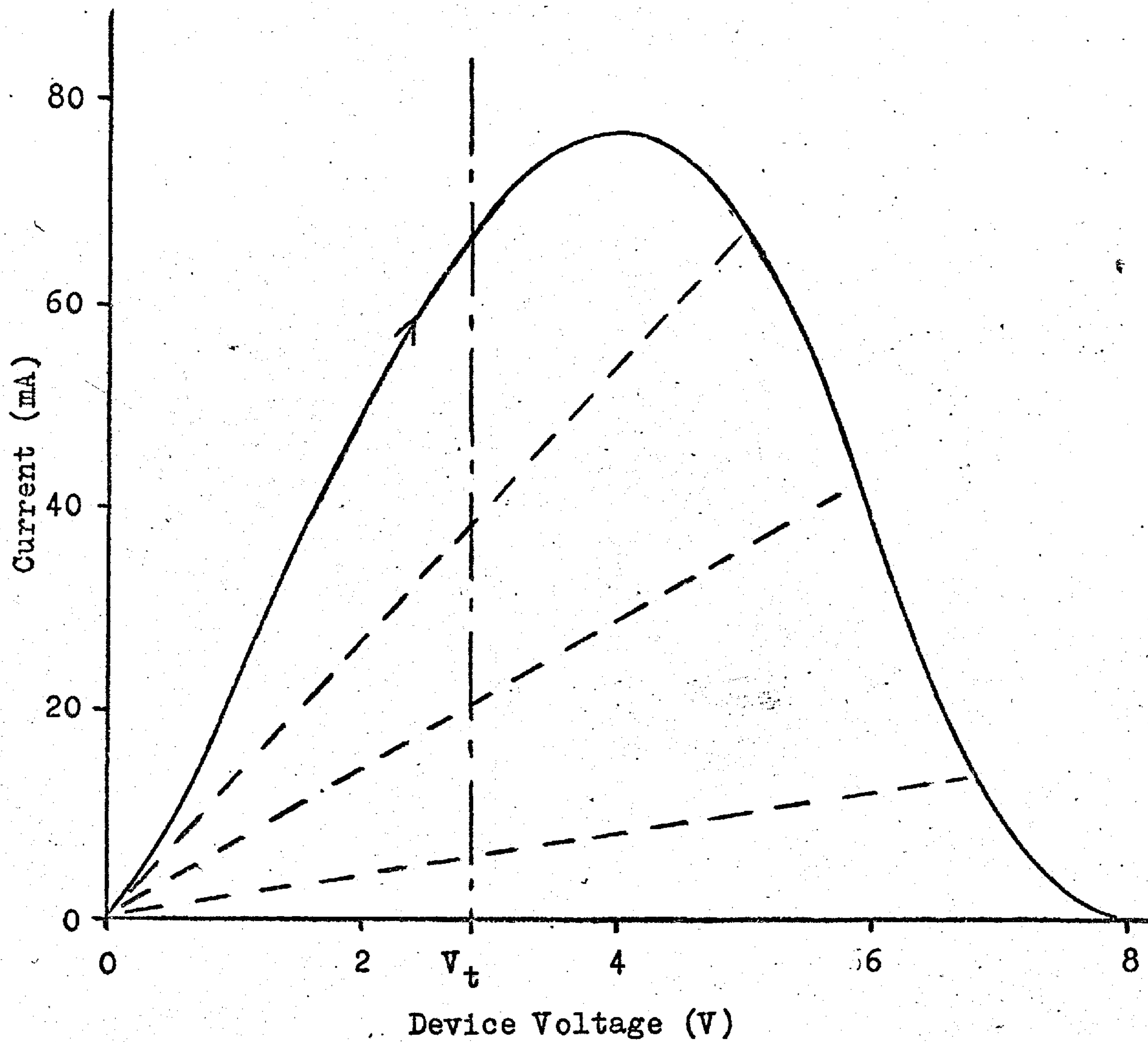

Figure 6.1 Current-voltage characteristics of Simmons and Verderber type devices.

characteristic could then be restored by applying a voltage to the devices in excess of a well defined threshold voltage. Hickmott[56] found that thin alumina films sandwiched between suitable electrodes could be made to exhibit d.c.characteristics almost identical to those observed by Simmons and Verderber[51] in SiO. The storage of the high resistance state and the existence of a threshold voltage for restoration of the original conductivity was also noted by Hickmott.

In contrast to the results of Feldman and Gutierez, both Simmons and Verderber and Hickmott assert the need for a forming process before switching or negative resistance can be obtained. This process consists of applying a high field to the devices for a given length of time dependent on the temperature of the device. The lower the temperature the longer time that is required to form devices. In particular Verderber et al.[52] report that no devices could be formed below -50°C. The forming process is shown to be electrode dependent[52,56] and is supposed in references 51, 52 to be caused by the migration of positively charged ions into the insulator film. Both Simmons and Verderber[51] and Hickmott[56] attribute the high formed conductivity to impurity band conduction and Simmons and Verderber[51] give a detailed account of a possible conduction mechanism based on the assumption that the impurity states are introduced by the positive ions driven into the insulator during forming. Their theory depends on a high density of ions ($\sim 10^{26}/m^3$) penetrating the whole of the insulator thickness

(up to 3000Å, ref. 52) under the action of the field without actually causing a catastrophic short. This may be possible in a highly disordered film, but it hardly seems likely that this density of ions could penetrate, under the influence of an electric field alone, a distance of the order of 10 μm in a highly perfect ZnS single crystal, without causing catastrophic and irretrievable breakdown.

However, there are similarities in the operation of the oxide film switches described by Simmons and Verderber[51,52] and Hickmott[56] and the ZnS single crystal devices described here. The above authors note that the voltage applied to a device must be rapidly reduced to zero if a transition from a high conductivity state to a low conductivity state is to occur. This was also observed for ZnS (5.3.4). In addition, they note the virtual independence of temperature of the high conductivity state which was also found in the case of ZnS (5.4.3).

A memory effect at zero bias is noted by the above authors and in particular Simmons and Verderber[51] note a much more permanent memory at 77°K than 300°K. Kulp[60] has found that optically induced conductivity in CdS crystals can be stored at temperatures up to 220°K. Above this temperature a gradual time dependent decay was observed. From the rate of decay and from saturation photo currents he deduced that the product of the number of traps and their capture cross-section rose by a factor of 10^4 between 205°K and 270°K. All these observations are in accordance with the observed memory effect in ZnS. A similar

rapid decay of the high conductivity state was observed (5.4.3) in ZnS devices at 233°K. This was also the temperature of the sharp discontinuity in the T.S.C. curves (5.6.2).

Finally, Litton and Reynolds[53] found that the passage of too great a current quenched optically stimulated stored conductivity in CdS. This may have been due to local heating as they suggest. However, it seems unlikely that a crystal cooled to 4.2°K could be locally heated to 230°K. Perhaps it is more likely that the same switch OFF mechanism was being observed as was observed here in ZnS and in references 51 and 56 in oxide films.

6.2 Proposed band model for switching crystals

6.2.1 General description

The experimentally observed forming process which has to occur in order to achieve conductivity switching in both ZnS and thin oxide film switching devices, suggests that the insulating medium is permanently (or semi-permanently) changed by the application of an electric field at room temperature. It is logical to argue that this change is brought about by the introduction of electrode material into the insulator since forming is electrode dependent. However, it does not seem likely that electrode material could penetrate any more than a very thin surface layer of the ZnS crystals in the concentrations which would be required to produce a bulk conductivity large enough to explain the low resistance of the ON states of these devices. We therefore present a model based on the modification of the

surface depletion barriers which are generally present at metal-ZnS interfaces. This model explains all the experimental observations qualitatively and gives a quantitative value for the ON state resistance of devices which is in good agreement with experimentally obtained values.

Figure 6.2 shows the general energy band picture for a crystal of ZnS sandwiched between two metal electrodes and having shallow surface layers of fixed distributed positive charges. If the concentration of charge at the surface is great enough then thin depletion barriers result and the potential of the conduction band inside the surface is brought so close to the Fermi level that a large concentration of free electrons resides there in thermal equilibrium. The conduction band may then communicate freely with the metal electrodes by means of electrons tunnelling through the thin surface barrier.

In the central portion of the crystal there is an accumulation of electrons and so the conduction band moves away from the Fermi level in this region with a resultant decrease in free carrier concentration. It will be shown however, that this rise in potential will only be of the order of a few kT in a thin crystal and that the conduction band is practically flat in the centre of the crystal. Thus the ON state resistance is defined by the central portion of the crystal with the surfaces acting in effect as ohmic (majority carrier injecting) contacts.

In the OFF state some of the positive barrier charge is assumed to be neutralized, so reducing the band pull-down

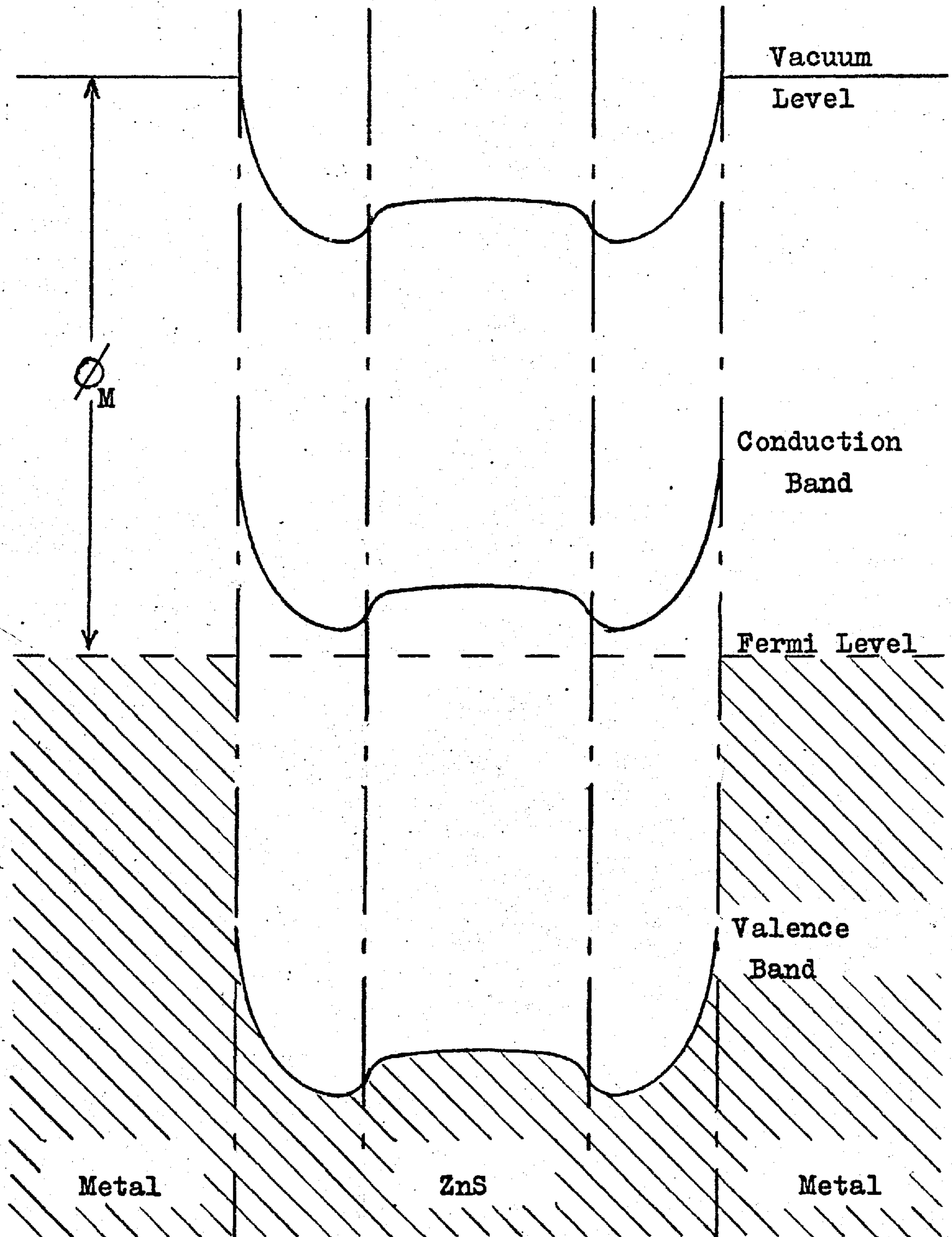

Figure 6.2 General band picture of a Metal-ZnS-Metal sandwich structure.

effect. A barrier is thus created to the passage of electrons from metal to ZnS and this results in a very high resistance state.

6.2.2 Potential distribution in a device for zero applied voltage.

We assume a symmetrical device for ease of calculation and consider the barrier region shown in Figure 6.3. We take for simplicity a constant concentration of surface charge penetrating a distance "d" into the crystal. Beyond this point the fixed charge is assumed equal to the very small concentration of donors normally present in the crystals. (This abrupt distribution does not differ too greatly from the complementary error function distribution which would be expected for impurities diffused into the crystal from a constant concentration source.)

We take our origin of distance x at a point distance d beneath the surface of the crystal and the potential of the conduction band at this point as the origin of voltage (Figure 6.3).

Let N_i/m^3 be the concentration of positive charges in the barrier region, and N_d/m^3 be concentration of donors in the bulk.

Then Poisson's equation gives

$$\frac{\partial^2 V}{\partial x^2} = -\frac{e(N_d - n)}{\epsilon_r \epsilon_o} \qquad 6.1$$

for $x > 0$

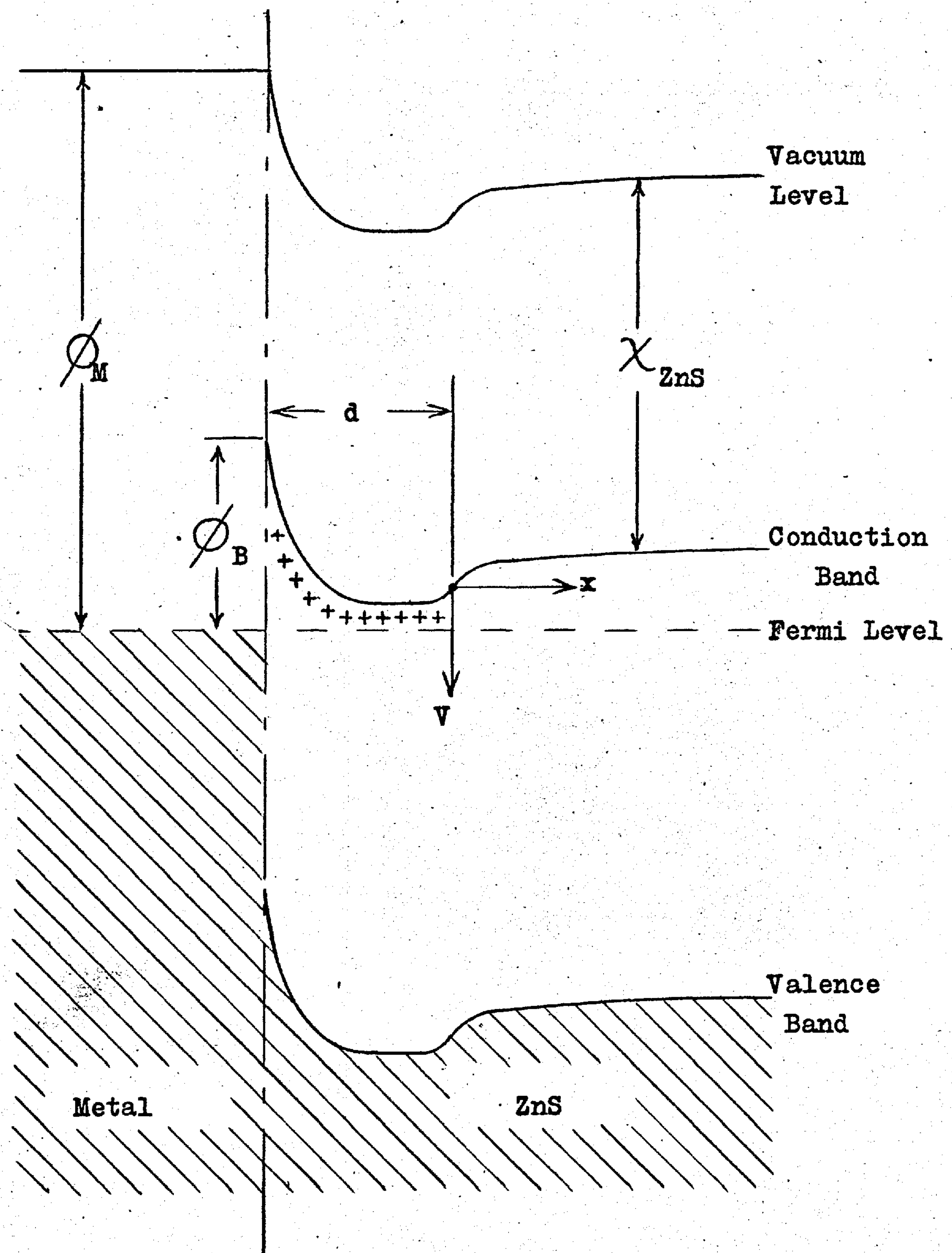

Figure 6.3 Band diagram of a Metal-ZnS interface.

and $$\frac{\partial^2 V}{\partial x^2} = -\frac{e(N_d + N_i - n)}{\epsilon_r \epsilon_o} \qquad \text{———— 6.2}$$

for $x < 0$

where n/m^3 is the concentration of free electrons, ϵ_r is the relative permittivity of ZnS and ϵ_o is permittivity of free space.

Now by assumption $N_i \gg N_d$

∴ Equation 6.2 becomes

$$\frac{\partial^2 V}{\partial x^2} \approx -\frac{e(N_i - n)}{\epsilon_r \epsilon_o} \qquad \text{———— 6.3}$$

for $x < 0$

Let n_o/m^3 be the concentration of free electrons at $x = 0$

$$\therefore \quad n = n_o \exp\left(\frac{eV}{kT}\right) \qquad \text{———— 6.4}$$

for all x.

∴ Using $\dfrac{\partial^2 V}{\partial x^2} = \dfrac{1}{2} \dfrac{\partial \left(\frac{\partial V}{\partial x}\right)^2}{\partial V}$

and substituting equation 6.4 in equation 6.1 gives

$$\left(\frac{\partial V}{\partial x}\right)^2 - \left(\frac{\partial V}{\partial x}\right)_0^2 = -\frac{2e}{\epsilon_r \epsilon_o} \int_0^V \left[N_d - n_o \exp\left(\frac{eV}{kT}\right)\right] dV \qquad \text{———— 6.5}$$

for $x>0$, i.e. $V<0$.

$$\therefore \quad \left(\frac{\partial V}{\partial x}\right)_0^2 - \left(\frac{\partial V}{\partial x}\right)^2 = \frac{2eN_d V}{\epsilon_r \epsilon_o} - \frac{2n_o kT}{\epsilon_r \epsilon_o}\left[\exp\left(\frac{eV}{kT}\right) - 1\right] \qquad 6.6$$

as $x \rightarrow \infty$, $V \rightarrow V_\infty$, and $\dfrac{\partial V}{\partial x} \longrightarrow 0$, where V_∞ is defined by the position of the bulk Fermi level. In the absence of any other limiting conditions this would be such that

$$n_o \exp\left(\frac{eV_\infty}{kT}\right) = n_\infty = N_d \qquad \text{———— 6.7}$$

since we assume all donors ionized.

$$\text{Thus } \left(\frac{\partial V}{\partial x}\right)_0^2 = \frac{2eN_dV_\infty}{\epsilon_r\epsilon_o} - \frac{2N_dkT}{\epsilon_r\epsilon_o} + \frac{2n_okT}{\epsilon_r\epsilon_o} \qquad \text{———— 6.8}$$

$$\therefore \left(\frac{\partial V}{\partial x}\right)^2 = \frac{2N_dkT}{\epsilon_r\epsilon_o}\left[\exp\frac{e(V-V_\infty)}{kT} - \frac{e(V-V_\infty)}{kT} - 1\right] \qquad \text{———— 6.9}$$

Now for $x>0$ $V-V_\infty>0$

Thus $\exp\dfrac{e(V-V_\infty)}{kT} \gg \dfrac{e(V-V_\infty)}{kT}$

so long as $V-V_\infty > \dfrac{kT}{e}$

We may thus rewrite equation 6.9 as

$$\left(\frac{\partial V}{\partial x}\right)^2 = \frac{2n_okT}{\epsilon_r\epsilon_o}\exp\left(\frac{eV}{kT}\right) \qquad \text{———— 6.10}$$

so long as the condition $V-V_\infty > \dfrac{kT}{e}$ is fulfilled. (V_∞ is defined by equation 6.7).

Since N_d is small (for very high resistivity material) and n_o is large (high concentration of surface charge) we see from equation 6.7 that $V_\infty \gg \dfrac{kT}{e}$ and therefore equation 6.10 is valid at the origin. The field at the origin is thus given by

$$\left(\frac{\partial V}{\partial x}\right)_0 = -\sqrt{\frac{2n_okT}{\epsilon_r\epsilon_o}} \qquad \text{———— 6.11}$$

and is independent of the bulk donor concentration N_d.

Equation 6.10 may be integrated to give

$$\left[\exp\left(-\frac{eV}{2kT}\right) + 1\right] = e\left(\sqrt{\frac{n_o}{2kT\epsilon_r\epsilon_o}}\right)x \qquad \text{———— 6.12}$$

where $x>0$, $V<0$.

Thus for small V, the potential rises (for electrons) sharply with a slope equal to $\left(\frac{\partial V}{\partial x}\right)_o$. At larger V the potential becomes a logarithmic function of x. The central barrier therefore consists of an abrupt rise in potential of several kT followed by a much more gradual rise over a comparatively large distance.

From equation 6.3

$$\left(\frac{\partial V}{\partial x}\right)^2 - \left(\frac{\partial V}{\partial x}\right)_o^2 = -\frac{2eN_iV}{\epsilon_r \epsilon_o} + \frac{2n_okT}{\epsilon_r \epsilon_o}\left[\exp\left(\frac{eV}{kT}\right) - 1\right] \quad 6.13$$

for $x<0, V>0$

Now $\frac{\partial V}{\partial x}$ must be continuous at $x = 0$

.˙. Using equation 6.11 in equation 6.13

$$\left(\frac{\partial V}{\partial x}\right)^2 = -\frac{2eN_iV}{\epsilon_r \epsilon_o} + \frac{2n_okT}{\epsilon_r \epsilon_o} \exp\left(\frac{eV}{kT}\right) \quad \text{———————} \quad 6.14$$

for $x<0$.

Suppose that the minimum conduction band potential (for electrons) occurs at $x = -x_c$

Then at $x = -x_c$, $V = V_c$, $\frac{\partial V}{\partial x} = 0$

.˙. from equation 6.14

$$\exp\left(\frac{eV_c}{kT}\right) = \frac{N_i}{n_o}\left(\frac{eV_c}{kT}\right) \quad \text{———————} \quad 6.15$$

If, as we assume, the depth of penetration of the positive surface charge is great enough to prevent the depletion and accumulation layers overlapping, then the space charge density

at $x = -x_c$ is zero (since the electron charge just neutralizes the fixed charge eN_i).

$$\therefore n = N_i \text{ at } x = -x_c \qquad \text{———} \quad 6.16$$

Using equation 6.15 and 6.16 we obtain

$$N_i = N_i \quad \frac{eV_c}{kT} \qquad \text{———} \quad 6.17$$

$$\text{i.e. } V_c = \frac{kT}{e} \qquad \text{———} \quad 6.18$$

$$\text{and } n_o = \frac{N_i}{2.72} \qquad \text{———} \quad 6.19$$

The value of n_o given by equation 6.19 may now be used in equation 6.12 to give the conduction band potential in the central part of the crystal (where $x>0$).

Figure 6.4 shows the potential of the conduction band plotted against distance within this central region of the crystal for 77°K and 300°K. The abrupt rise followed by the very much more gradual rise in potential is clearly shown. The curves shown in Figure 6.4 do not take into account the concentration of bulk donors. If this were large enough (room temperature resistivity $<10^4 \Omega m$) the conduction band potential would become constant at the point where its height above the Fermi level was equal to that in normal bulk material. This would lead to a "flat band" condition in the centre of the crystal and the resistivity would be determined by the nett donor density. It is likely, however, that the nett donor concentration in these crystals was low (bulk room temperature resistivity

Figure 6.4 Conduction band potential in the central region of a device.

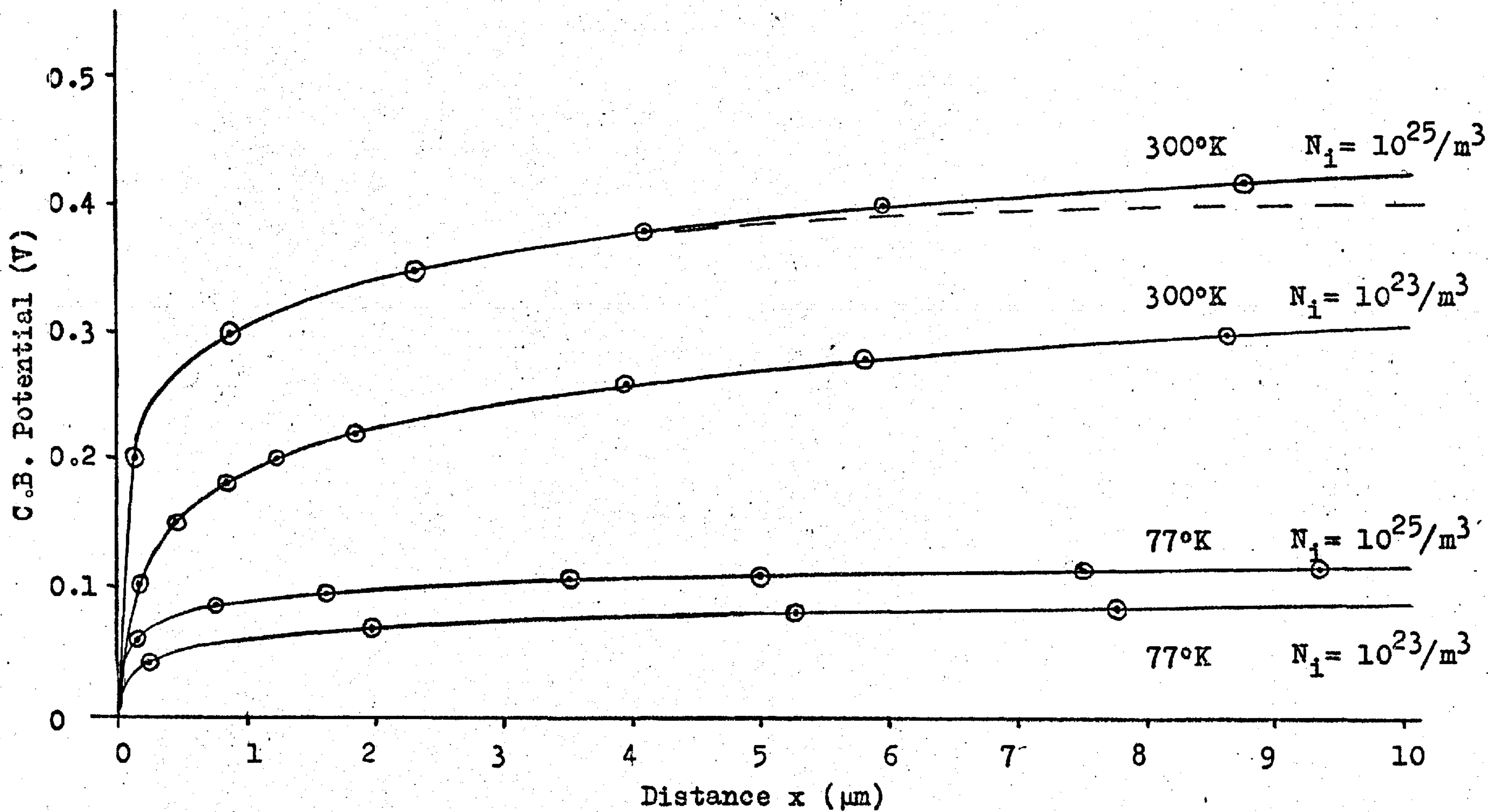

$>10^8 \Omega$m). The room temperature Fermi level corresponding to $10^8 \Omega$m resistivity is given by Table 4.1 as 0.735eV below the conduction band. As the Fermi level at the surface of the crystal is very close to the conduction band, the position of the Fermi level in the centre of the crystal is given approximately by the potential curves of Figure 6.4. These show that the bulk Fermi level is not reached until the thickness of the central region is much greater than 10μm. Crystals of the order of 20μm thick, therefore, impose artificial boundary conditions on the shape of the conduction band since the symmetry of the device demands that the slope of the conduction band, $\frac{\partial V}{\partial x}$, shall be zero near the centre of the crystal.

Assuming negligible nett donor concentration, equation 6.10 can be modified to include this boundary condition with the result that

$$\left(\frac{\partial V}{\partial x}\right)^2 = \frac{2n_o kT}{\epsilon_r \epsilon_o}\left[\exp\left(\frac{eV}{kT}\right) - \exp\left(\frac{-eV_m}{kT}\right)\right] \qquad 6.20$$

where $x>0$, $V<0$, $-V_m$ is the mid-crystal potential of the conduction band.

Integrating equation 6.20 gives

$$\sin^{-1}\left\{\exp\frac{-e(V+V_m)}{2kT}\right\} - \sin^{-1}\left\{\exp\left(\frac{-eV_m}{2kT}\right)\right\}$$

$$= \left\{e\sqrt{\frac{n_o}{2kT\epsilon_r\epsilon_o}}\cdot\exp\left(\frac{-eV_m}{2kT}\right)\right\}x \qquad 6.21$$

The dotted curve shown in Figure 6.4 was plotted for

$N_i = 10^{25}m^{-3}$ and a crystal thickness of 20μm, using equation 6.21. By substituting equation 6.4 into equation 6.21 we find that

$$n_m \approx \frac{\pi^2 kT \epsilon_r \epsilon_o}{2e^2 x_m^2} \qquad 6.22$$

where n_m = concentration of electrons in the conduction band at the centre of the crystal

x_m = value of x at the centre of the crystal.

Since the surface barriers on the crystal are by definition thin, x_m is approximately half the thickness of the crystal t. Thus equation 6.22 becomes

$$n_m \approx \frac{2\pi^2 kT \epsilon_r \epsilon_o}{e^2 t^2} \qquad 6.23$$

Equation 6.23 shows that n_m is independent of N_i and depends only on temperature and crystal thickness. A typical value of n_m would be $1.5 \times 10^{17}/m^3$ for T = 77°K and t = 20μm.

6.2.3 Current conduction in devices in the ON state

In the ON state the depletion barriers at the surfaces of the crystal are supposed to be so thin that electrons may tunnel freely between the metal electrodes and the conduction band of the ZnS. Thus, by assumption, the contacts have a low resistance (compared with the rest of the device) in the ON state. Due to the relatively low free electron concentration in the centre of the crystal most of the applied voltage will be dropped in this region and current flow will be regulated by this part of the crystal.

Figure 6.5 shows the effect on the band diagram of applying a small voltage to the switched ON device. The origins of V and x are the same as in Figure 6.3.

The current flow equation in the central region is

$$j = e\left[\mu n E + D_n \cdot \frac{\partial n}{\partial x}\right]$$

$$= e\mu\left[nE + \frac{kT}{e} \cdot \frac{\partial n}{\partial x}\right] \qquad 6.24$$

where j is the current density in A/m^2

E is the electric field in the conduction band in V/m

μ is the electron mobility in $m^2/Vsec$.

If the bulk donor concentration is small, then the only space charge in the central region is that of electrons.

Hence Poisson's equation is

$$\frac{\partial E}{\partial x} = -\frac{ne}{\epsilon_r \epsilon_o} \qquad 6.25$$

Let the voltage corresponding to the Fermi level be V_F. Since a voltage is applied to the device, V_F will be a function of x.

$$\text{By definition } n = N_c \exp\frac{e(V - V_F)}{kT} \qquad 6.26$$

$$\therefore \frac{\partial n}{\partial x} = \frac{en}{kT}\left(\frac{\partial V}{\partial x} - \frac{\partial V_F}{\partial x}\right)$$

$$= -\frac{enE}{kT} - \frac{en}{kT}\frac{\partial V_F}{\partial x} \qquad 6.27$$

By substituting equation 6.27 into equation 6.24 we obtain

$$j = -ne\mu \frac{\partial V_F}{\partial x} \qquad 6.28$$

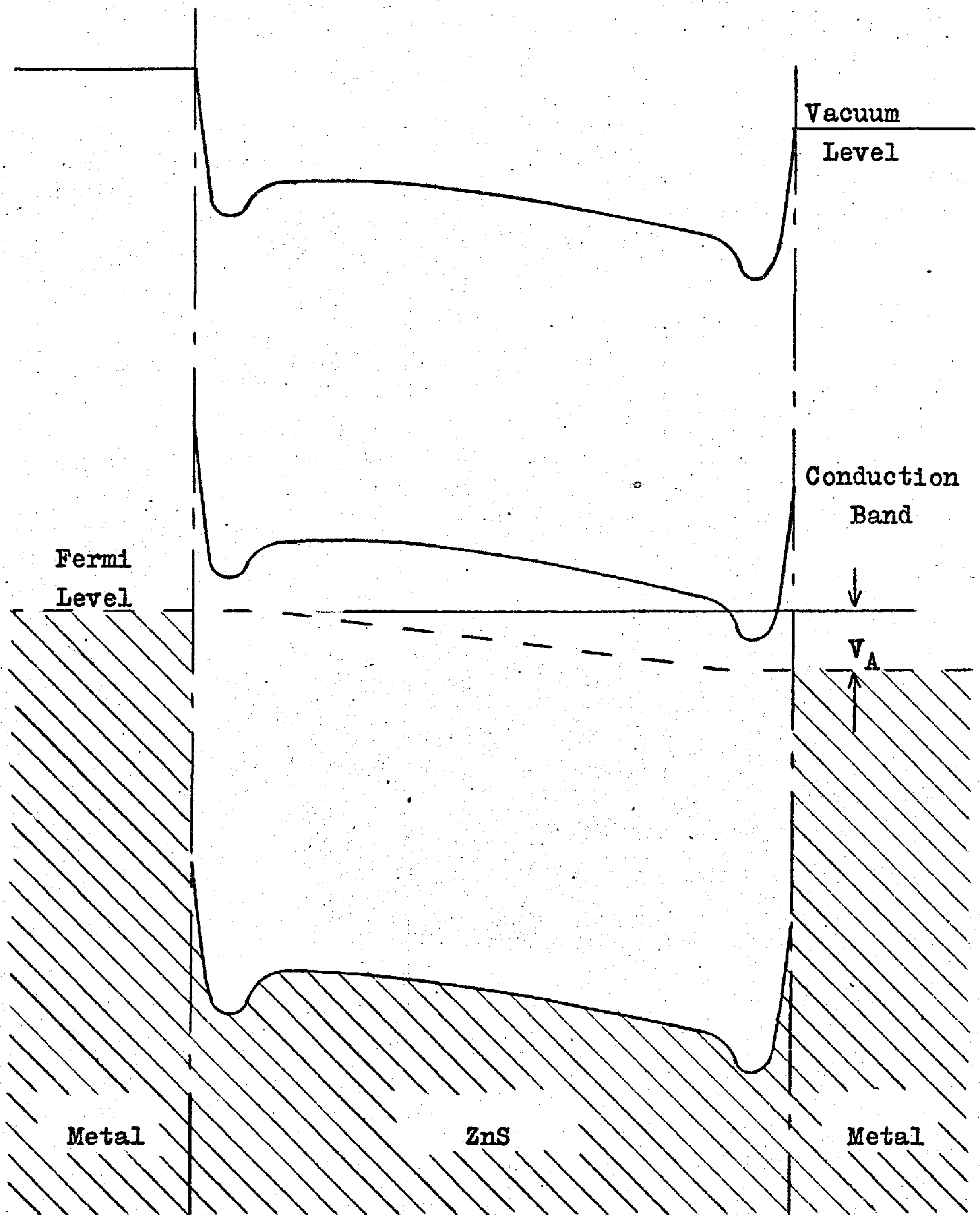

Figure 6.5 Efect on Band Diagram of applying a small voltage.

Since the electron quasi Fermi level must be continuous across the device and since at zero current the Fermi potential is independent of x, the voltage applied to the device must be

$$\int_0^t \frac{\partial V_F}{\partial x} \cdot dx .$$

$\therefore$ The applied voltage V_A is given by

$$V_A = \int_0^t \frac{\partial V_F}{\partial x} dx = \int_0^t \frac{-j}{ne\mu} dx = \frac{-j}{e\mu} \int_0^t \frac{1}{n} dx \qquad 6.29$$

since j is independent of x for a one dimensional model.

For small currents we assume that the electron distribution in the crystal is not significantly different from the zero current distribution.

Equations 6.4 and 6.21 may be combined to give $\frac{1}{n}$ as a function of x thus

$$\frac{1}{n} = \frac{1}{2n_m}\left\{1 + \left(\frac{2n_m}{n_o} - 1\right) \cos 2K_1 x + 2\left(\frac{n_m}{n_o}\right)^{\frac{1}{2}}\left(1 - \frac{n_m}{n_o}\right)^{\frac{1}{2}} \sin 2K_1 x\right\} \qquad 6.30$$

where n_m is the concentration of electrons at the centre of the crystal for zero current flow and

$$K_1 = e\sqrt{\frac{n_m}{2kT\epsilon_r\epsilon_o}} \qquad 6.31$$

Thus, by integrating equation 6.30 we obtain

$$\int_0^t \frac{1}{n} dx = \frac{1}{2n_m}\left\{t + \frac{2}{K_1}\left(1 - \frac{n_m}{n_o}\right)^{\frac{1}{2}}\left(\frac{n_m}{n_o}\right)^{\frac{1}{2}}\right\} \qquad 6.32$$

where it is assumed that the potential drop in the surface layers is small.

From equation 6.21 we see that

$$K_1 t = 2K_1 x_m \approx \pi \qquad 6.33$$

Since n_m is typically of the order of $10^{17}/m^3$ and n_o may be of the order of $10^{25}/m^3$, equation 6.32 therefore reduces to

$$\int_0^t \frac{1}{n} dx = \frac{t}{2n_m} \qquad 6.34$$

Substituting equation 6.34 into equation 6.29

$$V_A = -\frac{jt}{2e\mu n_m} \qquad 6.35$$

Using the approximate equation 6.23 for n_m gives

$$V_A = -\frac{jet^3}{4\pi^2 kT\mu \epsilon_r \epsilon_o} \qquad 6.36$$

The ON state resistance is therefore given by

$$R_{ON} = \frac{V_A}{I_{ON}} = \frac{et^3}{4\pi^2 kT\mu \epsilon_r \epsilon_o A} \qquad 6.37$$

where A is the area of the current channel.

For a typical device

$$t = 20\mu m$$

$$A \approx 10^{-6} m^2$$

$$\mu = 3 \times 10^{-2} \ m^2/Vs \text{ (Reference 1m)}$$

$$T = 77°K$$

$$\therefore R_{ON} = 14k\Omega \qquad 6.38$$

This theoretical value of R_{ON} is in very good agreement with experimentally obtained values (Section 5.3.1) which were typically between 10kΩ and 20kΩ.

Although the t^3 dependence of R_{ON} could not be verified quantitatively by experimental results (through lack of data) a very much smaller value of R_{ON} was observed for a thinner than average crystal, suggesting that R_{ON} does increase rapidly with thickness. Additional evidence is given by Dearnaley[59] who notes that the degree of forming of Simmons and Verderber type devices follows an approximate t^3 law.

Equation 6.37 shows that R_{ON} is expected to be independent of surface charge concentration, provided that the surface barriers are sufficiently low resistance not to contribute significantly to the total resistance of the device. This would explain why many devices had similar values of R_{ON}. The ability to vary R_{ON} by controlling the switch ON conditions probably arises from the dependence of R_{ON} on A, the area of the current conducting channel. The cross-section area of this channel is likely to depend on the switch ON current. The ON state resistance can thus depend on the switch ON current used, as was found experimentally (Section 5.3.3.). When the current channel has expanded to almost the area of the contacts it cannot continue to increase its area for increasing switching current drive. There is therefore, a lower limit to the ON state resistance obtainable from a given device. Reproducible values of ON state resistance may therefore be obtained most

easily by driving the device very hard at switch ON so as to obtain the limiting value of R_{ON}. This effect was observed in practice.

The temperature dependence of R_{ON} is given by the term $\frac{1}{kT\mu}$ in equation 6.37. The temperature range of most interest is 77°K to 200°K over which range experimental devices showed negligible change in ON state resistance. The three main scattering mechanisms in 11 – V1 compounds are optical phonon scattering (dominant at the higher temperatures), piezo-electric scattering and ionized impurity scattering (dominant at lower temperatures), (Ref. 1n). Very little quantitative experimental data is available on the temperature dependence of mobility in ZnS. One reference (1j) shows that in doped powder samples the dominant scattering mechanism appears to be optical phonon scattering above 200°K and ionized impurity scattering below 200°K. However, in pure single crystals it is more likely that piezo-electric scattering becomes dominant at low temperatures as is shown to be the case for CdS in reference 1p. The "cross-over" point between the two mechanisms would then lie right in the centre of the temperature range of interest, so that the temperature dependence of the mobility would be expected to lie somewhere between the T^{-} dependence for piezo-electric scattering and the $\exp\left(\frac{\hbar\omega_1}{kT}\right)$ dependence for optical phonon scattering. Thus qualitatively μ decreases with increasing temperature in the range of interest at a rate which could, in principle, account

for an almost zero temperature coefficient. However, the simple derivation of R_{ON} does not take account of any redistribution of carriers by the applied field, of possible electron traps in the central part of the crystal, nor of the possibility that the conduction band is degenerate at the bottom of potential well at the surface barriers. It would therefore, be unreasonable to expect any more than qualitative agreement for the temperature dependence so calculated.

6.2.4 Conduction in the OFF state

The model for the ON state relies on there being a sufficiently high concentration of fixed positive charge at the surfaces of the device to cause the surface depletion layers to become transparent to electrons tunnelling into the conduction band of the ZnS from energies close to the Fermi energy in the metal. If, during the switch OFF process, some of this positive charge is removed, then electrons will no longer be able to pass freely from metal to ZnS. According to the way in which the surface charge is removed either the surface depletion layer may become thicker, so that electrons can no longer tunnel through it, or else the potential of the conduction band near the surface of the ZnS crystal may rise sufficiently far above the metal Fermi level to cut off the supply of electrons from the crystal, even though the depletion layer remains thin enough to permit tunnelling. In either case the effective device resistance will be drastically increased. The two cases are illustrated in

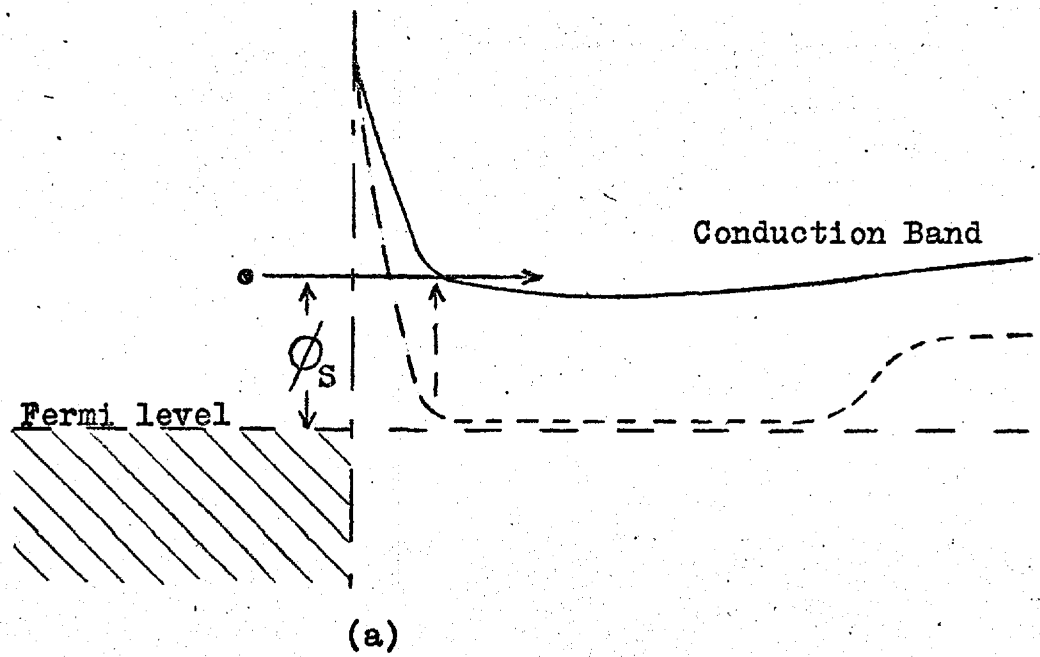

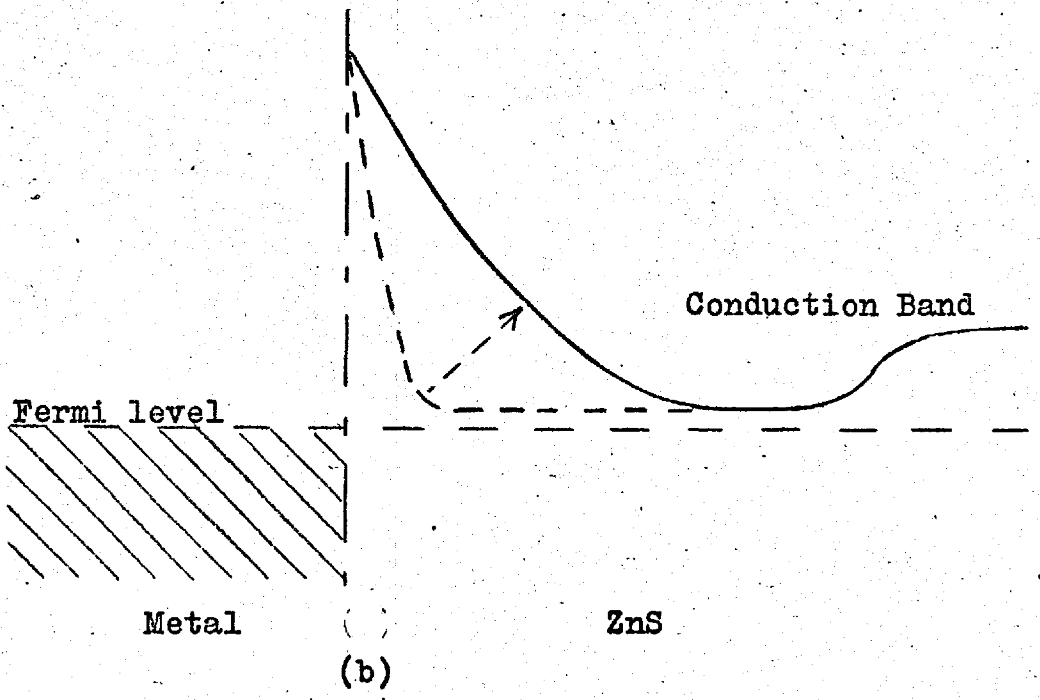

Figure 6.6 Posible potential profiles at the Metal-ZnS interface in the OFF state.

Figures 6.6(a) and (b). The dotted lines show the profile of the conduction band edge in the ON state. The band diagram of Figure 6.6(a) shows that electrons surmounting the barrier ϕ_s may tunnel into the conduction band of the ZnS (phonon assisted tunnelling). Thus ϕ_s is an artificially low Schottky barrier and the I - V characteristics of such a device would be expected to be of the form log I α $V^{\frac{1}{2}}$. The concentration of electrons on the ZnS side of the surface depletion layer is equal to the residual positive charge in this region in order to meet the condition of charge neutrality. Thus ϕ_s must be proportional to kT in order to maintain the correct concentration of electrons in the conduction band for charge neutrality. Both the log I α $V^{\frac{1}{2}}$ dependence and the ϕ_s α kT dependence were observed in practice (Section 5.5.3 and Table 5.3). The linear dependence of ϕ_s on kT is very good evidence for the existence of the mechanism of conduction shown in Figure 6.6(a), since constant values of ϕ_s would be expected if the log I α $V^{\frac{1}{2}}$ characteristics were a result of either Schottky or Poole-Frenkel emission in the normally accepted sense.

6.2.5 Origin of the positive charge

In principle, any thin layer, containing sufficient stable positive charge in the surface of a crystal would fulfil the requirements of the model for the ON state. Simmons and Verderber[51,52] have suggested that gold diffuses into their devices under the action of the electric field and that the forming process is simply this electrically activated diffusion.

Evidence also exists for the field activated diffusion of silver ions into quartz crystals[63]. No doubt the high fields involved do have some effect on the diffusion of silver from the electrodes into the ZnS crystals discussed here. However, this does not explain how positive charge can be injected into both the surfaces with a d.c. forming voltage unless the silver ions diffuse right through the crystal in sufficient concentration to form the cathode barrier, without actually causing a catastrophic short circuit between the two electrodes. Copper, silver and gold are all known to diffuse very rapidly into the II - VI compounds by an interstitial mechanism[1k] and the annealing of gold doped CdTe at temperatures as low as 100°C has been shown to produce significant changes in electrical conductivity[1q]. Evidence has also been found for significant room temperature diffusion of copper into II - VI compounds[64].

It is therefore not unreasonable to suggest that silver atoms diffuse into the surfaces of ZnS crystals from silver contacts at room temperature, at least to a depth of the order of 100Å, by an interstitial mechanism. These atoms would, in their unformed state be neutral and would therefore not be expected to alter the crystal conductivity by a significant amount (as compared with conductivity switching).

The centres which hold the positive charge must have an extremely small capture cross-section at temperatures below 233°K if they are not to be discharged by conduction band electrons. The existence of centres with a very small capture

cross-section is known in II - VI compounds. Wright et al.[61] found a capture cross section of $10^{-34}m^2$ for the storage centre in CdS crystals showing conductivity storage phenomena. Such a centre might well have a potential profile as shown in Figure 6.7. The potential diagram is drawn for electrons and is referred to the conduction band edge (since this represents the free electron energy in ZnS). Jonscher[49] has previously suggested that some electron traps in insulators may have this type of potential profile. In this case, however, it would represent the positive charge centre (Ag^+ ion) with a certain amount of negative charge screening around it. Because of the screening of the centre, conduction band electrons would have to surmount the barrier ϕ_1 before they could be trapped at the charge centre. Since most of the conduction band electrons have energies confined to a few kT above the conduction band edge, it is to be expected that, at low enough temperatures, the capture cross section of such a centre would be very small. In addition there should be a narrow range of temperature over which the capture cross section would change by many orders of magnitude, corresponding to the temperature at which a significant number of electrons can surmount the barrier ϕ_1. This effect has been observed by Kulp[60] for CdS conductivity storage crystals where the capture cross section increased by a factor of 10^4 over the temperature range 205°K to 270°K.

The same effect is also implied by the measurements on ZnS devices in this work. The ON state was shown to be unstable

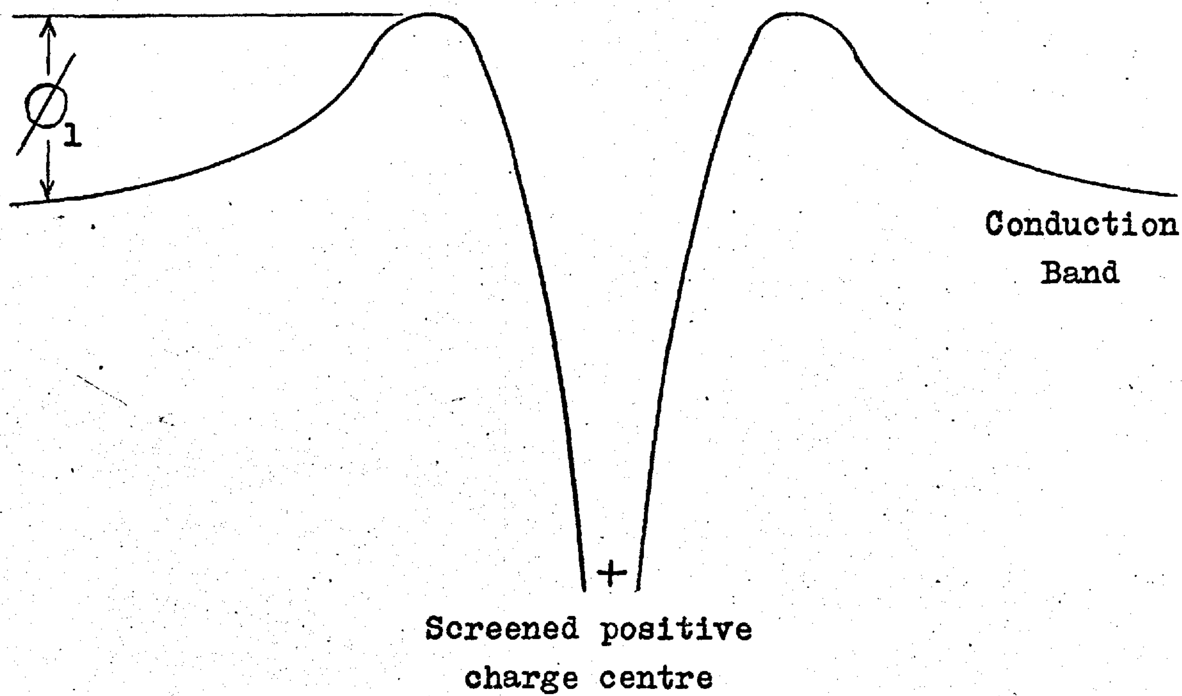

Figure 6.7 Possible potential profile of a screened positive charge centre.

above about 230°K at which temperature time dependent decay took place. Also the sudden discontinuity of the T.S.C. curves suggests that rapid discharging of charged centres could be taking place. The fact that the ON state resistance increased rapidly above 230°K also implies a discharging of positively charged centres since, by this means, the device was switching itself OFF.

Structurally, wurtzite ZnS consists of a close packed lattice of large sulphur ions with small zinc ions in half the interstitial positions between the sulphur ions. The interstitial sites in the lattice for foreign impurity atoms are thus the unoccupied half of the interstitial positions between the sulphur ions. They are therefore screened from the zinc ions by the electron clouds of the surrounding sulphur ions. Identifying the conduction and valence bands with the zinc and sulphur ions respectively(36) we see that this amounts to a screening of the interstitial position from the conduction band. On the other hand valence band holes would not be screened from the interstitial position and could thus be trapped at neutral interstitial silver atoms. The nett effect would be to ionize the neutral interstitial atoms. It is therefore proposed that the positive charge at the surface of the crystal arises from the ionization of neutral interstitial silver atoms which have diffused into the material from the contacts. The ionization process is thought to be one of hole trapping rather than impact ionization or field assisted removal of electrons,

although all three processes may play some part in ionizing the silver atoms.

6.2.6 The forming process

Equation 4.15 may be used to calculate the positive charge required in the surface for given barrier thicknesses. Thus it can be shown that approximately 10nC of charge is required for a barrier 100Å thick, or 20nC of charge for a barrier 50Å thick (assuming an active device area of $10^{-6}m^2$). This charge has to be supplied to both cathode and anode barriers before a device can be switched to the high conductivity state. Since devices could be formed with direct current, the positive charge at the cathode could not have been generated by the removal of electrons from the charge storage centres in the ZnS to the adjacent electrode, since the field at the cathode would have opposed this motion of electrons. Impact ionization of the centres is also unlikely, since most of them are so close to the cathode that the electrons do not have a chance to acquire enough energy from the field to ionize them. Since forming occurs at fields of the order of 5×10^7V/m and is temperature dependent it is unlikely that the positive charge at the cathode barrier is generated by tunnelling of electrons out of the storage centres into the ZnS conduction band. It is probable that this kind of tunnelling would require fields an order of magnitude higher.

Other possible mechanisms for the ionization of the

centres are the trapping of valence band holes, phonon assisted tunnelling of electrons from the storage centres to the conduction band, or Poole-Frenkel emission of electrons into the conduction band. All these mechanisms are thermally activated processes and could thus account for the temperature dependence of the forming process.

Figure 6.8 shows tha band diagram for an unformed device with a high voltage applied to it. There is negligible band bending at the surfaces since there is very little positive surface charge in unformed devices. If holes and electrons enter the device by Schottky emission from the anode and cathode respectively, then the ratio of hole to electron current is:

$$\frac{I_p}{I_n} = \exp \frac{e(\phi_n - \phi_p)}{kT} \qquad 6.39$$

where ϕ_n and ϕ_p are the zero field barriers to electrons and holes entering the conduction and valence bands respectively. Aven and Mead[36] have found that the barrier $e\phi_n$ for silver on ZnS is 1.62eV. Thus, since the band gap of ZnS is 3.6eV, $e\phi_p$ must be 1.96eV and hence $e(\phi_n - \phi_p) = -0.36$eV.

∴ At room temperature

$$\frac{I_p}{I_n} \approx 10^{-6}$$

and at 77°K

$$\frac{I_p}{I_n} \approx 3 \times 10^{-24}$$

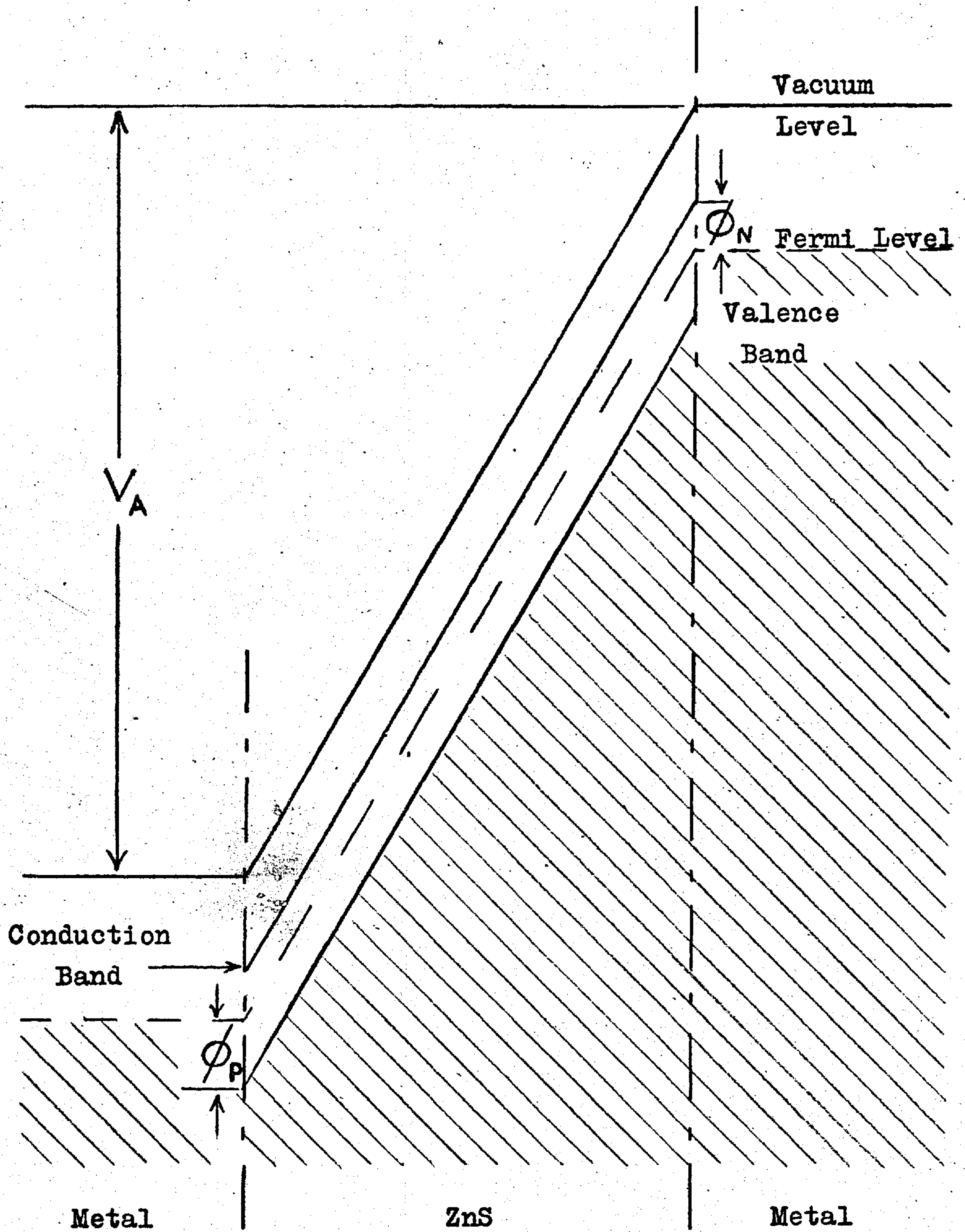

Figure 6.8 Unformed device with a high voltage applied.

With an electron current of 1mA, at room temperature it would take ten seconds for the hole current to supply 10nC to the anode barrier. At 77°K the time required would be approximately 10^{15} hours. Thus Schottky emission of holes from the anode predicts a slightly longer room temperature forming time than found in practice (of the order of two seconds), but it does account for the inability to form devices at low temperatures.

It is interesting to note that Verderber et al.[52] found that forming times varied from ten seconds at room temperature to more than one hour at -40°C. Equation 6.39 predicts that forming times for ZnS at the above two temperatures would be in the ratio of 50 to 1, if Schottky emission of holes is the mechanism responsible for forming. This type of mechanism might therefore also explain Verderber's results.

6.2.7 The switch ON process

It has been established experimentally (Section 5.3.4) that the charge required to switch OFF a device is typically less than 800pC. Thus only a small fraction of the charge in the surface barriers can be neutralized in the switch OFF process. It therefore follows that only this small fraction of the total surface charge has to be supplied in the switch ON process. In addition, the large concentrations of positive charge at the surfaces of the crystals, even in the OFF state, cause considerable band bending at all times in formed devices. The hole current due to Schottky emission from the anode no

longer flows since the effective barrier to holes at the anode is increased (see Figure 6.9). There must therefore be some other mechanism by which holes are supplied to the valence band in order to be trapped at the cathode charge centres. It is likely that the high density of positive charge centres in formed devices form some kind of impurity band at the crystal surface through which holes could enter the crystal. A possible mechanism for switch ON would therefore involve impurity band conduction through the surface barrier of the devices followed by tunnelling of holes from impurity centres to the valence band. These processes are not strongly temperature dependent and could therefore operate equally well at 300°K or 77°K, but only in formed devices. Thus, it is necessary to form devices at room temperature first before switching can occur at 77°K.

6.2.8 The switch OFF process

As has already been mentioned, the charge involved in the switch OFF process is typically less than 800pC, or of the order of $\frac{1}{100}$ of the total surface barrier charge. This is in good agreement with the model for the OFF state of the device, as given in section 6.2.4, in which the conduction band potential changes very little between the ON and OFF states. Another feature of the switch OFF process is the need to remove the applied voltage very rapidly (see also references 51,56).

Consider the device in the ON state. For small applied voltages the carrier distribution in the device is unaffected by the applied voltage and the potential profile of the

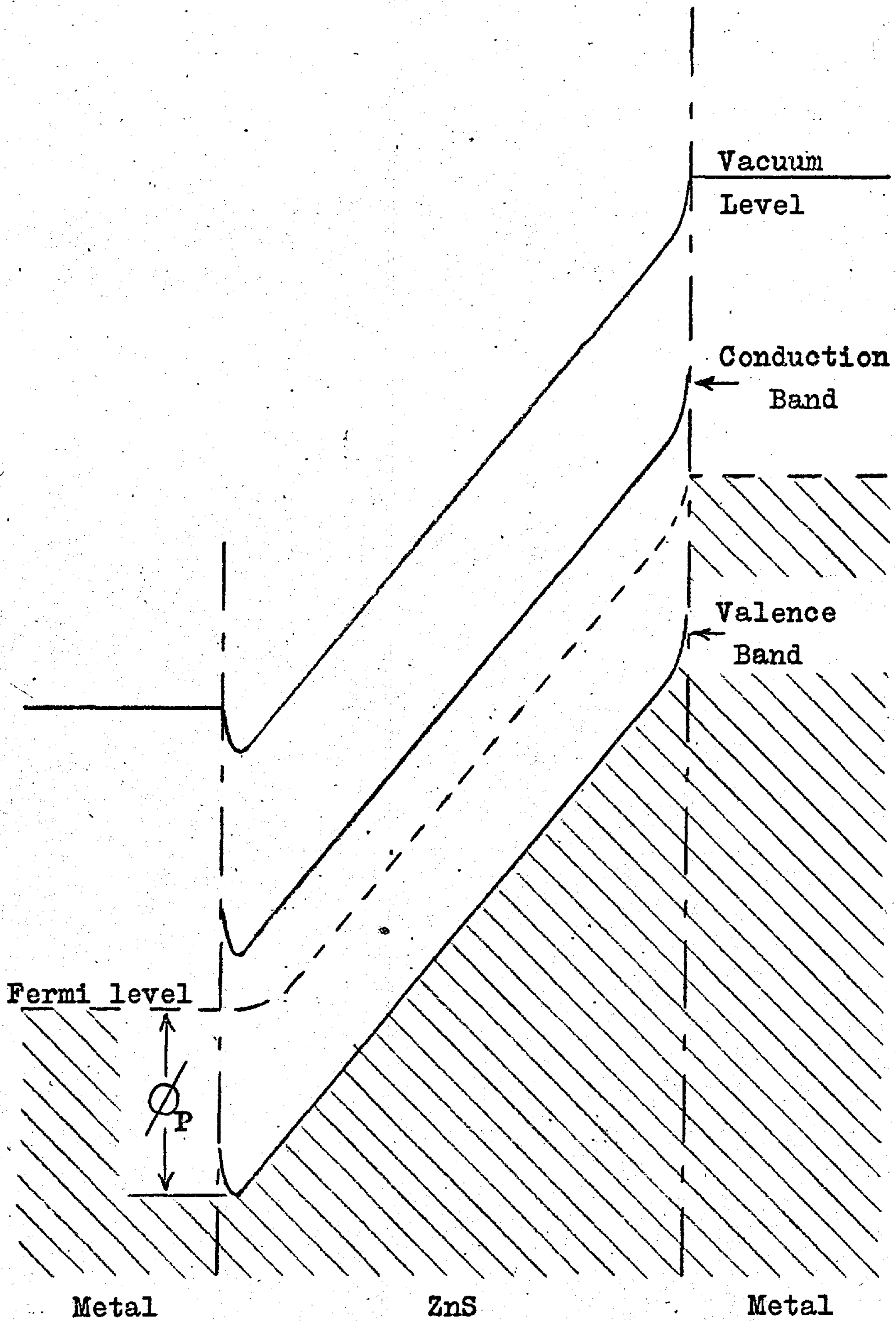

Figure 6.9 High voltage applied to a formed device.

conduction band as is shown in Figure 6.5. However at relatively high applied voltages ($\approx$20V) a larger concentration of electrons is injected from the cathode potential well into the central part of the device. If the voltage is reduced gradually, then the carrier distribution remains in equilibrium with the contacts since all the injected electrons have time to escape. If however, the applied voltage is reduced to zero in a short enough time, the electrons do not have time to escape from the device. They must return to the potential well inside the surface barriers since it is energetically favourable for them to do so. However, in doing this, they effectively neutralize some of the positive space charge in the barriers and increase their thickness so that the electrons can no longer tunnel out of the device as easily as they could previously. The band diagram at this stage is illustrated in Figure 6.10. Obviously this state is unstable since the electron quasi Fermi level is above the metal Fermi level. The raising of the electron quasi Fermi level with respect to the conduction band greatly increases the concentration of electrons at energies above the threshold $e\phi_1$, (see Figure 6.7) for capture by the positive charge centres. A sudden collapse of part of the positive charge therefore occurs, corresponding to the number of electrons with energy greater than $e\phi_1$. The discharging process must be extremely fast since the positive centres have a relatively large capture cross section for electrons with

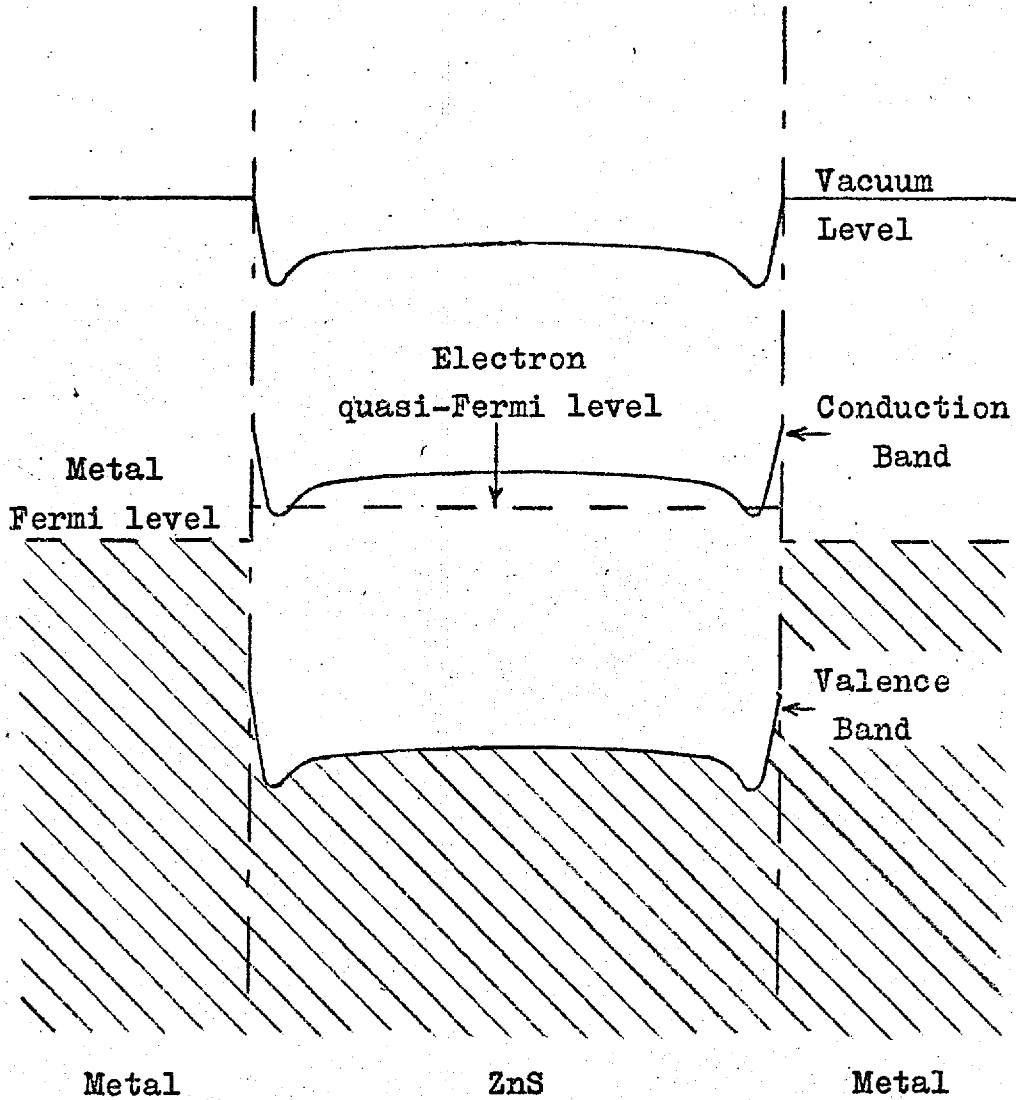

Figure 6.10 Meta-stable state of a device in the process of switching OFF.

energy greater than $e\phi_1$. The discharge of the positive centres must result in a band diagram as shown in Figure 6.6. The device has therefore been switched to the OFF state.

Obviously, the device cannot be switched OFF until a significant number of electrons is able to surmount the screening barrier $e\phi_1$. A certain minimum voltage must therefore be applied to the device in order to inject enough carriers into the central region of the crystal so that they may later turn OFF the device. There is therefore, a threshold voltage for switch OFF by the pulse method. The device may, however, also be turned OFF by a d.c. method. In this case a larger voltage must be applied in order to produce a finite voltage drop across the contact barriers. The cathode then injects excess electrons into the device moving the quasi Fermi level for electrons into the conduction band in the potential well. Electrons are then able to discharge the centres as before.

It is seen from the above arguments that there are two threshold voltages for switch OFF, the one for fast pulse switching being lower than the d.c. value. The existence of a threshold voltage is confirmed by the experimental results (Section 5.3.4). The threshold was also found to vary with pulse length such that higher voltages were required for longer pulses.

6.3 Discussion of the model and conclusion

The proposed model for the switching devices relies on three postulates:

1. The existence of thin depletion layers at the metal ZnS interface.
2. The existence of charge storage centres with extremely low capture cross-sections.
3. The interstitial diffusion of silver at low temperatures.

All three postulates have been shown to be well established experimentally by previous workers, whereas all other models including one by Mott[65], appear to rely to some degree on unestablished principles.

In addition all the experimentally observed aspects of switching and memory are predicted at least qualitatively by the model, and in some instances it has been possible to show quantitative agreement.

Thirdly, it is physically realistic in its requirements. For instance, it does not require the massive field assisted diffusion of electrode material throughout the device whilst at the same time requiring that there be no interelectrode short circuit as does the model of Simmons and Verderber[51].

Some reference has already been made to the explanation of the results of previous workers using the model proposed here. One interesting phenomenon which has been observed with amorphous switches is the existence of a "dead time" during

which the device may not be switched from the high to the low impedance state[51]. We recall that the switch OFF mechanism proposed involves electrons injected into the central part of the device neutralizing some of the positive charge in the surface barrier. The positive space charge is neutralized by the electron space charge even before recombination takes place. If there exist shallow electron traps in the device, then it is conceivable that the electrons, which would normally recombine with the positive charge centres, are temporarily prevented from doing so by being trapped. During this time it would be impossible to reconstitute the positive charge since the charge centres would not have been neutralized by recombination with electrons. There would therefore be a dead time which would reflect the lifetime of the trapped electrons and the density of the traps. In an amorphous material the density of traps may well be high so that a substantial dead time would be expected. In single crystal ZnS, on the other hand, the density of shallow traps is likely to be much smaller so that only a very short dead time (or none at all) would be expected. Unfortunately, it has not been possible to ascertain whether or not a dead time exists in the ZnS devices owing to the practical difficulty of producing repetitive switching because of the high switch ON voltages required.

In conclusion, it may be said that the discovery of conductivity switching in single crystal material is a major advance in switching device technology since it has provided

a very suitable vehicle for the theoretical and experimental investigation of switching phenomena.

References

1. AVEN and PRENER

Physics and Chemistry of II-VI Compounds.

(North Holland, 1967).

(a) Page 595

(b) " 139

(c) " 638

(d) " 79

(e) " 330

(f) " 596 and 604

(g) " 159

(h) " 358

(j) " 595

(k) " 233

(m) " 603

(n) " 551 et seq.

(p) " 581

(q) " 257

2. F. SEITZ

The Modern Theory of Solids. (McGraw Hill, 1940).

3. G. DESTRIAU

J.Chim.Phys., 33, 587, (1936)

4. E.J. ALLEN and J.L. CRENSHAW

Am.J.Sci., 34, 310, (1912)

5. R. FRERICHS
Naturewissenschaften, 33, 387, (1946)
Phys.Rev., 72, 594, (1947)

6. A. ADDAMIANO and P. A. DELL
J.Phys.Chem., 61, 1020, (1957)

7. D.C. REYNOLDS and S.J. CZYZAK
Phys.Rev., 79, 543, (1950)

8. J. NISHIMURA and Y.TANABE
J.Phys.Soc.Japan, 14, 850, (1959)

9. K.PATEK, M.SKALA, L.SOUCKOVA
Czech.J.Phys.B., 12, 313, (1962)

10. W.W. PIPER and S.J. POLICH
J.Appl.Phys., 32, 1278, (1961)

11. H. SAMELSON
J.Appl.Phys., 32, 309, (1961)

12. R. NITSCHE, H.U. BÖLSTERLI and M. LICHTENSTEIGER
J.Phys.Chem.Solids, 21, 199, (1961)

13. F. JONA and G. MANDEL
J.Phys.Chem.Solids, 25, 187, (1964)

14. H. SAMELSON
J.Appl.Phys., 33, 1779, (1962)

15. L.C. GREENE, D.C. REYNOLDS, S.J. CZYZAK and W.M. BAKER
J.Chem.Phys., 29, 6, 1375, (1958)

16. M.E. BISHOP and S.H. LIEBSON
J.Appl.Phys., 24, 660, (1953)

17. A. KREMHELLER

J.Electrochem.Soc., 107, 422, (1960)

18. P.D. FOCHS

J.Appl.Phys., 31, 1733, (1960)

J.Appl.Phys., 34, 1762, (1963)

19. I. DEV

Brit.J.Appl.Phys., 17, 761, (1966)

20. R.J. CAVENEY

J.Phys.Chem.Solids, 29, 851, (1968)

21. J.J. GILMAN

The Art and Science of Growing Crystals

(John Wiley & Sons, 1963)

(a) Page 269

(b) " 249

22. Dr. E.A.D. WHITE

Private Communication

23. I. BERTOTI, E. LENDVAY, M. FARKAS-JAHNKE, M. HARSY and P. KOVAKS

Acta Physica Hungaricae, 21, 121, (1966)

24. A. ADDAMIANO and M. AVEN

J.Appl.Phys, 31, 36, (1960)

25. A. EBINA and T. TAKAHASHI

J.Appl.Phys., 38, 3079, (1967)

26. H. KUKIMOTO, S. SHIONOYA, T. KODA and R. HIOKI

J.Phys.Chem.Solids, 29, 935, (1968)

27. P. GOLDFINGER and M. JEUNEHOMME
Trans.Faraday.Soc., 59, 2851, (1963)

28. R. COLIN
Technical Documents Liaison Office Unedited Rough Draft Translation. Measures of Thermodynamic Values by Mass Spectrometer, Study of Sulfur and Zinc
A.D. No.257 163 (1960)

29. R.A. ISAKOVA, V.N. NESTEROV
Russian Journal of Inorganic Chemistry, 11, 522, (1966)

30. K. TANAKA, M. MANNAMI, K. WATANABE
Jap.J.Appl.Phys., 4, 493, (1965)

31. A.G. FITZGERALD, M. MANNAMI, E.H. POGSON, A.D. YOFFE
J.Appl.Phys., 38, 3303, (1967)

32. J. CHIKAWA and T. NAKAYAMA
J.Appl.Phys., 35, 2493, (1964)

33. V.G. HILL
Acta.Cryst., 9, 821, (1956)

34. R. MARSHALL and S.S. MITRA
Phys.Rev., 134, A1019, (1964)

35. A.N. GEORGOBIANI and V.I. STEBLIN
Phys.Stat.Sol., 21, K49, (1967)

36. M. AVEN and C.A. MEAD
Appl.Phys.Lett., 7, 8, (1965)

37. M. BUJATTI
Brit.J.Appl.Phys., Ser.2, 1, 581, (1968)

38. A. M. GOODMAN
J.Appl.Phys., 35, 573, (1964)

39. F.A. KRÖGER et al.
Phys.Rev., 103, 279, (1956)

40. G.H.BLOUNT, M.W. FISHER, R.G. MORRISON and R.H. BUBE
J.Electrochem.Soc., 113, 691, (1966)

41. W.A. THORNTON
J.Electrochem.Soc., 108, 636, (1961)

42. M. AVEN and D.A. CUSANO
J.Appl.Phys., 35, 606, (1964)

43. SPAKOWSKI
Proc.Fifth Photovoltaic Conf., Maryland, U.S.A.(1965)

44. G. B. ABDULLAEV et al.
Phys.Stat.Solidi, 26, 65, (1968)

45. H.D. BARBER
P-N Junctions in Intermetallic Semiconductors
Ph.D. Thesis, London University (1965)

46. P.N. KEATING
Phys.Chem.Solids, 24, 1101, (1963)

47. L. FASS
Private Communication

48. Fast Pulse Techniques
E-H Research Laboratories Inc., Oakland, California

49. A.K. JONSCHER
Thin Solid Films, 1, 213, (1967)

50. SERVINI
Direct current conduction in thin insulating films
Ph.D. Thesis, London University (1968)

51. J.G. SIMMONS AND R.R. VERDERBER
J.I.E.R.E., 34, 81, (1967)

52. R.R. VERDERBER, J.G. SIMMONS, B. EALES
Phil.Mag, 16, 1049, (1967)

53. F. ARGALL
Electronics Lett., 2, 282, (1966)

54. C.W. LITTON and D.C. REYNOLDS
Phys.Rev., 133A, 536, (1964)

55. C. FELDMAN and W.A. GUTIERREZ
J.Appl.Phys., 38, 2474, (1967)

56. T.W. HICKMOTT
J.Appl.Phys., 35, 2118, (1964)

57. J.F. GIBBONS and W.E. BEADLE
Solid State Electronics, 7, 785, (1964)

58. S.R. OVSHINSKY
Phys.Rev.Lett., 21, 1450, (1968)

59. G. DEARNALEY et al.
Conduction and memory phenomena in thin insulating films. U.K.A.E.R.E. report - R5992

60. B.A. KULP
J.Appl.Phys., 36, 553, (1965)

61. H.C. WRIGHT, R.J. DOWNEY, J.R. CANNING
Brit.J.Appl.Phys., Ser.2, 1, 1593, (1968)

62. M.A. LAMPERT

Phys.Rev., <u>125</u>, 126, (1962)

63. E.L. MILNE and P. GIBBS

J.Appl.Phys., <u>35</u>, 2364, (1964)

64. Dr. M. BROWN

Private Communication

65. N.F. MOTT

Contemporary Phys., <u>10</u>, 125, (1969)